# Evaluating Mid-term Storage Technology to Enhance Flexibility in a Renewable Offshore Hybrid Power System

Lymperios Lymperopoulos

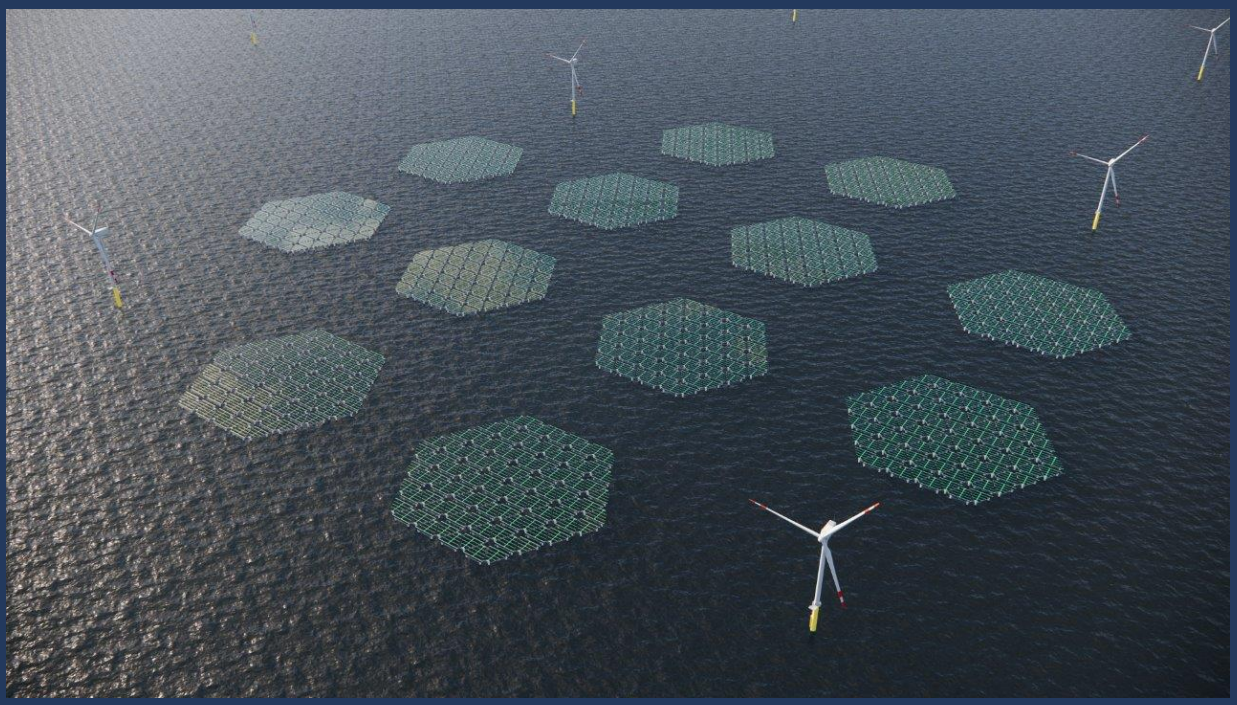

TU Delft

# Evaluating Mid-term Storage Technology to Enhance Flexibility in a Renewable Offshore Hybrid Power System

by

Lymperios Lymperopoulos

to obtain the degree of Master of Science in Sustainable Energy Technology
at the Delft University of Technology
to be defended publicly on August 29, 2024.

| | |
|---|---|
| Thesis committee: | |
| Chair: | Prof. Dr. D.A. von Terzi |
| Supervisor: | Dr. Ir. M.B. Zaayer |
| External examiner: | Dr. S.J. Pfenninger-Lee |
| Project Duration: | November 28th, 2022 – August 29th, 2024 |
| Student number: | 5547431 |

Wind Energy Group, Faculty of Aerospace Engineering, Delft University of Technology
An electronic version of this thesis is available at....

# Acknowledgements

This master's thesis marks the culmination of my MSc Sustainable Energy Technology journey at Delft University of Technology. Reflecting on the past three years, I am filled with gratitude for the incredible support and guidance I have received.

First and foremost, I would like to express my deepest appreciation to my supervisor, Prof. Zaayer. Thank you for granting me the opportunity to work on such a fascinating and creative project that perfectly aligned with my interests and career aspirations. Your unwavering support, understanding, and flexibility have been invaluable throughout this process.

I am also profoundly grateful to my fellow SET peers, project teammates, professors, and teaching assistants. Your collective support, knowledge, and camaraderie have enriched my experience over the past two years. The collaborative spirit and shared experiences have been a cornerstone of my academic journey.

A special thank you goes to the friends I have made during these three years. Your encouragement and motivation, especially during the challenging final year, were instrumental in helping me persevere. Your willingness to support me even after completing your own work demonstrates the true essence of friendship and solidarity.

Furthermore, I would like to extend my heartfelt gratitude to my friends back home. Despite the distance, your unwavering support and encouragement have been a constant source of strength.

Lastly, but most importantly, I wish to express my deepest gratitude to my parents and my brother. Your love, support, and motivation have been my bedrock, not just for the past three years, but for the entirety of my 25-year journey. Your belief in me has been the driving force behind my achievements, and for that, I am eternally grateful.

# Abstract

In 2022, global carbon dioxide emissions surged to a record high of 36.8 gigatons, highlighting the urgent need for a sustainable energy transition despite a temporary decrease during the COVID-19 pandemic. This trajectory underscores the imperativeness to replace fossil fuels with renewable energy sources, which are expected to double their capacity in the next five years. However, the integration of intermittent renewables like wind and solar presents challenges in stabilizing electricity grids, necessitating innovative solutions to balance supply and demand effectively.

This thesis presents a thorough exploration of mid-term storage strategies aimed at enhancing flexibility in hybrid offshore power systems that integrate wind and solar energy. A multi-criteria analysis was employed to identify the most suitable storage technologies for medium-term applications, resulting in the selection of Compressed Air Energy Storage (CAES), Lithium-ion batteries, and Lead-acid batteries as the top three candidates.

A specific study area, already equipped with offshore wind turbines, was selected for this research. Weather data were obtained and analyzed to reduce power mismatches and their associated costs. A multi-objective optimization approach was applied, focusing on minimizing the hourly loss of load and total capital costs associated with the hybrid renewable energy system.

In the base case scenario examined, which comprised 100% wind power, CAES emerged as the storage technology with the lowest total capital cost. However, by varying the proportions of offshore wind and solar energy, it was found that adjusting the mix to 80% offshore wind and 20% solar led to a significant reduction in the annual loss of load, thus reducing the total capital cost of the renewable hybrid system.

The results, depicted through Pareto optimal graphs underscore CAES as the most cost-effective solution when integrated with a predominantly offshore wind generation mix. The findings provide valuable insights into sustainable energy storage solutions and strategic planning for future developments in renewable energy.

# Abbreviations/Symbols

## Abbreviations

Table 1: List of Abbreviations

| Abbreviation | Definition |
|---|---|
| AHP | Analytic Hierarchy Process |
| MCA | Multi-Criteria Analysis |
| EST | Energy Storage Technology |
| CAPEX | Capital Expenditure |
| PHES | Pumped Hydro Energy Storage |
| CAES | Compressed Air Energy Storage |
| LAES | Liquid Air Energy Storage |
| PTES | Pumped Thermal Energy Storage |
| Li-ion | Lithium Ion |
| LA | Lead Acid |
| VRFB | Vanadium Redox Flow Battery |
| SoC | State of Charge |
| HES | Hybrid Energy System |
| PV | Photovoltaic |
| FPV | Floating Photovoltaic |
| MOOPs | Multi-Objective Optimization Problems |
| MPC | Model Predictive Control |
| R&D | Research and Development |
| DC | Direct Current |
| AC | Alternating Current |

# Symbols

Table 2: List of Symbols

| Symbol | Definition | Unit |
|---|---|---|
| $A$ | Rotor swept area | [$m^2$] |
| $A_m$ | Module azimuth | [°] |
| $A_{panel}$ | Area of solar panel | [$m^2$] |
| $A_s$ | Sun azimuth | [°] |
| $a$ | Wind shear exponent | [-] |
| $a_m$ | Elevation of the module | [° ] |
| $a_s$ | Sun elevation | [°] |
| $C_{sto}(t)$ | Storage capacity at time (t) | [Wh] |
| $C_{sto}(t-1)$ | Storage capacity at time (t-1) | [Wh] |
| $C_{PV,cap}(t)$ | PV farm capacity | [W] |
| $C_{W,cap}(t)$ | Wind farm capacity | [W] |
| $c_p$ | Power coefficient | [-] |
| $c_{wake}$ | Wake loss coefficient | [-] |
| $\Delta P(t)$ | Power imbalance at time (t) | [W] |
| $\Delta P_{final}(t)$ | Final power imbalance at time (t) | [W] |
| $E_{D,t}$ | Energy demand at time (t) | [Wh] |
| $E_{gen,total}$ | Total annual energy generated | [Wh] |
| $E_{in}$ | Energy input | [Wh] |
| $E_{out}$ | Energy output | [Wh] |
| $E_{PV,farm}$ | Total power production of a PV farm | [Wh] |
| $E_{PV,farm,new}$ | New solar energy after adjusting the number of PV panels | [Wh] |
| $E_{PV,farm,t}$ | Energy generated by PV panels at time (t) | [Wh] |
| $E_{sto(t)}$ | Energy stored at time (t) | [Wh] |
| $E_{total}$ | Total annual energy generated after considering grid losses | [Wh] |
| $E_{w,farm,new}$ | New wind energy after adjusting the number of wind turbines | [Wh] |
| $G_{dif}$ | Diffuse solar irradiance component | [$W/m^2$] |
| $G_{dir}$ | Direct solar irradiance component | [$W/m^2$] |
| $G_{gro}$ | Ground-reflected solar irradiance component | [$W/m^2$] |
| $G_{tot}$ | Total solar irradiance on the surface | [$W/m^2$] |
| $h$ | Hub height | [m] |
| $h_{ref}$ | Reference height | [m] |
| $\eta_{abs}$ | Grid absorption rate (energy lost as heat) | [%] |
| $\eta_{dis}$ | Distribution losses | [%] |
| $\eta_{drive}$ | Efficiency of drive train | [%] |
| $\eta_{grid}$ | Total efficiency of the grid | [%] |
| $\eta_{inv}$ | Inverter efficiency | [%] |
| $\eta_{PV}$ | Efficiency of PV panel | [%] |
| $\eta_{sto}$ | Efficiency of storage technology | [%] |
| $\eta_{sto,1}$ | Efficiency of the storage technology always 1 | [%] |
| $N_{PV}$ | Number of PV panels | [-] |
| $N_w$ | Number of wind turbines | [-] |
| $N_{w,new}$ | Number of new wind turbines required | [-] |
| $N_{w,original}$ | Original number of wind turbines | [-] |

| | | |
|---|---|---|
| $P_{D_{normilised}}$ | Normalized power demand | [W] |
| $P_{D_{normilised}}(t)$ | Normalized power demand at time (t) | [W] |
| $P_{discharge}(t)$ | Power discharged from storage at time (t) | [W] |
| $P_G(t)$ | Power generation at time (t) | [W] |
| $P_{PV,farm}$ | Total power production of a PV farm | [W] |
| $P_{PV,farm}(t)$ | Power output by a PV farm at time (t) | [W] |
| $P_{PV,rated}$ | Rated power per PV panel | [W] |
| $P_{w,farm}$ | Total wind power generated by a wind farm | [W] |
| $P_{w,farm,new}$ | Total installed wind power after adjustment | [W] |
| $P_{w,farm}(t)$ | Power output by a wind farm at time (t) | [W] |
| $P_{w,rated}$ | Rated power per wind turbine | [W] |
| $P_{cap}(t)$ | Cost per unit of PV capacity | [€/W] |
| $Q_n$ | Nominal Capacity | [Wh] |
| $Q_t$ | Available capacity | [Wh] |
| $\rho$ | Air density | [kg/m$^3$] |
| $r_{PV}$ | Ratio of solar power | [-] |
| $S_{cap}(t)$ | Storage capacity | [W] |
| SF | Scaling factor for normalizing power demand | [-] |
| $s_f$ | Shading factor | [-] |
| $SoC(t)$ | State of Charge at time (t) | [-] |
| $SoC(t-1)$ | State of Charge at time (t-1) | [-] |
| $\Sigma P_D$ | Cumulative power demand over the same period | [Wh] |
| $\theta$ | Optimal tilt angle of module | [°] |
| $\alpha$ | Albedo | [-] |
| $v(h_{ref})$ | Velocity at reference height | [m/s] |
| $v_{cut-in}$ | Cut-in wind speed | [m/s] |
| $v_{cut-out}$ | Cut-out wind speed | [m/s] |
| $v_{rated}$ | Rated wind speed | [m/s] |
| $W_{cap}$ | Cost per unit of wind capacity | [€/W] |

# Contents

# List of Figures

# List of Tables

# 1 Introduction

## 1.1. Energy Transition

In 2022, the worldwide carbon dioxide ($CO_2$) emissions from energy combustion and industrial processes increased by 321 Mt/y, resulting in a new record high of 36.8 Gt of $CO_2$ per year [1]. Figure 1.1 presents the trend of global $CO_2$ emissions from the year 1900 to 2022. The graph demonstrates that the trajectory of $CO_2$ emissions has generally been increasing over this time period. However, a notable deviation occurred during the COVID-19 pandemic, resulting in a temporary decrease in emissions. Nevertheless, following this period, the emissions quickly rebounded and resumed their upward trend, reaching maximum levels. Worldwide concerns about climate change, the Climate Agreement, and the energy crises created by geopolitical tensions have all contributed to accelerating the transition to a sustainable energy sector. Thus, replacing traditional fossil-fueled power plants with clean, renewable generation is key to the essential energy sector transition. The IEA report [2] states that the worldwide goal is that the total capacity of installations of renewable power will grow to almost double in the next five years. This will allow renewable power to overtake coal as the largest source of electricity generation and assist in keeping alive the possibility of limiting global warming to a maximum of 1.5 °C.

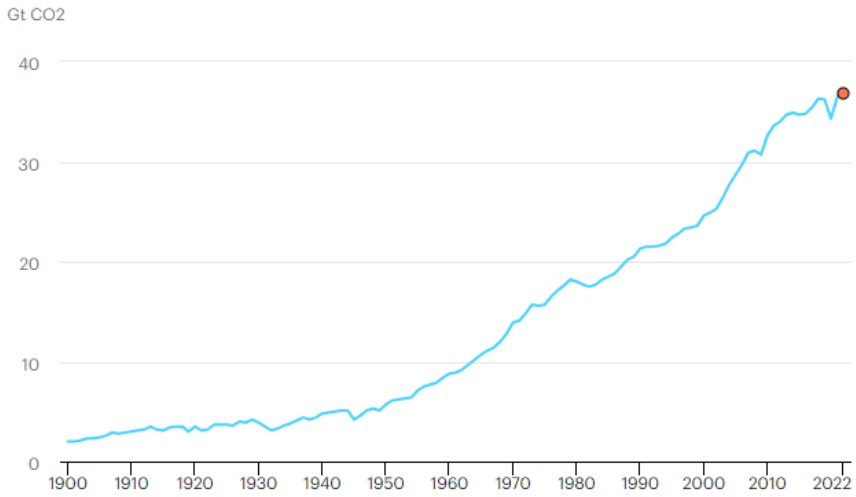


Figure 1.1: Global $CO_2$ emissions from energy combustion and industrial processes (1900-2022) [2]

### 1.1.1. Balancing Supply and Demand

The energy transition, despite its potential benefits, encounters significant challenges in terms of stabilizing and maintaining the smooth operation of electricity grids. Energy generation from conventional fossil-fuelled power plants can be regulated depending on the energy demand, and therefore electricity grids have sufficient flexibility to balance changes in demand. On the contrary, wind turbines and photovoltaics, which are the two dominant renewable energy sources, are inconsistent and non-dispatchable as the availability of

natural resources determines their energy generation potential. This variability can hinder the penetration of wind and solar energy into the electricity market due to the instability created to the power system and the associated balancing costs required to use current technologies such as fossil fuel generators.

### 1.1.2. Hybrid Solar and Wind System

Currently, the additional flexibility required to balance Renewable Energy Sources (RESs) is provided by the limited storage capacity, which is led by Pumped Hydro Energy Storage (PHES) and by traditional power plants [3]. Thus, due to the rising electricity demand, conventional power plants are operating more often than before in part-load, and therefore more startups of these facilities are required. Part-load operation reduces the efficiency of the traditional power plants operation (full-load), forcing the power plants to use relatively more fuel than before to produce the same amount of electricity and consequently increasing $CO_2$ emissions. This paradox could be avoided if the required flexibility is provided by different elements [3], to reduce the effect of this intermittency. Combinations of renewable energy technologies will be required to achieve a smoother power output and reduce (or even eliminate) the use of traditional fossil-fueled power plants. Wind based hybrid systems with photovoltaics are the most promising sources for power generation due to their advantageous complementary nature. Wind speeds are often low in periods when the solar resources are at a peak. On the other hand, the wind is often stronger in seasons when there are less solar resources. The dependence of hybrid renewable energy systems in highly unpredictable weather patterns introduces a significant level of complexity in their design. The inherent variability and intermittency of renewable sources, make it impossible to achieve a perfect resolution of the mismatch between energy generation and demand.

### 1.1.3. Storage

Storage is a key technology that will limit the challenges posed by the intermittency of the sources. Energy storage can eliminate the time mismatch between energy demand and generation by taking excess electricity from the grid when generation surpasses demand, storing it, and returning it when there is insufficient electricity production to meet the demand [4]. The discharge time scales are divided into four main categories [5] also depicted in Figure 1.2:

1. Very-short-duration storage (<5 min)
2. Short-duration storage (5 min–4 h)
3. Medium-duration storage (4–200 h)
4. Long-duration storage (>200 h)

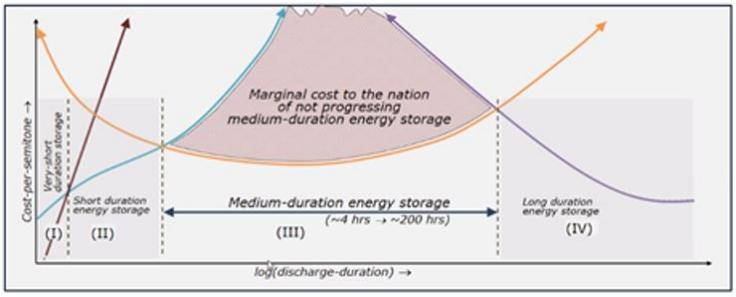


Figure 1.2: The four main durations of energy storage

Due to the various discharge time scales, no single storage technology is suitable for all durations. Therefore, a combination of storage technologies will be necessary to effectively manage the intermittence of renewable energy generation sources.

### 1.1.4. Overview of Current Hybrid Wind, Solar, and Storage Systems

In the past, there have been several projects focused on onshore hybrid renewable energy systems that combine wind and solar technologies. These projects have primarily been implemented in off-grid settings and have involved the integration of battery backup systems. Additionally, some projects have explored grid-connected configurations [6]. The largest hybrid renewable energy system in Europe is in the Netherlands.

Vattenfall commissioned an onshore hybrid energy park in the Dutch province of South Holland. The Haringvliet energy park consists of a 38MW solar park, a 22MW wind farm composed of 6 wind turbines, and 12 containers with 288 batteries for a total power of 12MW. The amount of green electricity the park will produce corresponds to approximately the annual consumption of 39,000 households [6, 7].

Another pertinent illustration of a hybrid system that closely corresponds to the generation technologies explored in this thesis is located in China. China accounted for over half of the world's total onshore and offshore wind power capacity. The cumulative worldwide capacity for onshore and offshore wind power surpassed 830 GW by the year 2021. During the same period, China installed more offshore wind generation capacity than every other country installed over the last five years [8], showing how devoted China is to reach their 2060 net-zero targets. China has recently completed the world's first commercial pilot offshore hybrid generating facility, including a floating wind turbine and a floating photovoltaic park, as shown in Figure 1.3. The installation is located off the coast of Haiyang, in Shandong Province in eastern China. China's State Power Investment Corporation (SPIC) commissioned the pilot hybrid offshore energy generator that includes one floating wind turbine and two solar arrays. The solar floaters are connected to the wind turbine and a sub-sea cable transmits power from the site to the onshore power grid [9, 10]. This example proves that offshore energy hybrid systems are possible and countries are exploring this potential.

Figure 1.3: Pilot project of an offshore hybrid system in China
[10]

## 1.2. Introduction to Medium-Term Storage

The variability of supply of the hybrid power plant over a medium-term storage period (4hrs -200hrs) is primarily caused by the diurnal and seasonal variations of the regional weather. Studies have concluded a strong correlation between weather patterns and wind speeds [11, 12]. The diurnal variation of offshore wind speeds shows distinct patterns between day and night. Although offshore wind speeds can exhibit slightly higher values at night, these changes are relatively small because the overall variability of offshore winds is lower compared to onshore winds. This consistent wind behavior offshore is due to the reduced influence of land-based temperature variations and surface friction, making offshore wind a more reliable energy source. Additionally, if an offshore wind farm is located near the coast, the timing of peak wind speeds may differ slightly, compared to a wind farm situated further offshore due to the varying influence of the landmass on wind patterns.

According to a study conducted by Coelingh, Van Wijk, and Holtslag [11] on diurnal variations of offshore wind speed, the results indicated minimal diurnal fluctuations at the offshore platforms. Another study by Coelingh, Van Wijk, and Holtslag [12] demonstrates that the offshore platforms also don't exhibit any seasonal dependence. A significant atmospheric factor that exerts a considerable influence on weather patterns is the presence of high- and low-pressure systems. These systems play a pivotal role in shaping daily weather variations. High- and low-pressure areas arise due to the upward and downward movement of air, leading to the formation of a pressure gradient force. Variation in pressure across different locations

generates both horizontal motion of wind and vertical motions within the atmosphere [13]. However, it is essential to note that at higher altitudes, the influence of the earth's surface on wind speed diminishes. Instead, the prevailing wind patterns at these altitudes are primarily driven by synoptic air pressure gradients and the Coriolis force [14]. For solar radiation, the diurnal patterns are during daytime and night-time. Solar radiation is also heavily dependent on seasonality change, with higher solar radiation in summer months compared to winter.

## 1.3. Problem Formulation

Currently, fossil-fueled power plants provide enough flexibility to balance changes in demand as their output energy can be controlled depending on the required energy. However, as discussed above, variable renewable sources are inflexible as the availability of the natural resources determines their output. Consequently, the grid loses flexibility as more renewables replace fossil-fueled generation. As the penetration of renewables continues to increase, the task of effectively matching energy supply and demand becomes progressively more challenging, particularly within the time range of 4 to 200 hours. Consequently, the utilization of storage technologies becomes imperative to address this specific time range, highlighting the significance of medium-term energy storage as an essential component for the energy transition.

The main problem identified during the outset of this thesis was that while examining the current storage configurations, it was found that medium-term storage has not yet been investigated in-depth. Medium-term storage is not yet widely used and most research has been based on short-term storage and recently on long-term storage [15]. Using medium-term storage will allow the hybrid renewable energy system to become more flexible and improve the balance between supply and demand. As stated in a seminar [15] on medium-term energy storage by Prof. Seamus Garvey, "Medium-term storage is the most important category of energy storage by the significant way but yet it doesn't appear in any policy document or recognised at all. However, more than 60% of all energy emerging from storage comes from medium-duration storage technologies" [5].

## 1.4. Objective

Building upon the problem analysis presented in the preceding section, the primary objective of this research is to develop the design of the building blocks to determine the most optimum medium-term storage technology to match the desired demand by electricity generated from a hybrid off-shore system.

The sub-objectives of this thesis are:

- Determine, analyse and compare the energy demand pattern and the intermittency of energy generation sources.
- Identify and optimise the potential medium-term storage technologies to ensure a secure and feasible storage configuration.
- Simulate and evaluate the impact of the design medium-term storage system on the hybrid generation system required to meet the demand.

## 1.5. Scope

The scope of this research focuses on the simulation of an offshore generation and onshore storage hybrid system in the Netherlands. The choice of the Netherlands is based on its ambitious renewable energy targets and significant investments in offshore wind power. This study will specifically examine mature, currently viable onshore storage technologies, given that offshore storage technologies are still in the research phase with limited literature available. The analysis will exclude the transmission of energy from offshore generation to the onshore grid, focusing exclusively on generation and storage technologies. Additionally, only the capital costs of each technology will be considered, as including operational costs would add significant complexity due to the variability in maintenance, operational lifetimes, and efficiency losses over time. The primary objective is to evaluate and propose a reliable and cost-effective hybrid energy system using current technology, contributing to the Netherlands' renewable energy goals. The study will consider technologies that have undergone extensive testing and development to ensure reliability and practicality in present-day applications.

## 1.6. Approach

A comprehensive outline of the steps followed in this thesis comprises of the following key components:

1. Energy Demand and Generation Analysis: The first step involved analyzing daily data on solar radiation, wind speed, and electricity demand to determine, analyze, and compare energy demand patterns with the intermittency of energy generation sources. This analysis was supported by a detailed discussion of the data sources used and culminated in the presentation of a normalized figure representing the power demand.
2. Integrated Multi-Criteria Analysis Model: The possible medium-term energy storage technologies where identified. Then the research utilizes an integrated MCA model based on the Analytic Hierarchy Process (AHP). This model facilitates the systematic evaluation and comparison of alternative technologies for medium-term storage. By assigning weights to criteria and scoring the technologies, the MCA model enables the narrowing down of suitable options for the subsequent optimization.
3. Computational Model Development: A computational model is developed to optimize the configuration of medium-term storage technologies. This model takes into account various parameters and constraints. Through a multi-objective optimisation, the Pareto optimal solutions are determined, enabling to demonstrate the optimal medium-term storage technologies.
4. Simulation and Impact Evaluation: A simulation model was developed to assess the impact of the designed medium-term storage system on the hybrid generation system's ability to meet demand. This step involved evaluating the performance of the selected storage technologies through different case studies, determining the most effective energy generation mix, and analyzing its effect on the capital cost. Additionally, a sensitivity analysis was performed to provide further insights into the robustness and overall effectiveness of the system.

## 1.7. Thesis Description

This section outlines the structure of the thesis. Chapter 2 introduces and evaluates various medium-term energy storage technologies through a multi-criteria analysis, ultimately selecting the top three technologies based on specifically chosen criteria. Chapter 3 then delves into a comprehensive examination of the simulation model developed, detailing the methodology and equations employed. Following this, Chapter 4 focus on the study location in the Netherlands, analyzing pertinent data such as local weather patterns and electricity demand trends. Chapter 5 presents the findings from the simulation model, encompassing an assessment of the selected storage technologies performance and a sensitivity analysis that provides additional insights. This chapter also compares outcomes from two different case studies and determines the most effective energy generation mix and its impact on the capital cost of the medium-term storage system. Finally, Chapter 6 concludes the thesis by summarizing the key discoveries, exploring the implications of the research, and offering recommendations for future studies.

# 2

# Selection of Medium-term Storage Technologies

In this chapter, the focus will be on identifying alternative technologies suitable for medium-term storage. An integrated Multi-Criteria Analysis model based on the Analytic Hierarchy Process was chosen to narrow down the selection of technologies for the optimization phase. A total of eight energy storage technologies were initially selected for evaluation. Each of these technologies were assessed using six different criteria. Based on the Multi-Criteria Analysis, three storage technologies emerged as the most promising options. These technologies underwent further analysis and evaluation in the subsequent stages of the thesis. The first section delves deeper into the need for medium-term storage. The following section introduces a range of potential energy storage technologies. The subsequent section provides an in-depth explanation of the MCA which was conducted and elucidated the outcomes derived from this analysis. The final chapter presents a comprehensive overview of all the storage technologies explored, providing the necessary background literature information required for the MCA.

## 2.1. Medium-term Storage Technologies

In this thesis, the technologies which will be analysed and examined need to comply with the time frame of medium duration storage i.e. a minimum of 4hrs and a maximum 200hrs. Thus, the analysis did not consider technologies with very high frequencies, very short discharge times or small capacities. Therefore the technologies that were not considered, included flywheels and supercapacitors. Not all main parameters and limitations are accounted for at this point of the report, as particular details are not yet specified (eg. spatial limitations) due to the generic nature of the analysis. The thesis is focused on the Netherlands as was stated in Section 1.5, and therefore certain geographical limitations become apparent. For instance, technologies, like pumped hydro storage, are not applicable in the Dutch storage portfolio due to the country's flat topography. The Netherlands has limited hydraulic head as a result of minimal elevation changes across its landscape. Therefore, alternative storage technologies that are more suitable for the Netherlands' geographic characteristics will be explored and evaluated in this study.

In paper [3], the authors propose that the ideal storage technology should satisfy several key criteria. These criteria include a minimum nominal power rating to enable operation at the electricity grid level (10 MW), an appropriate capacity over power ratio suitable for load shifting (t>1h), high roundtrip efficiency, short startup times, and cost-effectiveness. Additionally, the ideal storage technology should not be dependent on location-specific geographical features. To ensure a consistent approach, a constraint was imposed in the study, specifying that all storage facilities would be situated onshore, despite potential advantages that might be associated with offshore locations, as mentioned in Section 1.5. Nevertheless, most offshore technologies are in the research phase and are not ready to enter the market.

## 2.2. Multi-Criteria Analysis

As denoted in the previous section, the tool used to assess and compare the different storage technologies is MCA. The utilisation of a Multi-Criteria Analysis (MCA) aims to provide a structured methodology for the selection of the most suitable list of options for the chosen criteria. MCA was determined the most suitable technique given the multi-dimensional and complex nature of storage technologies to be assessed,

which typically involve a range of conflicting criteria featuring different forms of data and information. The MCA used in this study follows a technique known as the simple additive weighting method. This method, which is described in detail in the paper [16], is a popular and widely used decision-making approach that considers different criteria. The simple additive weighting method utilises a straightforward and intuitive weighted additive model, which in this case incorporates the AHP to determine the overall performance of the various options being evaluated. The AHP was chosen due to its transparency and ability to reveal the relative merits of alternative solutions in a MCA problem [17]. AHP is a simple mathematical method that provides a structured approach to decision-making by breaking down complex problems into a hierarchical structure of criteria and alternatives. AHP also allows obtaining weights of evaluation criteria by comparing these criteria through pairwise comparison matrices. The primary objective of the simple additive weighting method is to derive global scores, obtained as the weighted sum of individual performance scores, that clearly indicate the best option for addressing the problem under consideration. However, it is important to acknowledge that the simple additive weighting method lacks the theoretical accuracy of more formal decision-making methods. It may resemble basic weighted average calculations and may have limited connections to the broader MCA theory. Despite this limitation, the simplicity and transparency of this method makes it widely adopted and applicable in practical decision-making scenarios [17].

Finally, four steps are followed to conduct the MCA and are defined as follows [18]: The first step is identifying all possible energy storage technologies (ESTs). The second step involves the identification and selection of criteria enabling the comparison of these storage technologies. In the third step, weights are assigned to the criteria, completing the MCA. In the final step, the possible ESTs are scored against each criterion. Below, these four steps are further analyzed and then applied, to conduct the MCA.

Step 1: From literature review [19, 20, 21], as many as possible storage technologies meeting the requirements for medium-term energy storage were identified. Using the same structure as paper [22] Figure 2.1 was developed, illustrating the eight possible energy storage technologies (ESTs) and introduces the abbreviations for each storage technology.

These technologies are categorized based on their method of converting and storing electricity as extracted from paper [22]. Specifically, the identified ESTs are grouped into three categories [23]: mechanical, electrochemical, and chemical, as depicted in Figure 2.1.

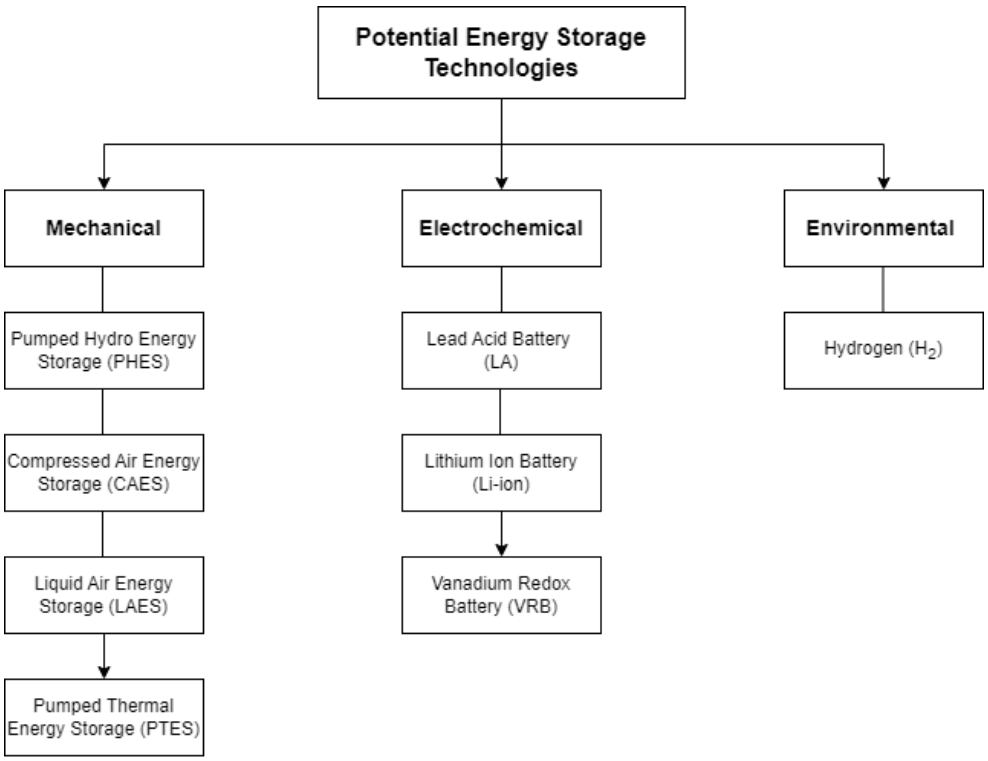


Figure 2.1: Potential Energy Storage Technologies

Step 2: In this step, the identification and selection of criteria enable the comparison of the potential ESTs. The Analytic Hierarchy Process (AHP) was used to evaluate the multiple options and make a choice based on a set of criteria. AHP relies on a hierarchical structure that allows the problem to be divided into smaller sub-problems, which can be examined independently, ensuring no criteria overlap, reducing the dependence and interaction between the criteria. This approach simplifies the overall problem enabling the identification of the criteria. Thus following the AHP process from literature [22, 24] first, the three main criteria were selected, consisting of Technical, Economical, and Environmental aspects. Subsequently, seven criteria were chosen, which are depicted in Figure 2.2. These selected criteria are crucial for facilitating an unbiased and thorough evaluation of the alternative storage technologies, ultimately guiding the selection of the most suitable energy technology. While socio-political factors are acknowledged as significant considerations for Multi-Criteria Analysis (MCA) it is determined that they fall outside the scope of the current study and will not be further investigated.

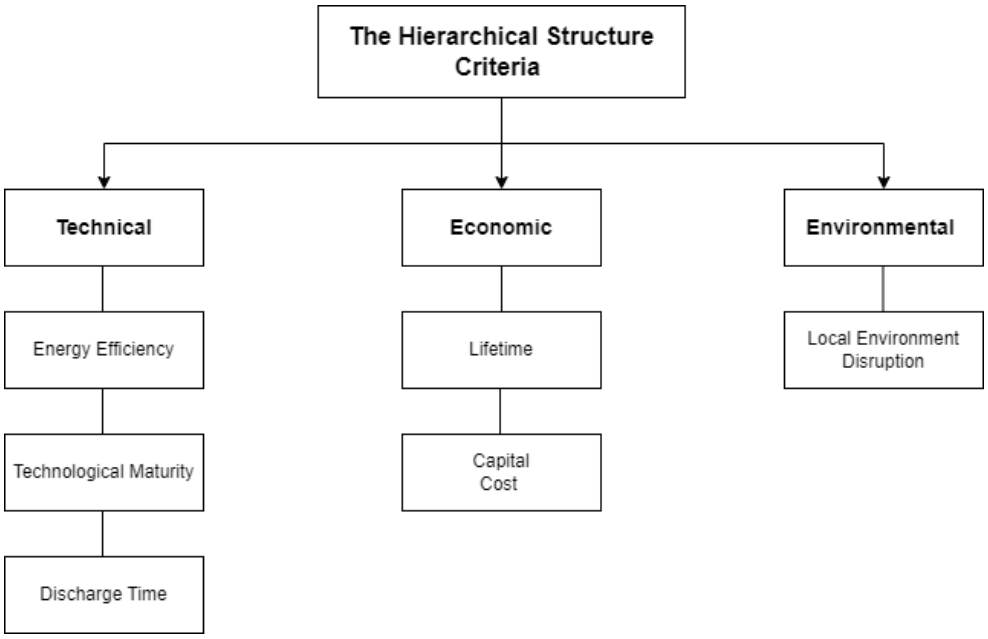


Figure 2.2: Selected main criteria and criteria used for the MCA

STEP 3: This step involves selecting the weights for the criteria for the Multi-Criteria Analysis. To assign the appropriate weights to the criteria, previous MCA studies on related topics of storage technologies were consulted as references [22, 24]. However, it is important to note that the ideal method for determining the weights would involve input from experts in the field. Unfortunately, due to practical constraints, this approach was not feasible for this thesis.

Instead, a thorough analysis was conducted to assess the importance of each criterion within the context of this thesis and its relevance to the subsequent model. Careful consideration was given to identifying and prioritizing the criteria that are crucial for the research objectives and the model's effectiveness. This analysis served as the basis for assigning appropriate weights to the criteria in order to reflect their relative importance accurately.

Using the hierarchical structure with the three categories illustrated in Figure 2.2, the selected criteria were systematically evaluated to ensure an unbiased allocation of weights. Initially, weights were assigned to higher-level categories: 60% to the technical category, 30% to the economic category, and 10% to the environmental category. The detailed breakdown of weights for the lower levels within these categories is provided in Table 2.3.

The importance of technological maturity is evident when examining Table 2.3, aligning with the emphasis placed on it in section 1.5 of the introduction. This importance arises from the fact that the hybrid system is planned for construction and implementation based on present data and technologies. Therefore, selecting mature technologies ensures a higher level of reliability and reduced risk in the

implementation phase. In the table, technological maturity is given a relative weight of 40% within the technical criterion, which translates to 24% of the overall decision-making weight, making it the highest and highlighting its significant role in the process. Discharge time is crucial in meeting the medium-term storage requirements (4-200 hours) specified in this thesis. The table assigns a 30% weight to discharge time within the technical criterion, contributing 18% to the overall decision. This underscores its critical role in the hybrid system's performance. Energy efficiency is another key criterion, particularly important in the context of renewable energy technologies. It is widely regarded as a crucial factor and is assigned a high weight in most MCA studies. In line with this, energy efficiency is given a 30% weight within the technical criterion, translating to an 18% impact on the overall decision, emphasizing its vital role in achieving an efficient hybrid system.

Capital expenditure (CAPEX) is highly relevant in the analysis. Within the economic criterion, which has an overall weight of 30%, CAPEX holds a relative weight of 65%, contributing 19.5% to the overall decision-making weight. Lifetime, while still considered, holds a lesser weight compared to CAPEX within the economic criterion. With a relative weight of 35%, it contributes 10.5% to the overall decision. This reflects the project's focus on short-term implementation, where CAPEX is prioritized over long-term considerations like lifetime.

Lastly, the local environmental disruption criterion, although assigned a relatively low overall weight of 10%, is crucial for reducing CO2 emissions and protecting both global and local environments. This importance is comparable to lifetime, reflecting its focused but limited impact in this analysis.

| Main Criterion | Relative Weight | Criterion | Relative Weight |
|---|---|---|---|
| Technical | 60% | Energy Efficiency | 30% |
| | | Technological Maturity | 40% |
| | | Discharge Time | 30% |
| Economic | 30% | Lifetime | 35% |
| | | Capital Expenditure (CAPEX) | 65% |
| Environmental | 10% | Local Environmental Disruption | 100% |

Figure 2.3: Selected weights for each main and criterion

STEP 4: In the final step the possible ESTs are assessed and scored for each criterion presented in Figure 2.3. The scoring of the criteria for each storage option evaluated is accomplished by assigning a value between 1 (low performance) and 9 (high performance) [18, 25]. From papers [19, 20, 21] Table 2.1 was developed, playing a crucial role in generating the results. Section 2.4 provides a comprehensive overview of the eight storage technologies selected in Step 1, offering the necessary background literature, including the advantages and disadvantages of each, to support the MCA and the construction of Table 2.1. This ensures a deeper understanding of the selected technologies and effectively contextualizes the results presented. Table 2.1 presents the selected ESTs alongside the selected criteria, and it provides the corresponding qualitative or quantitative data for each technology-criterion combination. The information in this table served as a foundation for developing Table 2.3 and facilitated the scoring process. Scoring

each criterion involved different methods due to the variation in data types. To determine the scores for the quantitative criteria, such as CAPEX (Capital Expenditure), the technology with the lowest cost was assigned the highest score (9), reflecting its desirability. Conversely, for efficiency, the technology with the highest efficiency among the alternative ESTs was identified and assigned a score of (9), indicating the highest performance. Then, for the remaining alternative ESTs, the relative score was assigned according to Table 2.2. This approach ensured that the scoring was proportionate and reflected the relative performance of each EST in relation to the highest value.

Table 2.1: Literature review on possible ESTs and the selected criteria

| ESTs / Criteria | Efficiency (%) | Discharge time (h) | Lifetime (years) | Technology Maturity | Environmental Impact | CAPEX (€/kW) |
|---|---|---|---|---|---|---|
| Pumped Hydro Energy Storage | 65-85 | 1-24+ | 30-60 | Mature | High/Medium | 500-2000 |
| Compressed Air Energy Storage | 50-60 | 1-24+ | 40 | Mature | High | 900-2300 |
| Liquid Air Energy Storage | 50-60 | 1-12+ | 20-40 | R&D – Pre-commercial | Low | 1000-3000 |
| Pumped Thermal Energy Storage | 30-50 | 1-6+ | 25 | R&D – Pre-commercial | Low | 350-450 |
| Lithium Ion | 85-95 | min-h | 8-15 | Commercial | Medium/Low | 150-1300 |
| Lead Acid | 70-80 | s-h | 3-10 | Mature | High | 100-500 |
| Vanadium Redox Flow | 65-85 | s-10h | 10-20 | R&D – Pre-commercial | Medium/Low | 500-2300 |
| Hydrogen | 30-50 | 1-24+ | 20-30 | Developing | Low | 2000-5000 |

For criteria with qualitative data (lifetime, technology maturity and environmental impact), specific score ranges were established for the ESTs, and the match or non-match of the data to these ranges determined the scores. Table 2.2 enables the translation of these ranges into appropriate criteria scores, facilitating the scoring process within the MCA. By aligning each technology's performance across various criteria with the predetermined weights (Step 3), it becomes possible to systematically assign scores reflecting their relative performance.

Table 2.2: Scoring system for the criteria evaluated

| Scores | Efficiency (%) | Discharge Time | Lifetime (years) | Technology Maturity | Environmental Impact | CAPEX (€/kW) |
|---|---|---|---|---|---|---|
| 1 | 10-20 | s-hr | 5 | R&D - Pre-commercial | High | 3200+ |
| 2 | 20-30 | s-hr | 10 | R&D - Pre-commercial | High | 2800-3200 |
| 3 | 30-40 | min-hr | 15 | Developing | Medium/High | 2400-2800 |
| 4 | 40-50 | min-hr | 20 | Developing | Medium/High | 2000-2400 |
| 5 | 50-60 | 1-6hr | 25 | Developing/Commercial | Medium | 1600-2000 |
| 6 | 60-70 | 1-24hr | 30 | Commercial | Medium/Low | 1200-1600 |
| 7 | 70-80 | 1-24hr | 35 | Commercial | Medium/Low | 800-1200 |
| 8 | 80-90 | 24hr+ | 40 | Mature | Low | 400-800 |
| 9 | 90-100 | 24hr+ | 45+ | Mature | Low | 0-400 |

The total scores of the MCA analysis have been derived and are presented in Table 2.4. To determine the total score for a specific alternative EST, the selected weights from Figure 2.3 are multiplied by the corresponding scores from Table 2.3. This multiplication takes place for each criterion. The resulting values are then summed up, considering all criteria, to obtain the final score for the alternative EST. By multiplying the weights by the scores and summing the results, accounts for the relative importance of each criterion, as indicated by the weights, and combines it with the performance of each EST across all criteria. Consequently, the resulting total score, presented in Table 2.4, provides a comprehensive assessment of the alternative EST's and the overall suitability within the hybrid energy system.

Table 2.3: Scores per suitable ESTs for the selected criteria

| Criteria | Efficiency | Discharge time | Lifetime | Technology Maturity | Environmental Impact | CAPEX |
|---|---|---|---|---|---|---|
| Pumped Hydro Energy Storage | 7 | 9 | 9 | 9 | 3 | 6 |
| Compressed Air Energy Storage | 5 | 9 | 9 | 8 | 2 | 5 |
| Liquid Air Energy Storage | 5 | 7 | 6 | 3 | 8 | 4 |
| Pumped Thermal Energy Storage | 7 | 5 | 5 | 2 | 8 | 1 |
| Lithium Ion | 8.5 | 5 | 2 | 6.5 | 6 | 8 |
| Lead Acid | 7 | 3 | 1 | 8 | 8 | 8 |
| Vanadium Redox Flow | 7 | 4 | 3 | 2 | 6 | 6 |
| Hydrogen | 3.5 | 4 | 5 | 4 | 8 | 1 |

Table 2.4: MCA total scores

| ESTs / Criteria | Efficiency | Discharge time | Lifetime | Technology Maturity | Environmental Impact | CAPEX | Total Scores |
|---|---|---|---|---|---|---|---|
| Weights (%) | 0.18 | 0.18 | 0.105 | 0.24 | 0.1 | 0.195 | 1 |
| Pumped Hydro Energy Storage | 7 | 9 | 9 | 9 | 3 | 6 | 7.46 |
| Compressed Air Energy Storage | 5 | 9 | 8 | 8 | 2 | 5 | 6.45 |
| Liquide Air Energy Storage | 5 | 7 | 6 | 3 | 8 | 4 | 5.09 |
| Pumped Thermal Energy Storage | 7 | 5 | 5 | 2 | 8 | 1 | 4.16 |
| Lithium Ion | 8.5 | 5 | 2 | 6.5 | 6 | 8 | 6.36 |
| Lead Acid | 7 | 3 | 1 | 8 | 8 | 8 | 6.19 |
| Vanadium Redox Flow | 7 | 4 | 3 | 2 | 6 | 6 | 4.55 |
| Hydrogen | 3.5 | 4 | 5 | 4 | 8 | 1 | 3.83 |

## 2.3. Discussion of MCA results

Based on the results presented in Table 2.4, it is evident that Pumped Hydro Energy Storage (PHES) emerges as the most suitable alternative EST according to the MCA. However, as discussed previously in Chapter 2, Pumped Hydro Energy Storage is not feasible for the region under consideration. Consequently, the focus shifts to the three alternative ESTs that follow PHES from the results of the MCA. These options are Compressed Air Energy Storage (CAES), then Lead Acid batteries (LA), and lastly Lithium-ion batteries (Li-ion). In the subsequent subsection, a comprehensive exploration of these three selected alternative ESTs will be provided. This detailed analysis will encompass their technical aspects, method of use and other relevant considerations. By delving deeper into the specifics of each alternative EST, a better understanding of their potential within the context of the hybrid energy system can be achieved.

## 2.4. Analysis of possible storage technologies

This subsection provides a concise overview of the eight selected storage technologies and aims to offer a better understanding of how the MCA results were concluded.

### 2.4.1. Mechanical Energy Storage (MES)

Mechanical Energy Storage, built on the direct storage of potential or kinetic energy, is among the oldest energy storage methods, alongside thermal storage. This approach allows for the direct storage of exergy [26]. The four MES technologies that were investigated further are Pumped Hydro Energy Storage (PHES), Compressed Air Energy Storage (CAES), Liquid Air Energy Storage (LAES) and Pumped Thermal Energy Storage (PTES).

1. Pumped Hydro Energy Storage (PHES)

   PHES is the most mature and widely deployed grid-scale storage technology, accounting for about 96% of the global storage power capacity and 99% of the global storage energy volume [27]. PHES requires two water reservoirs at different elevations to generate power as water flows from the top reservoir to the bottom, passing through a turbine. For charging, PHES operates by storing electrical energy by pumping water into the upper reservoir to produce a potential difference, in periods of low energy demand.

   Advantages [19]:

- High round-trip efficiency 65-85%.
- Very long life expectancy, approximately 30-60 years.
- Potentially highly cost-effective in suitable locations, resulting in a low cost per kilowatt-hour (kWh).

Disadvantages [19]:

- Constrained by specific geographical features, significantly limiting the number of suitable sites.
- High capital cost primarily due to the extensive civil engineering, site preparation, mechanical and electrical equipment required, and the long development and construction periods.

2. Compressed Air Energy Storage (CAES)

   CAES is a commercially matured technology. Traditional CAES operates by storing electrical energy by compressing air and storing it under pressure in an underground cavern/reservoir or above ground in pipes or vessels. The compressor is powered by electricity to compress the air, which is then stored under pressure. For the discharge process, compressed air and natural gas are used to pre-heat the stored compressed air before it is expanded in a turbine to produce electric energy. Innovative CAES solutions are proposed and are under R&D to eliminate some of the environmental issues and increase the efficiency of the system [28]. However, this thesis does not identify these alternatives as they are out of scope.

   Advantages [29]:

   - Very long life expectancy of around 40 years.

   Disadvantages [30]

   - The conventional CAES setup involves the direct use of fossil fuels, which leads to the emission of pollutants into the environment.
   - Low efficiency 50-60%.
   - Geographical constraints, relying on the presence of salt formations, depleted reservoirs, porous aquifers, and unused mines.

3. Liquid Air Energy Storage (LAES)

   LAES is an emerging technology that stores thermal energy by air liquefaction. Electricity drives a liquefaction cycle when charging, and the liquefied air is stored in a thermally insulated tank at cryogenic temperatures [21]. In the discharge cycle, the pressure of liquid air is increased and is then converted to high-pressure air by passing through a heat exchanger. The high-pressure air is used to generate electricity in an expansion turbine. Thermal storage is used to retain cold from the evaporation that will be recovered in a counterflow heat exchanger to reduce the energy required by the liquefaction cycle [31, 32]. Currently it Pre-commercial level but Highview Power has successfully constructed and demonstrated two LAES plants, one with a capacity of 350 kW and another with 5 MW. Additionally, they are constructing a commercial plant with a capacity of 50 MW and an energy storage capacity of 250 MWh [31].

   Advantages [33]:

   - LAES boasts a high energy density, typically ranging from 1 to 2 orders of magnitude greater than some alternative storage methods. This is primarily due to the fact that liquid air takes up only about 1/700th of the volume compared to gaseous air, allowing for the storage of substantial quantities of air in relatively compact containment structures.
   - There are no site constraints limiting its deployment.

   Disadvantages:

   - Relatively low round-trip efficiency, estimated at around 50% to 60% due to the energy-intensive air liquefaction process [32].
   - High capital cost 1000-3000 €/kW [3]

   .

4. Pumped Thermal Energy Storage (PTES)

   PTES is a technology still in the development stage with pilot projects. Electricity is converted into heat using a large-scale heat pump, and this heat is stored in a hot material such as water or gravel inside an insulated tank. The heat is then converted back into electricity using a heat engine. PTES is combined with common thermodynamic cycles, but interest is limited due to the acknowledged inefficiency of thermal engines in generating electricity, typically around 20-50%. However, integrating a heat pump with a thermal engine to establish a complete charge and discharge cycle can make the system more attractive [34, 35].

   Advantages [34]:

   - Quite high life expectancy of 20–30 years.
   - Location-independent.

   Disadvantages [34]:

   - Low efficiencies 20-50%.

### 2.4.2. Electrochemical Energy Storage (EES)

Electrochemical energy storage encompasses various types of batteries. These batteries operate by converting the chemical energy stored within their active materials into electrical energy through a reversible electrochemical oxidation-reduction reaction [36]. The three EES technologies investigated further are Lead Acid batteries (LA), Lithium-Ion batteries (Li-ion) and Vanadium Redox Flow batteries (VRFB).

1. Lead Acid (LA)

   LA is the most mature rechargeable battery for commercial applications. It consists of electrodes of lead metal and lead oxide in a sulfuric acid solution. During discharge, lead and lead oxide turn into lead sulfate, and the electrolyte's sulfuric acid concentration diminishes. During charging, lead metal is deposited on the negative electrode and lead oxide on the positive electrode, increasing the sulfuric acid concentration [37].

   Advantages [4, 37]:

   - High energy efficiency of around 70%-80%.
   - Low capital costs 100-500 €/kW.

   Disadvantages [4, 38]:

   - Relatively small cycle life (400-1000 cycles), translating to a lifespan of approximately 3 to 10 years, depending on usage and maintenance.
   - Contains lead, which is known to have a negative environmental impact due to its toxicity.

2. Lithium Ion (Li-ion)

   Li-ion batteries have become one of the primary energy storage solutions in modern society. Their applications and market share have expanded rapidly and continue to grow steadily [39]. Li-ion operates by the intercalation principle, a reversible injecting of a guest atom into a solid host structure without causing a significant disruption of the lattice structure. In Li-ion batteries, lithium ions are transported between the two electrodes, being de-intercalated from one to be re-intercalated to the other [40].

   Advantages:

   - High capital cost ($900-1300/kWh).
   - High efficiency 85-95%.

   Disadvantages:

   - High capital cost ($900-1300/kWh).
   - It is fragile and requires a protection circuit to maintain safe operation.
   - Low average lifetime of a Li-ion battery is typically estimated to be between 8 and 15 years.

3. Vanadium Redox Flow Battery (VRFB)

   Vanadium Redox Flow Battery (VRFB) is the most advanced type of flow battery, utilizing vanadium ions as charge carriers. The operation of VRFB is based on the redox reactions of different ionic forms of vanadium in two separate electrolyte solutions, typically stored in external tanks. During the charging process, electrical energy is used to pump these electrolyte solutions through the cell stack, where vanadium ions undergo oxidation and reduction reactions. This process stores energy in the form of chemical potential. During discharge, the flow of the electrolyte solutions is reversed, and the vanadium ions release the stored energy by reversing the redox reactions, which generates electricity[41, 42].

   Advantages:

   - Extended operating life 5000-20,000 cycles, which is approximately 10-20 years [43].
   - High energy efficiency around 65%-85%.
   - Ability to independently scale power and energy capacities.

   Disadvantages:

   - High and volatile prices of vanadium minerals, posing a risk for investments. Significant upfront capital investment due to the cost of vanadium and system components 500-2300 €/kW.

### 2.4.3. Chemical Energy Storage (CES)

CES utilizes chemical materials from which energy can be extracted immediately or latently through physical sorption, chemical sorption, intercalation, electrochemical, or chemical transformation [44]. Only one CES technology, Hydrogen (H2), was investigated further.

1. Hydrogen ($H_2$)

   Hydrogen energy storage converts electrical power into hydrogen. This stored energy can later be released by using hydrogen as fuel in either a combustion engine or a fuel cell. Hydrogen is produced from electricity through electrolysis of water. The most mature and commercially utilized technology for this is the Alkaline Electrolyzer, with an efficiency ranging from 43% to 66%. Hydrogen can be stored in underground caverns or steel containers for smaller applications and converted back into electricity in fuel cells, which can achieve efficiencies up to 70% [44].

   Advantages [32]:

   - Hydrogen is characterized by an exceptionally low self-discharge rate.
   - Hydrogen energy storage systems can be readily scaled up to accommodate very large storage capacities.

   Disadvantages [32]:

   - Whole process of power to power has a very low efficiency of around 30-50%.
   - Hydrogen energy storage has a high capital cost 2000-5000 €/kW.
   - Safety issues arise as hydrogen is an extremely flammable and volatile substance.

# 3

# Model Description / Parametric Design

This chapter focuses on presenting and discussing the theory, formulas, and methodologies employed in the development of the simulation model. The model is designed to be generic, allowing for its application to various scenarios. However, certain assumptions are made, and the relevant literature supporting these assumptions is provided. The chapter begins with an overview of the work process, followed by subsections detailing each step in the development and execution of the model. Next, a comprehensive discussion of the different optimization techniques is presented, explaining their roles and implementations in detail. Finally, the chapter concludes with an outline of the optimization parameters that are input into the model, along with an explanation for their selection.

## 3.1. Model Overview

This subsection outlines the steps involved in designing the model to enable the analysis of a hybrid renewable energy system. Figure 3.1 presents a flow chart detailing the work process used in this thesis. The workflow begins with gathering power demand data and calculating wind and solar power generated from collected weather data. The next step is to determine the number of wind turbines and solar panels required for the selected energy mix. The flow chart also incorporates a normalization process to align power demand with the total annual energy output from renewable sources, ensuring that the data is scaled for accurate comparison.

The model starts from the far left where all the necessary inputs for the model are calculated using the equations discussed in the preceding Subsections 3.2 and 3.3. The power demand data are sourced from a database maintained by the electricity distributors.

Following normalization, the power imbalance is determined for each time step. This imbalance, derived from the difference between generated renewable energy and normalized demand, informs the control strategy for managing energy storage. Since this thesis focuses on medium-term energy storage, the imbalance is filtered to consider variations within the 4 to 200 hour range. This filtering process eliminates short-term and long-term variations from the dataset, refining the analysis to the relevant time frame.

Subsequently, the control strategy, depicted in Figure 3.7, manages the charge and discharge cycles of the energy storage system based on state of charge (SoC) constraints. This control strategy ensures efficient operation by charging the storage during periods of excess generation and discharging it when generation is insufficient to meet demand. This approach optimizes the use of renewable energy, maintaining a stable and reliable energy supply.

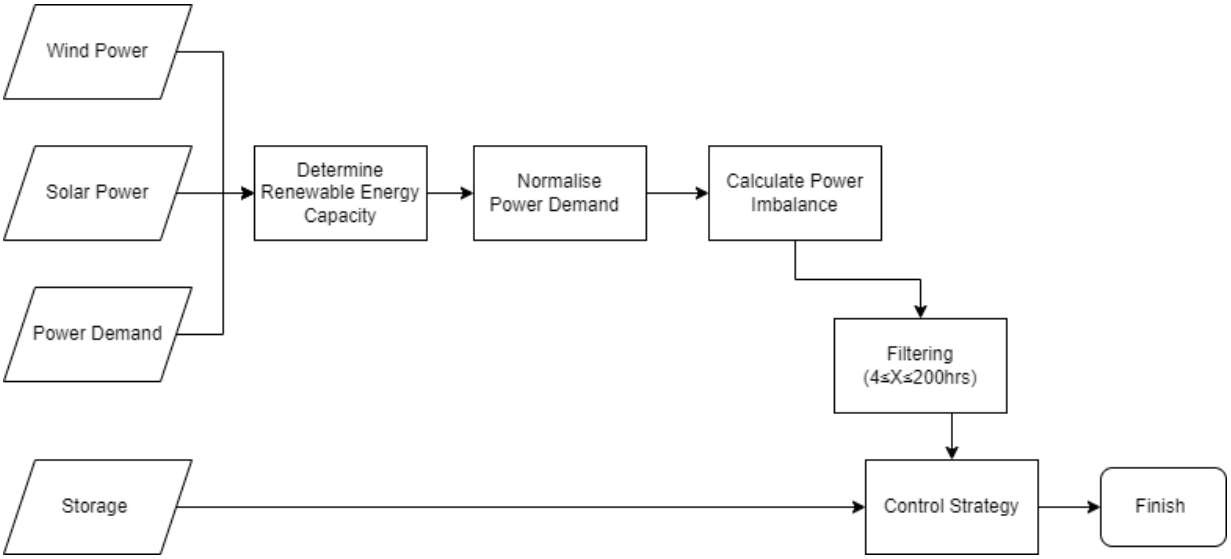


Figure 3.1: Flow chart depicting the work process

The control strategy is part of the control system that enables the provision of energy to the end users. The conceptual schematic shown in Figure 3.2 depicts the overall system architecture and the key components involved in transmitting energy from the hybrid system to the end users. It includes the electricity generation technologies, such as offshore wind turbines and offshore solar farm, which generate renewable energy. The system also includes an onshore storage technology. To ensure efficient transmission, the conceptual schematic incorporates electronic equipment such as converters, transformers, and control system.

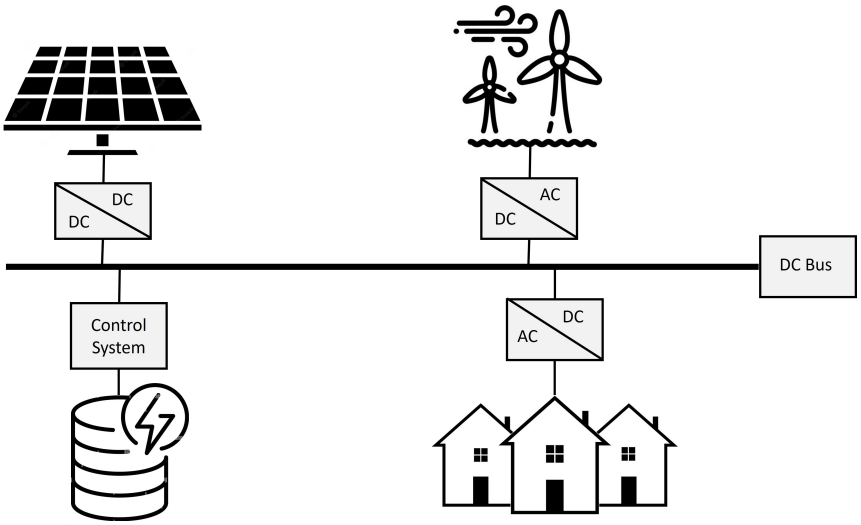


Figure 3.2: Schematic of the Energy configuration

The focus is on integrating the electricity generation technologies, the storage system, and the main on-land grid transmission line to ensure the delivery of energy to the selected demand. This involves considering various losses that occur during the transmission process and designing a conceptual schematic that illustrates the arrangement and the necessary equipment for the hybrid system.

The electronic equipment play a crucial role in managing the flow of electricity, converting the energy to the appropriate voltage levels, and maintaining stability and reliability throughout the transmission process [45]. The main on-land grid transmission line acts as the connection between the hybrid system

and the broader electricity grid. This allows the energy generated and stored in the hybrid system to be integrated into the existing power infrastructure, enabling it to supply energy to the selected demand.

## 3.2. Wind Power

To determine the wind power output, one of the critical factors is estimating the wind speed at the hub height of the wind turbines. The wind speed at different heights above the ground can vary significantly, a phenomenon known as wind shear. The wind shear needs to be accounted for in order to accurately predict the power production potential of a wind farm. There are two commonly used equations to extrapolate the wind shear: the power-law model and the logarithmic-law model [46]. The power-law model assumes a power relationship between the wind speed and the height above the ground, while the logarithmic-law model assumes a logarithmic relationship. In a study conducted by Lopez-Villalobos et al. (2022) [47], the accuracy of these models were compared. It was found that the logarithmic-law model tends to overestimate the wind speed, resulting in a higher percentage error compared to the power-law model. Specifically, the log-law model had an overestimation of 9% in the estimation of mean power at a height of 80 m and above for wind speeds measured at the standard height of 10m. Based on these findings, it is recommended to use the power-law model with a wind shear exponent ($\alpha$) of 1/7 [14] and [47]. The power- law model is depicted below by Equation 3.1:

$$v = v(h_{ref})\ (\frac{h}{h_{ref}})^{\alpha} \tag{3.1}$$

To determine the power generated by a wind turbine, the best approach would be to use the power curve of the specific wind turbine. However, as this is a generic approach, a general Equation 3.2 will be used to determine the power [14].

$$P_w = \begin{cases} 0 & \text{if } v < v_{\text{cut-in}} \\ \frac{1}{2} c_p \eta_{\text{drive}} \rho A v^3 & \text{if } v_{\text{cut-in}} \leq v \leq v_{\text{rated}} \\ P_{\text{rated}} & \text{if } v_{\text{rated}} \leq v \leq v_{\text{cut-out}} \\ 0 & \text{if } v > v_{\text{cut-out}} \end{cases} \tag{3.2}$$

Some constraints that need to be considered to ensure that the wind turbine calculations are accurate are the cut-in, nominal and cut–out wind speeds. The wind turbines cannot generate electricity for very low wind speeds of around 3.5 m/s, or extremely high wind speeds of around 25 m/s as specified on the power curve presented in Figure 3.3. As the wind exceeds the cut-in speed, the power output increases rapidly. However, around a certain speeds, known as rated wind speed, i.e. approximately 12–14 m/s, the power output reaches a maximum point called the rated power output. This is the maximum operation level of the electrical generator [14].

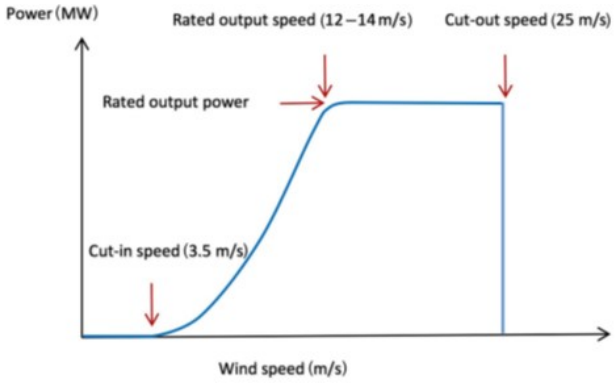


Figure 3.3: Theoretical Wind Power Curve [14]

The power coefficient has a theoretical maximum of 59.3% called Betz limit. However, in practice, the power coefficient ($c_p$) is typically around 40–50% [48], in the model, the constant value used was 45%. The

total efficiency of the drive train as determined through the literature review, has a range of 0.9 to 0.98 depending on the gearbox and generator use. The value that was used in the model was 0.95%. There is not yet a set configuration of a drive train for offshore wind turbines. As the wind energy industry is still in its early stages of development concerning drive train type and configuration, further research efforts are required, especially for floating and larger turbines, given the limited experience in these areas [49].

Finally, the wake effect is an important parameter to consider when investigating large wind farms. In the literature review, wake models were identified [50], allowing to determine the wake, but this is out of the scope of this thesis. Thus, it was concluded that the average power losses due to wind turbine wakes are of the order of 10% to 20% of total power output in large offshore wind farms. These values were determined in a study that was conducted for the Danish offshore wind farm Horns Rev, consisting of 80 wind turbines in an 8 × 10 grid configuration, with seven diameter spacing between each turbine [51]. In the model, a constant value of 15% was chosen as it falls within the appropriate range and was maintained consistently throughout all simulations. Consequently, Equation 3.2 was modified to include the wake loss coefficient ($c_{wake}$), which quantifies the reduction in power output due to the wake effect. In this thesis, the wake loss coefficient is defined as 85%. As discussed, the wake effect was determined for a wind field consisting of 8 wind turbines in a row. Therefore, the boundary condition is set such that if the number of wind turbines ($N_w$) is less than or equal to 8, the wake loss coefficient is not considered. Conversely, if the wind farm consists of more than 8 turbines, the wake effect must be taken into account. This simplification acknowledges that the real-world scenario is more complex and would require extensive analysis and experimental validation, which are beyond the scope of this thesis. Thus, the total wind power generated by a wind farm ($P_{w,farm}$) is represented by Equation 3.3.

$$P_{w,\text{farm}} = \begin{cases} 0 & \text{if } v < v_{\text{cut-in}} \\ \frac{1}{2} c_p \eta_{\text{drive}} \rho A v^3 \times N_{\text{w}} & \text{if } v_{\text{cut-in}} \leq v \leq v_{\text{rated}} \text{ and } N_{\text{w}} \leq 8 \\ c_{\text{wake}} \times \frac{1}{2} c_p \eta_{\text{drive}} \rho A v^3 \times N_{\text{w}} & \text{if } v_{\text{cut-in}} \leq v \leq v_{\text{rated}} \text{ and } N_{\text{w}} > 8 \\ P_{\text{rated}} \times N_{\text{w}} & \text{if } v_{\text{rated}} \leq v \leq v_{\text{cut-out}} \text{ and } N_{\text{w}} \leq 8 \\ c_{\text{wake}} \times P_{\text{rated}} \times N_{\text{w}} & \text{if } v_{\text{rated}} \leq v \leq v_{\text{cut-out}} \text{ and } N_{\text{w}} > 8 \\ 0 & \text{if } v > v_{\text{cut-out}} \end{cases} \tag{3.3}$$

## 3.3. Solar Power

Several steps and calculations are required to determine the total power output of the photovoltaic panel. This complicates the calculation more than for wind turbines. The first step is to determine the optimum tilt angle ($\theta$) of the PV panel by utilizing Equation 3.4. For the purpose of this thesis, it is assumed that the solar panels will have a fixed tilt angle. The Equation 3.4 is used to calculate the tilt angle has been derived empirically [52] as obtaining an accurate tilt angle requires conducting experiments specific to the location under consideration. The only input required is the latitude ($\phi$) of the location under consideration.

$$\theta = 0.764\phi + 2.14^{\circ} \tag{3.4}$$

The Angle of Incidence (AOI) of the solar panels is then calculated based on Equation 3.5. The sun azimuth ($A_s$) and the sun elevation ($a_s$) were determined by using a solar location calculator that was programmed in Python. Finally, the elevation of the module ($a_m$) was determined using Equation 3.6 and the module azimuth ($A_s$) [53]:

$$AOI = \cos^{-1}\left[\cos\left(a_m\right) \cdot \cos\left(a_s\right) \cdot \cos\left(A_m - A_s\right) + \sin\left(a_m\right) \cdot \sin\left(a_s\right)\right] \tag{3.5}$$

$$a_m = 90 - \theta \tag{3.6}$$

Equation 3.11 will be used to calculate the total solar irradiance incident on the solar panel. As the total irradiance is the sum of the direct irradiance ($G_{dir}$), diffused irradiance ($G_{dif}$) and the reflected irradiance ($G_{gro}$) as depicted by Equation 3.7 and Figure 3.4. The Direct Normal Irradiance (DNI) and Diffused Horizontal Irradiance (DHI) data will need to be collected for the specific region. The Sky View

Factor (SVF) will be determined using Equation 3.12. An important consideration that should be made while planning the offshore solar park is to eliminate shading losses.

Equation 3.7 will be utilized to calculate the total solar irradiance incident on the solar panel. This equation takes into account the direct irradiance (G$dir$) Equation 3.8 , diffused irradiance (G$dif$) Equation 3.9, and reflected irradiance ($G_{gro}$) Equation 3.10, as shown Figure 3.4. Finally by combining Equations 3.7-3.10 Equation 3.11 is formed. To calculate the total solar irradiance, data on Direct Normal Irradiance (DNI) and Diffuse Horizontal Irradiance (DHI) specific to the region of interest will be required. These data will be obtained for a specific region. Additionally, the Sky View Factor (SVF) will be determined using Equation 3.12, which quantifies the degree of sky obstruction. It is imperative to take shading losses into account during the planning phase of an offshore solar park. The proper positioning and design of solar panels play a vital role in minimizing shading from surrounding objects or structures, ultimately maximizing the capture of solar energy and optimizing the overall performance of the system. The advantage of offshore environments lies in their absence of limitations and minimal obstacles, which facilitates the effective reduction of shading losses through meticulous planning and design.

$$G_{tot} = G_{dir} + G_{dif} + G_{gro} \tag{3.7}$$

$$G_{dir} = s_f \cdot DNI \cdot \cos(AOI) \tag{3.8}$$

$$G_{dif} = SVF \cdot DHI \tag{3.9}$$

$$G_{gro} = DNI \cdot \cos(a_s) + DHI \cdot \alpha \cdot (1 - SVF) \tag{3.10}$$

$$G_{tot} = s_f \cdot DNI \cdot \cos(AOI) + SVF \cdot DHI + DNI \cdot \cos(a_s) + DHI \cdot \alpha \cdot (1 - SVF) \tag{3.11}$$

$$SVF = \frac{1 + \cos\vartheta}{2} \tag{3.12}$$

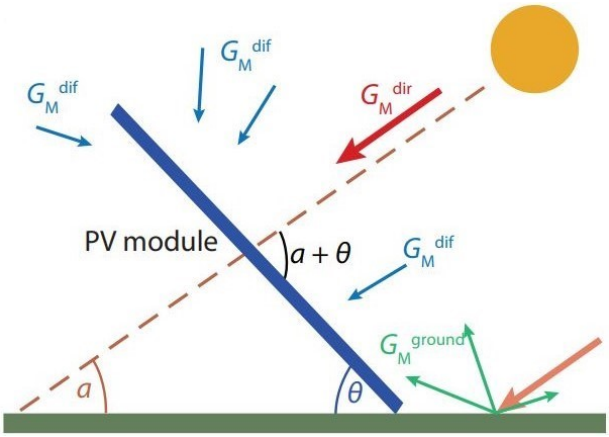


Figure 3.4: The three contributions to the total irradiance of the PV module [53]

The power output of a single PV panel can be determined using Equation 3.13. This equation requires knowledge of the solar panel's efficiency ($\eta_{PV}$) and its area ($A_{PV}$). In this thesis, a general approach is adopted based on research findings that indicate crystalline silicon panels, either single or polycrystalline, dominate the global market production, accounting for approximately 80% to 90% of installations. Among these two types, monocrystalline panels are selected for this thesis due to their higher energy efficiency, which typically ranges from 15% to 20% [54]. While cost considerations are also taken into account during the selection process, the emphasis is placed on energy efficiency, especially for an offshore project. The costs of the panels themselves are relatively small compared to other installation costs.

The efficiency of solar panels varies throughout the year due to the impact of fluctuating module temperatures ($T_M$). Ground-based solar PV installations often face reduced energy efficiency caused by elevated module temperatures. However, installing solar PV panels above water bodies can partially mitigate this issue. Such installations offer benefits such as preventing water evaporation and reducing the temperature beneath the solar panels, ultimately leading to increased energy production [55, 56]. So efficiency is assumed to be constant for the offshore PV panel.

$$P_{PV} = \eta_{PV} \cdot G_{tot} \tag{3.13}$$

Finally, to determine the overall power production of a photovoltaic farm, it is necessary to consider the number of PV panels that will constitute the farm. This can be calculated using Equation 3.14.

$$P_{PV,farm} = N_{PV} \cdot P_{PV} \tag{3.14}$$

## 3.4. Power Demand

Power demand is a critical factor that affects carbon emissions and system costs, and it is shaped by human activities in various settings such as industries, homes and workplaces. Behavioral approaches are crucial in explaining how individuals respond to internal and external factors that influence their energy consumption patterns [57]. As discussed in Chapter 1, the objective of this paper is not to precisely match a specific power demand and thus the power demand is normalized. The normalized demand represents a sensible example of a profile that exhibits variability characteristics, which could be considered representative of future needs for supply profiles of hybrid power plants. This approach ensures that the demand profile used in the analysis is realistic and adequately reflects the dynamic nature of electricity consumption patterns in the Netherlands. The power demand data are sourced from a database maintained by the electricity distributors.

## 3.5. Storage

From Chapter 1 and Chapter 2, it becomes evident how crucial storage systems are for the energy transition. The Multi-Criteria Analysis (MCA) conducted in Chapter 2, led to the selection of two electrochemical and one mechanical Energy Storage Technologies (ESTs) to be investigated further. In the first subsection, the State of Charge (SoC) the efficiency, and finally, a table depicting the above parameters for the three chosen ESTs is presented.

### 3.5.1. State of Charge (SoC)

A vital parameter extensively used in storage technologies is the State of Charge (SoC). SoC is a relative quantity representing the ratio of the available capacity ($Q_t$) to the maximum possible charge stored in a battery, typically the nominal capacity ($Q_n$). This relationship can be mathematically expressed as shown in Equation 3.15 [58].

$$SoC = \frac{Q_t}{Q_n} \tag{3.15}$$

While SoC is predominantly associated with batteries, it is not restricted solely to them. In fact, SoC can be applied to a wide range of energy storage systems, provided they have the ability to store energy and their capacity can be quantified. To clarify the concept of SoC further, a storage system with a SoC of 1 indicates that it is fully charged and at its maximum energy capacity. Conversely, a fully discharged battery or storage system would have an SoC of 0.

### 3.5.2. EST Efficiency

Efficiency is a critical parameter in evaluating energy storage systems, as it directly impacts the overall performance and economic viability of the storage technology. Efficiency ($\eta_{sto}$) in energy storage refers to the ratio of the energy output ($E_{out}$) to the energy input ($E_{in}$), expressed as a percentage as seen in Equation 3.16. This ratio indicates how much of the stored energy can be effectively retrieved and used.

$$\eta_{sto} = \frac{E_{out}}{E_{in}} \times 100\% \tag{3.16}$$

As discussed in Chapter 2 high efficiency is desirable in energy storage systems as it ensures that a greater proportion of the stored energy is available for use, reducing losses and improving the system's cost-effectiveness. Conversely, lower efficiency implies higher energy losses during storage and retrieval, making the system less effective and potentially more expensive in the long run.

Focusing on the three energy storage technologies (EST's) identified as most suitable from the MCA, two are electrochemical storage technologies (lithium-ion and lead-acid batteries), and the third is a mechanical storage technology (Compressed Air Energy Storage). The significant difference in efficiency between these electrochemical and mechanical storage system's is primarily due to fundamental differences in their energy conversion processes, internal resistance, heat losses, and energy density.

Electrochemical storage systems, such as lithium-ion batteries, achieve high efficiency in their charge and discharge processes due to the nature of chemical reactions. The intercalation mechanism in lithium-ion batteries, in particular, involves minimal energy loss. Conversely, mechanical energy storage systems, especially CAES, involve multiple stages of energy conversion (compression, storage, and expansion), each with inherent potential for energy losses. The compression and expansion of air in CAES result in significant thermal losses, which are challenging to recover efficiently.

### 3.5.3. Model Parameters

In this subsection, the key parameters for the selected ESTs are presented, focusing on efficiency and State of Charge (SoC) metrics. Table 3.1 below summarizes these values, highlighting the performance characteristics of lithium-ion batteries (Li-Ion), lead-acid batteries (LA) and Compressed Air Energy Storage (CAES). This information can also be found in Section 2.4 where all references are included.

Table 3.1: Performance characteristics for the selected ESTs

| Parameters | Li-Ion | LA | CAES |
|---|---|---|---|
| Efficiency (%) | 85-95 | 70-80 | 50-60 |
| SoCmax (%) | 80 | 80 | 100 |
| SoCmin (%) | 20 | 20 | 0 |

## 3.6. Determination of Renewable Energy Capacity

Following the calculation for the inputs, the next step involves determining the total installed solar and wind power required to meet the selected generation mix. In order to achieve this the required number of PV panels ($N_{PV}$) and wind turbines ($N_w$) needs to be determined. It should be noted that this method can be approached in various ways. However, for the purposes of this thesis, the wind turbine is used as the primary generation system, leading to a variable ratio of solar power ($r_{PV}$), which influences the overall energy mix. To facilitate direct comparisons across all scenarios, the total annual energy generated ($E_{gen,total}$) is kept constant. This constant value is based on the amount of wind power that would be produced in a scenario with an energy mix consisting of 100% wind power. Essentially, in the 100% wind scenario, the total energy generated by wind power alone is set as a baseline. As the ratio of solar power increases, wind power is reduced accordingly, but the total energy output remains the same. This approach allows us to compare different energy mixes while maintaining consistent energy production levels across all scenarios. To determine the number of wind turbines ($N_w$) required Equation (3.17) below is used:

$$N_{\text{w,new}} = N_{\text{w,original}} - \left\lceil N_{\text{w,original}} \times \frac{r_{PV}}{100} \right\rceil \tag{3.17}$$

The new wind power, $E_{w,new}$, is then recalculated with the new number of wind turbines. The total energy required from PV units, $E_{PV\ total}$, is determined by subtracting the new wind energy from the total constant energy:

$$E_{\text{PV total}} = E_{\text{gen,total}} - E_{\text{w,new}} \tag{3.18}$$

Then the number of PV panels required, $N_{PV}$, is calculated by dividing the total required PV energy ($E_{PV\ total}$) by the energy generated by a single PV panel:

$$N_{\text{PV}} = \left\lceil \frac{E_{\text{PV total}}}{E_{\text{PV,panel}}} \right\rceil \tag{3.19}$$

Finally, the model determines the total installed solar power and total installed wind power, where the total installed solar power $P_{solar\ total}$ is calculated as the product of the number of PV units $N_{PV}$ and the rated power per panel $P_{panel\ rated}$ depicted by the Equation 3.20 below:

$$P_{\text{solar total}} = N_{\text{PV}} \times P_{\text{panel rated}} \tag{3.20}$$

Similarly, the total installed wind power $P_{w,new}$ is computed as the product of the number of wind turbines $N_{w,new}$ and the rated power per turbine $P_{turbine\ rated}$:

$$P_{\text{w,new}} = N_{\text{w,new}} \times P_{\text{w,rated}} \tag{3.21}$$

This approach ensures that the energy mix aligns with the specified solar ratio ($r_{PV}$), optimizing the system to reduce the need for energy storage. The methodology is consistent with strategies used in renewable energy studies, where balancing contributions from different sources is crucial to enhancing system reliability and reducing costs, which is discussed in more detail in Section 1.1.2.

## 3.7. Normalisation of Power Demand

Using the previously determined number of PV panels ($N_{PV}$) and wind turbines ($N_w$), the power demand is normalized based on the total annual energy generated ($E_{total}$). This normalization process involves adjusting the total power demand to match the total energy produced by the selected mix of renewable energy sources over a year. Essentially, this means scaling the energy demand to ensure it aligns with the annual energy output from the renewable energy sources the need for this step is further explained in Subsection 3.4.

The total annual energy generated, $E_{total}$, is calculated by summing the power output from the wind turbine farm ($P_{w,\text{farm}}$) Equation 3.3 and the photovoltaic park ($P_{\text{PV,farm}}$) Equation 3.14 over the course of the year, thereby converting the power values into energy. Lastly as discussed in Section 3.1 the grid also has some losses that need to be considered thus employing Equation 3.22 enables the determination of the grid losses using values from relevant literature [59, 60]. Resulting in the total efficiency of the grid to be approximately 90% [61].

$$\eta_{\text{grid}} = \eta_{abs} \cdot (1 - \eta_{\text{dist}}) \cdot \eta_{\text{inve}} \tag{3.22}$$

The total annual energy generated, Etotal, is calculated

$$E_{\text{total}} = (\sum P_{w,farm} + \sum P_{\text{PV,farm}}) \times \eta_{grid} \tag{3.23}$$

Next, to normalize the power demand, a scaling factor (SF) is introduced, which is the ratio of The total annual energy generated, $E_{total}$, to the cumulative power demand $\sum P_D$ over the same period as the renewable energy sources, thereby converting the power values into energy.

The total annual energy generated, Etotal, is calculated by using the Equation 3.24 below:

$$SF = \frac{E_{\text{total}}}{\sum P_D} \tag{3.24}$$

Finally, the scaling factor (SF) is introduced to normalize the power demand $P_{D_{\text{normalized}}}$, as shown in Equation 3.25:

$$P_{D_{\text{normalized}}} = P_D \times SF \tag{3.25}$$

## 3.8. Determine the Power Imbalance

The next step involves calculating the power imbalance at each time step by summing the renewable energy produced by the generation technologies mix selected, and then subtracting the normalised demand power for the same time step using Equation 3.26. This power imbalance will provide insight into how the battery will operate. Specifically, it determines whether, for a given time step, the generated energy exceeds or falls short of the required load. This crucial information feeds into the decision-making process, guiding the control strategy's determination of whether the energy storage system should be charged or discharged. The power imbalance is then filtered to meet the timeframe for medium-duration storage which spans from 4 to 200 hours as explained in Subsection 3.9.

$$\Delta P(t) = \Big(P_{w,farm}(t) + P_{PV,farm}(t)\Big) - P_{D_{\text{normalized}}}(t) \tag{3.26}$$

## 3.9. Filtering Power Imbalance

As discussed in the preceding Chapters, the analysis timeframe for medium-duration storage spans from 4 to 200 hours. However, the dataset under examination encompasses not only medium-term data but also exhibits short-term and long-term variations. To enhance the accuracy of the analysis, specifically for medium-term storage, it becomes imperative to eliminate the influence of these variations. In this regard, frequency domain filters emerge as the appropriate tools for the task. Frequency domain filters are typically employed to allow certain frequencies to pass unaffected through the filter, while effectively blocking others. In this context, the selected filter is designed to attenuate most of the variations occurring at frequencies below a specific threshold (below 4 hours) and above another threshold (beyond 200 hours). This strategic filtering approach serves to refine the dataset, enabling precise and focused analysis of medium-term storage characteristics.

Filters can be classified in many ways. One common method of classification is based on a filter's frequency selectivity, which categorizes filters according to the range of signal frequencies they allow to pass or block. This classification includes the following types: Low-pass, High-pass, Band-pass, and Band-stop filters. Figure 3.5 illustrates these four basic frequency responses. Below a brief summary of each signal frequency is provided [62]:

- Low-Pass Filter: This type of filter allows lower frequencies to pass through with minimal attenuation, while it attenuates or blocks higher frequencies that exceed a certain cutoff frequency. It is often used to eliminate high-frequency noise from a desired low-frequency signal.
- High-Pass Filter: In contrast, a high-pass filter permits higher frequencies to pass through, while it attenuates or blocks low frequencies. It is used when you want to remove low-frequency noise or extract higher-frequency components from a signal.
- Band-Pass Filter: A band-pass filter only allows frequencies within a specific frequency band to pass through, while frequencies outside this band are attenuated. This is useful when you need to isolate signals within a certain frequency range.
- Band-Stop Filter (Band-Reject Filter): This type of filter attenuates or blocks frequencies within a specific band while allowing others to pass. It's used to eliminate or suppress signals within a particular frequency range.

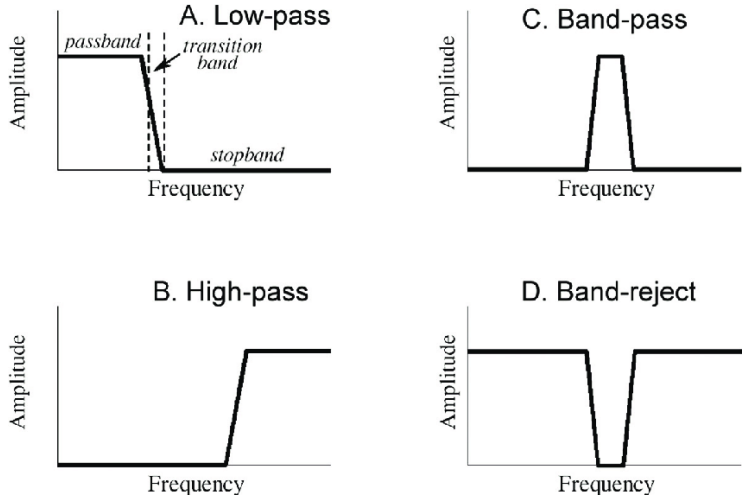


Figure 3.5: The four basic frequency responses [63]

In this thesis, a bandpass filter was determined as the most suitable filter. The data is sampled at a frequency of one sample per hour. This means that each data point represents an hourly measurement. The sampling frequency is thus set to 1 samples per hour. The high cut frequency corresponds to 1/4 samples per hour as the period is 4 hours. The low cut frequency corresponds 1/200 samples per hour as the period is 200 hours.

Butterworth filters serve as the foundational design for bandpass filters and fall under the category of filters classified based on their frequency response. Other types include Chebyshev Type I, Chebyshev Type II, and Elliptic filters. The Butterworth filter, an analog filter design, is distinguished for its flat frequency response in the passband and a smooth roll-off in the stopband. These filters are designed to achieve a maximally flat magnitude within the bandpass, making them an ideal choice for various applications, such as motion analysis. However, this comes at the expense of a relatively wide transition band.

An important parameter that needs to be taken into consideration when using the Butterworth filter is the filter's order. The flatness of the output response of a Butterworth filter increases with the filter's order. Higher-order filters provide greater precision, but in practical implementation, there's no ideal filter. The higher the Butterworth filter order, the more cascaded stages there are within the filter design, bringing the filter closer to an ideal "brick wall" response seen in Figure 3.6, although achieving a perfect response remains challenging in practice [64]. Thus, for this thesis a fourth-order Butterworth bandpass filter was used.

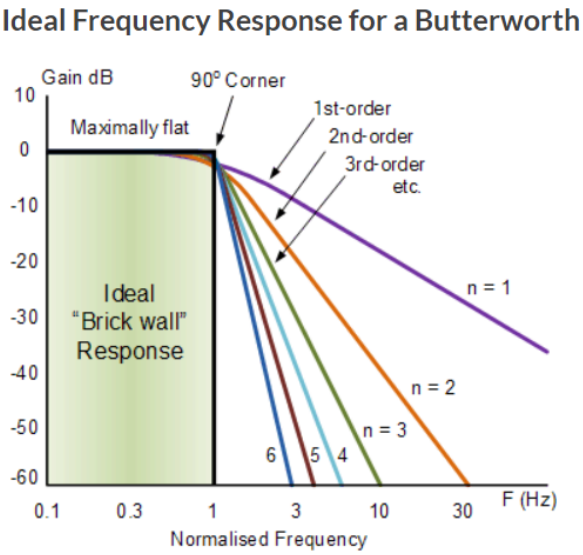


Figure 3.6: Frequency response of the Butterworth filter for various orders of the filter

Lastly, a linear filter is employed in tandem with the Butterworth filter for zero-phase filtering. This technique involves the application of an infinite impulse response filter to the signal, in both the forward and reverse directions. Notably, the order of the filter is doubled compared to the original filter order [65].

## 3.10. Control Strategy

This section provides an in-depth overview of the control strategy is used in this thesis. It is commonly known that the efficient and reliable operation of a hybrid renewable energy system relies significantly on the effective implementation of an appropriate control strategy. As a hybrid system combines different renewable energy sources, each with its own characteristics and variability, a control strategy becomes essential to optimize the system's performance and ensure its reliable operation [66]. The objectives of the control of a hybrid renewable energy system are:

1. Optimal Power Generation
2. Stability and Reliability

Research was conducted to identify the most suitable approach for developing the model required for this study. During this investigation, a wide range of software tools specifically developed for the design, analysis, and optimization of hybrid renewable energy systems were examined. In their paper, Sinha and Chandel [67] performed a comprehensive analysis of 19 software tools, including HOMER, Hybrid2, and SOMES. However, based on the broad perspective of this thesis, it was concluded that none of the available software options adequately met the requirements. As a result, the decision was made to employ the Python programming language for developing the required model. Python was deemed more suitable due to its flexibility and versatility in handling complex modeling and simulation tasks.

To calculate the required storage capacity for a given renewable penetration it is not only required to know the demand and generation profiles, but also requires modelling the operation of the storage (charge/ discharge). The numerical model developed for this purpose is presented below. To begin the analysis of the work process a flowchart was developed as shown in Figure 3.1 which illustrates the methodology adopted for coding the model.

The final step shown in the flowchart Figure 3.1 is the control strategy. Unlike the other processes, which remain constant and unalterable, the control strategy at this stage retains the flexibility to accommodate internal modifications. Control strategies play a vital role in addressing the integration challenges of intermittent renewable generation into the power grid. In general, control strategies can be categorized into classical and intelligent control strategies. Consequently, the control strategy tends to be complex, requiring continuous operation due to the intermittent nature of renewable energy sources and the pursuit

of multiple objectives. It is important to note, however, that within the scope of this thesis, the focus is not determining the most optimal control strategy. Thus, the control strategy which is depicted by a flowchart Figure 3.7 is employed to manage the charge and discharge cycles of energy storage devices. These devices are charged during periods of excess renewable generation and discharged when generation falls short of meeting demand following the SoC constraint as shown in Equation 3.29. While this basic control strategy is fundamental, it is worth noting that there is also literature exploring a range of optimization techniques to enhance efficiency and revenue generation, including forecasting methods and AI.

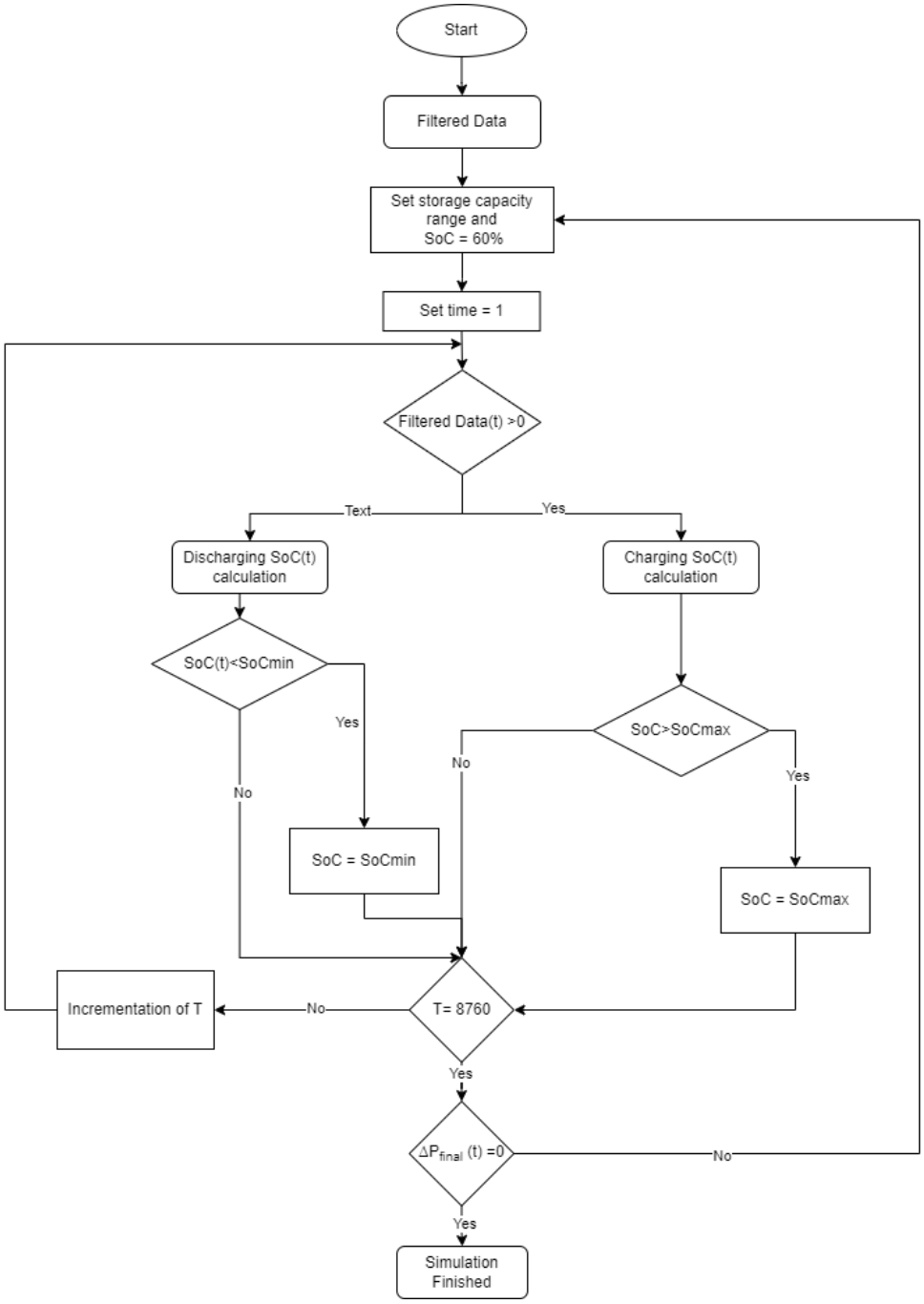


Figure 3.7: Flow chart depicting the control strategy used for this thesis

The power imbalance from Equation 3.26 is filtered with the method described in Section 3.9 to obtain the medium-term imbalance which on an hourly basis is used to determine the State of Charge (SoC) of

the storage system. When the filtered power imbalance exceeds zero, the excess power is used to charge the storage system. In this charging scenario, the SoC equation can be expressed as follows (3.27):

$$SoC(t) = SoC(t-1) + \frac{(E_{PV}(t) - E_D(t)) \cdot \eta_{sto,1}}{\eta_{inv}} \tag{3.27}$$

In the Equation 3.27 above, SoC(t) and SoC(t-1) represent the states of charge of the storage system at time t and t-1, respectively. The efficiency of the inverter is denoted as $\eta_{inv}$, and the efficiency of the storage technology ($\eta_{sto,1}$) is always 1 as explained below.

On the other hand, if the filtered power balance is below zero, the power not provided by the generation system will be covered by the storage system. Equation 3.28 shows the battery SoC(t) discharging equation:

$$SoC(t) = SoC(t-1) - \frac{(E_D(t) - E_{PV}(t))}{\eta_{inv} \cdot \eta_{sto,1}} \tag{3.28}$$

However, there is a constraint that requires the SoC to remain within certain limits, as shown in Equation 3.29:

$$SoC_{min} \leq SoC(t) \leq SoC_{max} \tag{3.29}$$

Battery systems used for renewable energy applications typically have a limited range of depth of discharge (DoD), often restricted to a maximum of 80% (for Li-Ion and LA), although this can vary slightly depending on the battery technology. Exceeding this limit can lead to over-discharge, potentially causing permanent damage to the battery. To ensure the longevity and efficiency of the battery, it is recommended that the SoC remains within an optimal range specific to each battery technology. For instance, maintaining the SoC within a specified range is considered ideal for optimal performance. This control strategy helps ensure that the battery operates in good condition, with a high probability of maintaining an adequate SoC and minimizing the loss of power supply probability (LPSP). LPSP refers to the likelihood that the energy storage system will be unable to meet power demand at any given time. By keeping the SoC within optimal limits, the effectiveness of the load control strategies is validated, contributing to an extended cycle life for the battery system [68].

Efficiency is a crucial parameter when evaluating storage technologies and was one of the selected criteria in the MCA, as discussed in Chapter 2. In traditional approaches, the efficiency of storage systems is typically accounted for by scaling up generation to compensate for efficiency losses. However, in this thesis, such approaches proved ineffective due to the filtering process used in the analysis. This filtering process alters the expected energy balance, resulting in inaccurate reflections of how efficiency losses impact the system's performance.

To address this issue, the efficiency of the storage technology ($\eta_{sto}$) was temporarily set to 1 in our model ($\eta_{sto,1}$). This simplification was necessary to prevent the filtered energy balance from distorting the dynamic relationship between generation, demand, and storage efficiency. If the actual efficiency were applied, it would have led to gradual, unrealistic changes in the SoC, ultimately requiring storage capacities far beyond practical or realistic levels.

Despite this adjustment, it was still important to incorporate storage efficiency ($\eta_{sto}$) into the model to ensure realistic outcomes. To achieve this, the initial storage capacity input into the model was adjusted to reflect the efficiency of the storage technology. As shown in Equation 3.30 and depicted in Figure 3.7, this efficiency-adjusted capacity ensures that the SoC is updated accurately to represent realistic performances.

$$C_{sto}(t) = C_{sto}(t-1) \cdot \eta_{sto} \tag{3.30}$$

To conclude in Figure 3.7 there is a check point ensuring that the filtered power imbalance ($\Delta P(t)$), including the energy storage technology ($E_s(t)$), at a specific time step, is zero by implementing Equation 3.31. This step is crucial for ensuring that there is no underproduction, allowing for the accurate determination of the appropriate storage capacity range needed to adjust the renewable energy capacity.

$$\Delta P_{final}(t) = \Delta P(t) + E_s(t) \tag{3.31}$$

## 3.11. Optimisation of Hybrid System

Analyzing hybrid systems poses significant challenges and requires thorough examination. The optimization objectives for these systems focus on attaining optimal operational conditions and conducting economic evaluations to maximize power generation efficiently and affordably, especially on days with extensive sunlight or wind. This involves considering the dependency of renewable sources, such as wind and solar, on meteorological conditions. Ultimately, the aim is to optimize performance to meet all physical and technical constraints, emphasizing the importance of techno-economic analysis in ensuring the effective utilization of renewable energy sources [69].

The integration of various optimal sizing techniques in the design of hybrid energy systems is gaining popularity. The optimal configuration and control method of the hybrid system are interconnected, intensifying the challenges associated with sizing, designing, and evaluating these systems. Introducing an optimal sizing approach becomes instrumental in ensuring peak performance, minimal investment, and optimal utilization of system components.

One of this thesis's primary objectives encompass optimising the storage capacity of the hybrid system to ensure a secure and feasible storage configuration. The optimization approach applied here employs a multi-objective framework, involving two distinct objective functions. The first objective is aimed at minimizing the power mismatch between the energy demand and the energy generated by the hybrid energy system. Simultaneously, the second objective concentrates on minimizing the overall capital cost associated with the hybrid energy system. Given the complexity introduced by these dual objectives, comprehensive research was undertaken to determine the most suitable optimization technique for this thesis. An in-depth examination of diverse optimization methods was conducted. This exploration aims to identify a suitable approach which is described in detail in Section 5.1.

### 3.11.1. Weighted Sum Method

The first method explored was the weighted sum method. This technique involves the combination of multiple objectives into a single objective by summing each objective, each multiplied by a predetermined weights. These weights are assigned based on the relative significance of each objective [70]. In this approach, the optimization problem can be formulated as follows:

$$\begin{aligned} &\min_x F(x) = \sum_{m=1}^{M} w_m f_m(x),\ m = 1,2\ldots,M \\ &\textit{subject to} \\ &g_j(x) \geq 0,\ j = 1,2\ldots,J \\ &h_k(x) = 0,\ k = 1,2,\ldots,K \\ &x_i^{(L)} \leq x_i \leq x_i^{(U)},\ i = 1,2,\ldots,n \end{aligned} \tag{3.32}$$

In these equations, $w_k$ represents the weight assigned to the $m$-th objective function.

### 3.11.2. Multi-objective Optimisation Method

The second method investigates is multi-objective optimization, a facet of multiple criteria decision-making that deals with mathematical optimization problems featuring more than one objective function to be simultaneously minimized or maximized [70]. Multi-objective optimization problems (MOOPs) have widespread applicability across real-world scenarios. They involve making optimal decisions while factoring in trade-offs among two or more conflicting objectives, all while adhering to constraints. In the context of a MOOP, the goal isn't to attain a solitary optimal solution, but rather a set of trade-off solutions. These trade-off optimal solutions are referred to as Pareto-optimal solutions. [71]. In its simplest form, a MOOP can be represented as follows: [70]:

$$\begin{aligned} &\min_x f_m(x),\ m = 1,2\ldots,M \\ &\textit{subject to} \\ &g_j(x) \geq 0,\ j = 1,2\ldots,J \\ &h_k(x) = 0,\ k = 1,2,\ldots,K \\ &x_i^{(L)} \leq x_i \leq x_i^{(U)},\ i = 1,2,\ldots,n \end{aligned} \tag{3.33}$$

When addressing MOOPs, two distinct approaches are available. Firstly, the classical methods usually require repetitive applications of an algorithm aiding in finding multiple Pareto-optimal solutions [70]. However, these do not guarantee that a Pareto-optimal solution is found. A classical approach to solving a MOOP is the parametric scalarizing approach, such as the weighted sum method, which is further elaborated in Subsection 3.11.1. The second approach for handling MOOPs involves the utilization of evolutionary algorithms (EAs). EAs adopt a population-based strategy wherein multiple solutions participate in each iteration, leading to the evolution of a new population of solutions in each iteration. This EA-based approach facilitates the calculation of multiple Pareto-optimal solutions within a single simulation run [70]. Genetic algorithms (GAs) are a class within the EAs that employ natural selection and an evolutionary process in their operations [72].

As explained by Mohapatra, Mishra, and Mishra [72], GAs maintain a pool of solutions that evolve over time. This is done in different generations where in each generation, the GA produces a new population using genetic operators such as selection, crossover, and mutation. Of course, an optimization procedure must be adapted such that it spreads the population to the Pareto front as best as possible instead of concentrating on some areas of it. Examples of such adapted procedures in the EA field are the non-dominated sorting Genetic Algorithm (NSGA-II), the Strength Pareto EA (SPEA-2), or the S-metric selection evolutionary multi-objective optimization algorithm (SMS-EMOA), to mention only a few [73]. These combinations of population-based optimization procedures and Pareto optimality, in general, will estimate the Pareto front roughly at the minimum, with less computational effort than it can be attained using the aggregation methods introduced for the assessment of the individuals of the same population-based methods.

## 3.12. Optimisation Parameters

This section comprises a detailed explanation and literature review aimed at defining the challenges encountered in determining the capital expenditure for the hybrid renewable system, and the three different storage systems. Given the novelty of these technologies in the market and their significant dependence on location and system size, detailed analysis was imperative. As a result, determining precise capital expenditures proved challenging, leading to the provision of ranges to accommodate the varying factors influencing costs.

### 3.12.1. Floating Photovoltaic

Determining the capital expenditure (CapEx) for floating photovoltaic (FPV) and storage technologies is a highly complex procedure that requires consideration of numerous parameters. These parameters include system size, location, local labor rates, market fluctuations, local climate conditions, environmental considerations, and transportation/access challenges [32]. Hence, for this thesis cost estimates from the literature are employed.

Estimating the CapEx for a FPV system is a notably intricate task, primarily due to the limited availability of publicly accessible data on this matter. FPV systems can be installed on artificial or natural water bodies. However, the selection of the floating structure type and anchoring solution is contingent on site-specific factors, resulting in considerable variability in the total system cost [74].

The National Renewable Energy Laboratory's report [74] was utilized to arrive at the CapEx estimation. This comprehensive report employs a bottom-up analytical approach to assess the installed costs of FPV systems with fixed tilt deployed on artificial water bodies under typical site conditions. It was determined that for a 10-MW fixed-tilt FPV system, the installed system cost stands at \$0.26/W , which is equivalent to a 25% increase relative to ground-mounted, fixed-tilt photovoltaic systems installed over bare ground. The higher structural costs associated with the floating platforms and anchoring systems contribute significantly to this premium. Furthermore, it's essential to acknowledge that the complexity of FPV systems necessitates

additional efforts for site investigation, planning, and design. As a result, the site investigation costs for FPV installations are currently higher due to the intricate nature of these installations. By relying on the comprehensive insights of the National Renewable Energy Laboratory's report, this study successfully incorporates a robust foundation to estimate the CapEx for floating photovoltaic systems.

### 3.12.2. Offshore Wind

Determining the cost of an offshore wind farm depends on various parameters, such as the type of wind turbine used, the foundation design etc [75]. The capital costs of a wind power project can be categorized into the following major components [76]:

Turbine cost: This encompasses expenses related to the turbine components such as blades, towers, and transformers.

Civil works: This includes construction costs for site preparation and the foundations for the towers.

Grid connection costs: These expenses cover transformers, substations, and the connection to the local distribution or transmission network.

Other capital costs: This category may include expenditures for the construction of buildings, control systems, project consultancy costs, and other miscellaneous expenses.

The Cost of the wind field was determined to be approximately €1700/kW [77]. This value was assumed based on the existence of a similar off-shore wind farm.

### 3.12.3. Li-ion and LA Batteries

The notion of capital cost encompasses diverse components that exhibit variations according to the technology type. Cost information for battery technologies is typically broken down into four components [78]:

- Capital cost: Battery packs cost varies by the type of technology used (€/kWh).
- Power conversion system (PCS): Includes costs for the inverter, packaging, and controls. This system affects all battery technologies similarly.
- Balance of plant (BOP): This includes components like site wiring and transformers, measured in €/kW.
- Construction and commissioning (C&C): Also known as engineering, procurement, and construction (EPC) costs. It covers site design, equipment procurement, transportation, labor, and installation costs.

From the literature, only the capital cost was available for both EES technologies. The estimated capital cost range for lead-acid (LA) batteries is between $200–$500/kWh. For lithium-ion batteries, the estimated range is $340–$450/kWh [78].

### 3.12.4. CAES

Accurately estimating the Capital Expenditure (CapEx) of Compressed Air Energy Storage (CAES) presents considerable challenges due to its inherently site-specific nature. Factors such as localized civil engineering expenses and environmental restrictions exert significant influence on CAES costs. The cost estimation process heavily relies on the unique characteristics of the chosen location. For example, utilizing an existing gas cavern can mitigate overall costs, whereas excavating a storage cavern from hard rock can lead to substantial cost escalations. Comparing CAES projects to previous endeavors is complex due to the limited operational CAES facilities and challenges in drawing parallels with pumped hydropower projects constructed decades ago under different energy and economic frameworks. This lack of direct comparability further complicates the cost estimation process in the CAES context. As a result, there exists a large range in capital costs for Compressed Air Energy Storage (CAES) systems, typically ranging from $1,050 to $2,300 per kW.

### 3.12.5. Conclusion of Optimisation Parameters

Since this thesis is based in the Netherlands, all costs will be presented in euros. Therefore, values obtained from literature sources in dollars need to be converted to euros for consistency. The average exchange rate for the year 2023 was used for conversion. According to [79], the exchange rate from dollars to euros was

0.9241 EUR. Table 3.2 displays the converted CapEx costs in euros for all the renewable energy technologies utilized for generation and storage.

Table 3.2: Converted capital expenditures (Capex) to euros for all renewable technologies

| Parameters | Values |
|---|---|
| Li-ion | €300–650/kWh |
| LA | €185–465/kWh |
| Offshore Wind farm | €1700/kW |
| Floating PV | €280/kW |
| CAES | €970-2310/kW |

# 4

# Specific Cases

In this chapter, the selected location is introduced. Next, the analysis of daily data for solar radiation, wind speed, and power demand, along with the sources used for data collection, will be discussed. The final section presents the normalized figure of the power demand. Additionally, a histogram is provided, examining and highlighting the importance of medium-term storage.

## 4.1. Location

The region which was selected for this study is in the Netherlands. The Netherlands was chosen because the Dutch government has set a target that by 2030, emissions will be reduced by 49% relative to 1990 and will be further reduced by 2050 by 95% relative to 1990. This concludes that to achieve the targets 70% of the electricity must be produced from renewable energy sources (wind and solar) by 2030 and 100% by 2050 [80]. In 2021, approximately 33% of the total electricity was produced from renewable sources [81]. Another factor taken into consideration is that the Climate Agreement states that an additional 7GW of offshore wind farm capacity is required in the Dutch sector of the North Sea between 2023 and 2030 [80]. As also discussed in paper [81] there is limited space for the development of onshore wind farms. Therefore the Netherlands will have to invest heavily in renewable sources, especially offshore power plants. The name of the wind farm chosen is called Hollandse Kust (Noord), located 18.5km from Egmond aan Zee, as shown in Figure 4.1 with the number three. This location was chosen as the Dutch government has ensured that all the conditions for planning and building wind farms, the measures to protect nature, and the necessary permits are as required. Additionally, the Dutch government provides that the energy from the wind farm will be delivered to land via an offshore grid [82].

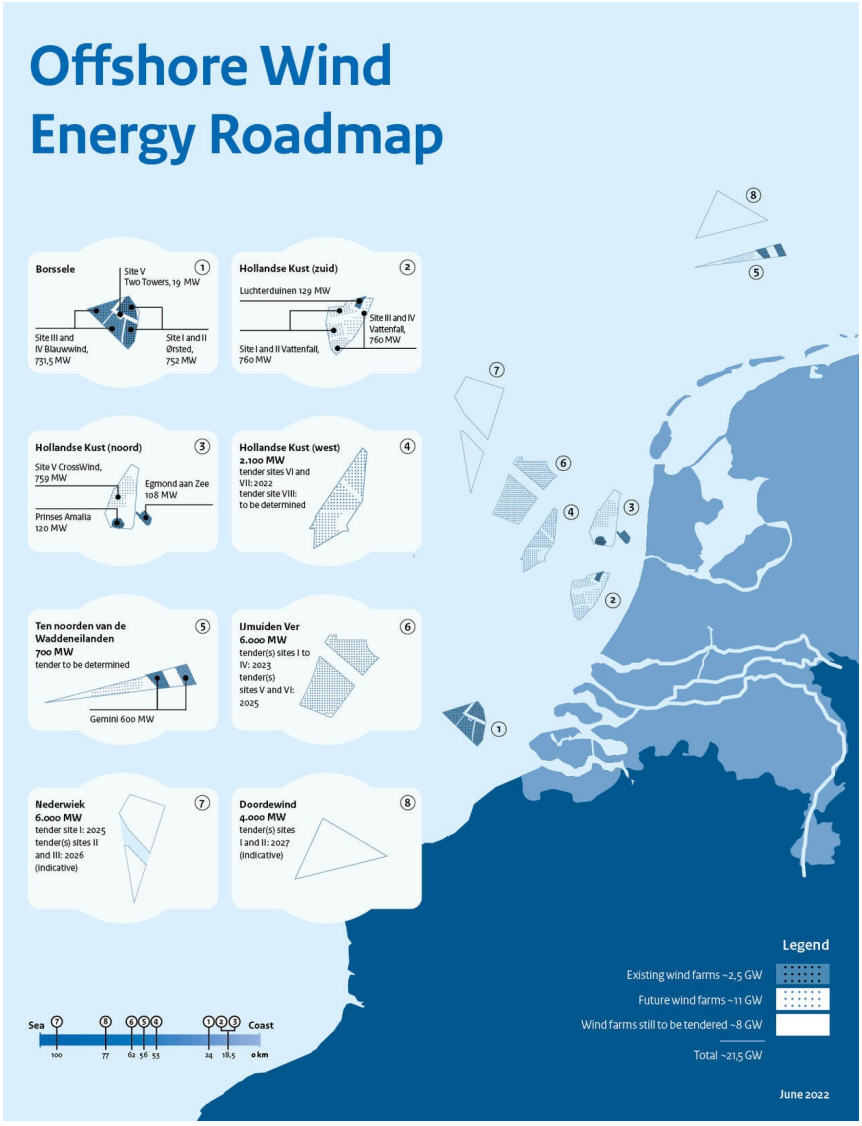


Figure 4.1: Dutch Offshore Wind Farm Zones [82]
Hollandse Kust (Noord) is depcited with the number three

## 4.2. Data Collection

The offshore region under investigation provided daily data for solar radiation and wind speed at the height of 10 meters above sea level. These data covered a four-year period from 2016 to 2019. The information was sourced from MERRA 2, a global atmospheric reanalysis developed by NASA. MERRA 2 utilizes satellite observations of earth, providing comprehensive data from 1980 to the present [83]. To ensure accuracy and to mitigate the impact of incorrect data collection or extreme conditions, an average of daily solar radiation values was calculated for the four-year period. This approach helps to minimize uncertainties and provides a representative measure of solar radiation levels in the offshore region over the specified timeframe.

The actual total load data for the Netherlands in 15-minute intervals for two specific periods, namely 2018-2019 and 2019-2020, were acquired from the European Network of Transmission System Operators for Electricity (ENTSO-E) Transparency Platform. This platform serves as a reliable source of diverse information concerning the European electricity market. ENTSO-E is an association that represents the transmission system operators (TSOs) responsible for electricity across Europe. The total hourly load of the Netherlands was calculated by averaging the four values of 15 minutes. Two years were considered in order to decrease the uncertainties of the data as described above. By considering two years' worth of data, the aim was to provide a more robust and comprehensive analysis, minimizing potential fluctuations and

outliers that could impact the overall assessment. While maintaining a constant annual demand serves as a useful simplification for analytical purposes, it is important to recognize its limitations, particularly as real-world demand tends to increase over time. Forecasting future power demand and understanding shifts in consumption patterns are crucial endeavors that require dedicated resources and research efforts. However, it is important to note that such forecasting lies beyond the scope of this paper. Our focus remains on the analysis of present conditions and the implications for the current energy system.

### 4.2.1. Generation Technologies Specification

The capacity and specifications of a 10 MW wind turbine and a monocrystalline solar panel are evaluated, both based on the current advanced technologies and that both generation technologies are located offshore. For this study, the wind turbine utilized is the 10 MW reference turbine developed by the Technical University of Denmark (DTU). This turbine was selected due to the comprehensive specification sheet available, which provided all necessary parameters for our analysis. Key specifications include a rotor diameter of 178 meters, a hub height of 119 meters, and a rated wind speed of 12 m/s, with a cut-in wind speed of 3 m/s and a cut-out wind speed of 25 m/s [84].

On the other hand, the selection of solar panels involved a more extensive review due to the wide range of available products and their varying specifications. As discussed in Section 3.3 average values for crucial parameters were adopted for a monocrystalline solar panel to ensure representatives. The selected parameters include a rated power output of 400W, with an efficiency of 18.5%, a typical module size of 1.9 $m^2$. These parameters, derived from a synthesis of contemporary literature and manufacturer data as seen in appendix Figures A.1, A.3, A.2, ensure a robust and realistic evaluation of solar energy potential in the context of our study. These values were chosen as they represent the most common and optimum configurations for offshore solar parks, allowing for significant energy capture due to the expansive and unobstructed nature of offshore installations.

By combining the data from the DTU 10 MW wind turbine and the averaged parameters for the monocrystalline solar panel, a comprehensive analysis of the renewable energy potential is provided, facilitating a deeper understanding of the performance and integration of these technologies in an offshore hybrid energy system.

## 4.3. Analysis of Demand and Generation Data

In this section, the data collected from the previous subsection will be analyzed using the methodology outlined in Figure 3.1 and the equations from Subsections 3.2, 3.3. The focus will be on emphasizing the annual and diurnal profiles and investigating the patterns of energy demand alongside renewable generation technologies. Moreover, based on the analyzed data and employing a normalization technique, we will examine the necessity of medium-term storage and determining its significance.

### 4.3.1. Power Demand

Figure 4.2 depicts the profile of the Netherland's hourly power demand alongside the average monthly demand. Figure 4.2 illustrates a notable increase in demand during the winter months (November- March) in contrast to warmer periods (April- October). This was expected as several factors contribute to this trend. For instance, reduced daylight hours and colder weather conditions play significant roles. Further analysis was conducted to observe the variations of the daily and weekly profile of the power demand.

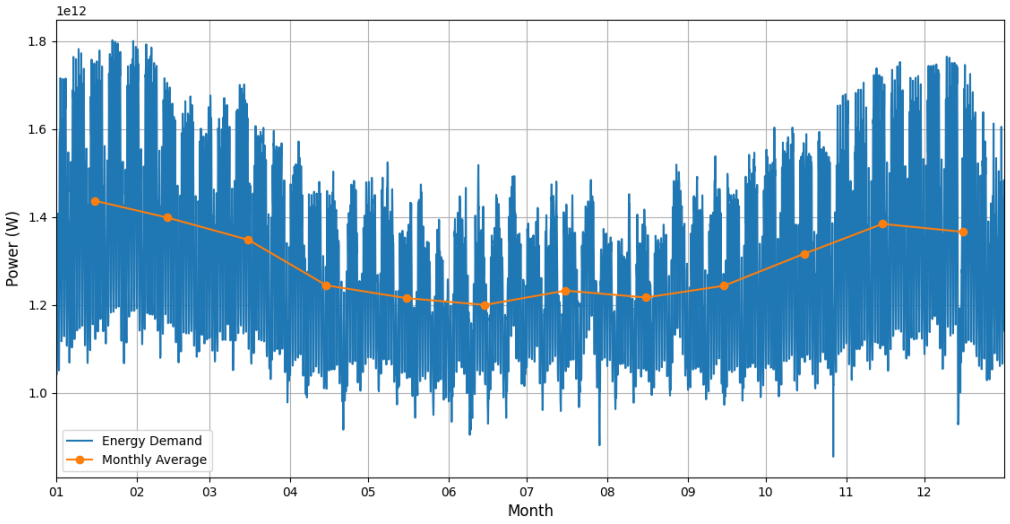


Figure 4.2: Annual hourly energy demand alongside the average monthly annual demand for the Netherlands

Figure 4.3 depicts three lines for comparison, providing insight into the daily power demand in the Netherlands. The red line signifies the lowest energy demand, the blue line represents the average daily energy demand, and the green line illustrates the highest energy consumption. As anticipated, the highest daily energy demand occurred during the winter month 22nd of January, while the lowest demand was recorded in the summer month 9th of June. Additionally, there is a noticeable peak in demand between 17:00-19:00 in all three cases. Furthermore, the patterns of the three lines are largely similar, with some variations observed during the summer months.

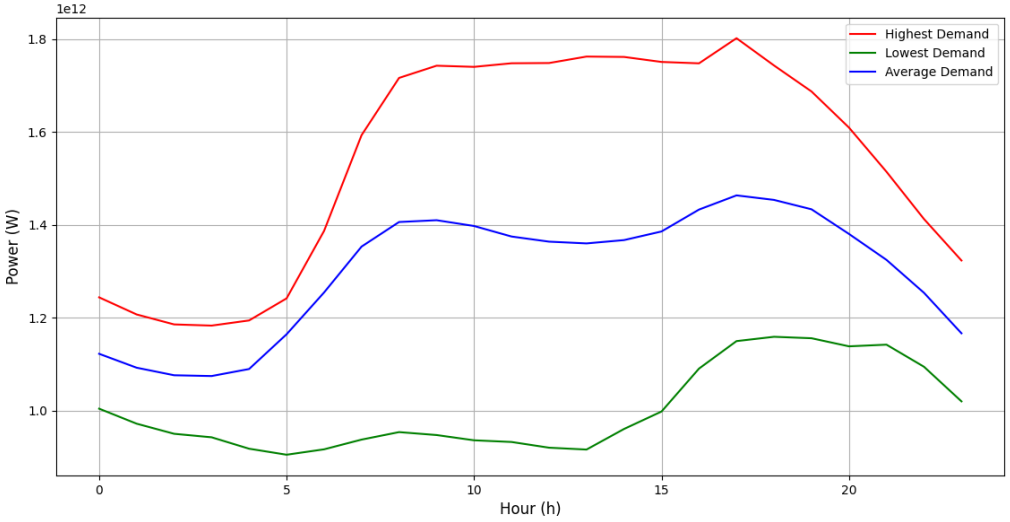


Figure 4.3: Comparison of power demand of the Netherlands including the higher, average, and lowest demand day

### 4.3.2. Wind Power Generation

Figure 4.4 illustrates the variable profile of annual hourly wind power generation from a single wind turbine stationed at the specified offshore location. This profile deviates from expectations outlined in Section 1.3, which were based on existing literature suggesting minimal seasonal and diurnal variations in offshore wind speeds. Discrepancies between the data obtained and these expectations are evident in Figures 4.4 and 4.6.

To address these discrepancies, further investigation was conducted using data from an alternative source. The Copernicus Earth observation program, a European Union initiative, provides accurate and reliable environmental information through a combination of satellite data, ground-based observations, and advanced modeling techniques [85]. The annual and average diurnal wind power results from the Copernicus database are depicted in Figure 4.5. A comparison between the two datasets reveals minimal differences, further validating the accuracy of the obtained data.

Possible factors contributing to the discrepancies between the dataset and the literature include the wind farm's proximity to the shore, variations in local atmospheric conditions, differences in measurement methodologies, and potential biases in data calibration between the sources. Despite these discrepancies, the data from MERRA 2 will be used for the analysis.

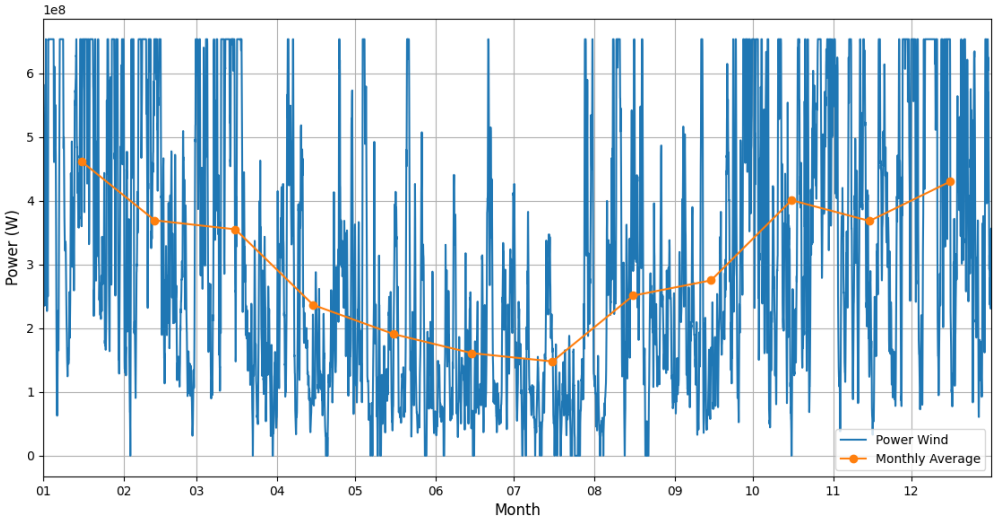


Figure 4.4: Annual hourly and average monthly wind power for a single wind turbine. Source MERRA 2

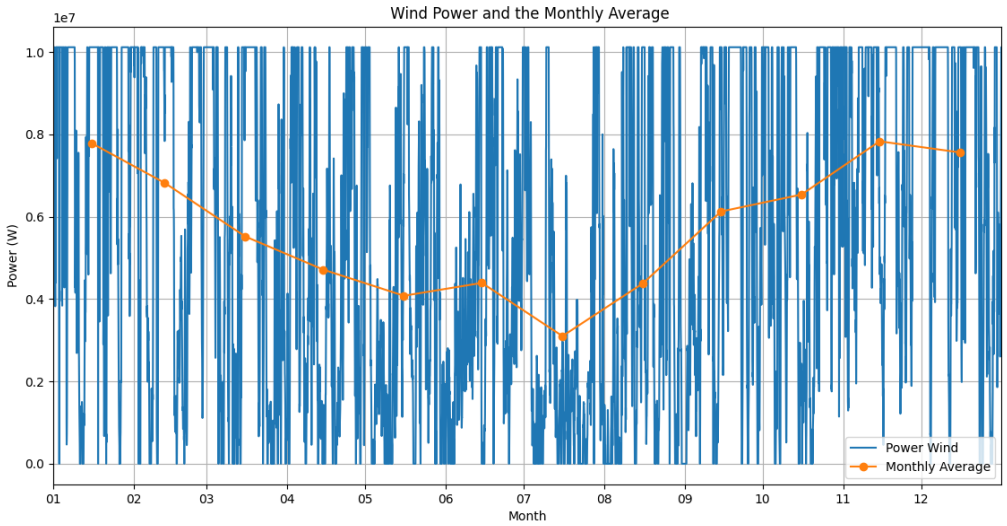


Figure 4.5: Annual hourly and average monthly wind power for a single wind turbine. Source Copernicus

Three graphs depicted in Figure 4.6 where required to capture the extreme volatility in power generation, due to the significant diurnal variations, especially evident in Figure 4.6c, underscore the dynamic nature of wind power generation. On the day with the high generation, peak power was sustained throughout the day seen in Figure 4.6a, while on the day of low generation, no power was produced during the day, with an increase at night seen in Figure 4.6b. From Figure 4.6c, it is clear that daytime generation power is lower compared to the power generated during the night.

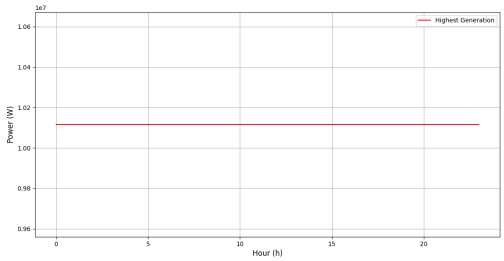


(a)

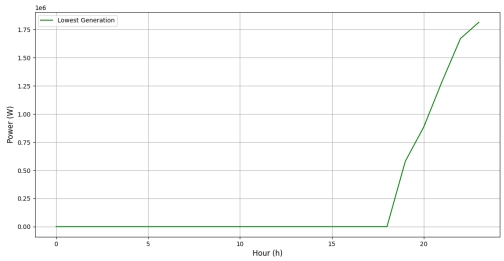


(b)

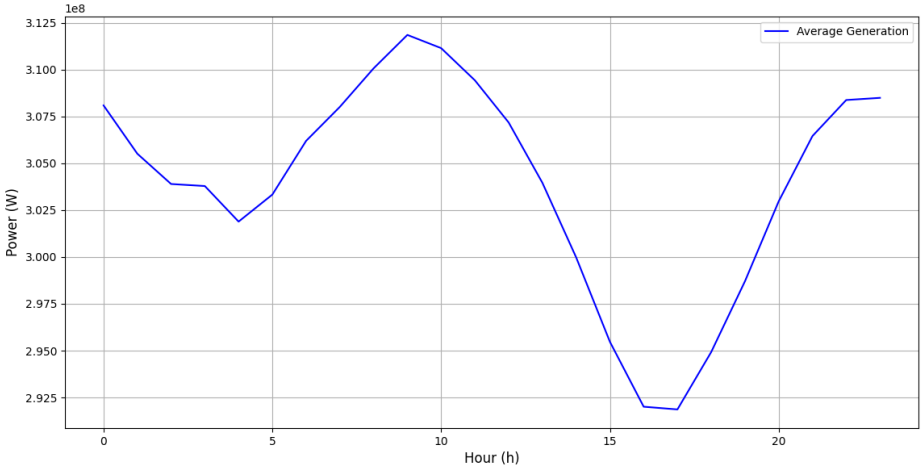


(c)

Figure 4.6: Comparison between the highest (a), average (b), and lowest (c) generations day

### 4.3.3. Solar Power Generation

Figure 4.7 illustrates the fluctuating profile of annual hourly solar power generation from a singular photovoltaic panel situated at the designated offshore location. As previously discussed in Section 1.3, solar radiation and consequent power output exhibit pronounced dependence on seasonal changes, with peak solar radiation occurring during summer months in contrast to reduced levels during winter, as corroborated by Figure 4.7. Examining the diurnal patterns portrayed in Figure 4.8, a substantial disparity between daytime and nighttime solar power generation is evident. Furthermore, distinct graphical representations emphasize the considerable variability inherent in solar energy production are presented in Figure 4.8.

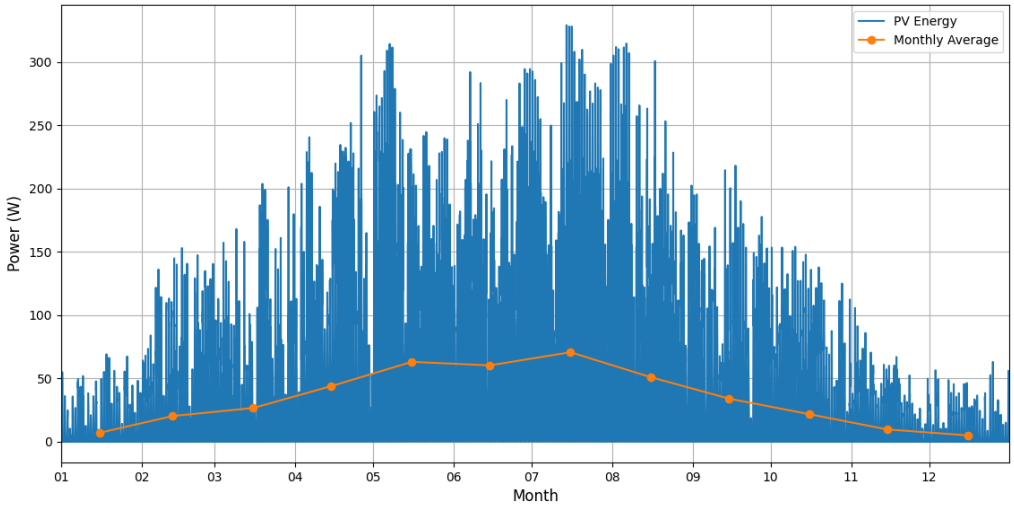


Figure 4.7: Annual hourly and the average monthly solar power for a single photovoltaic panel

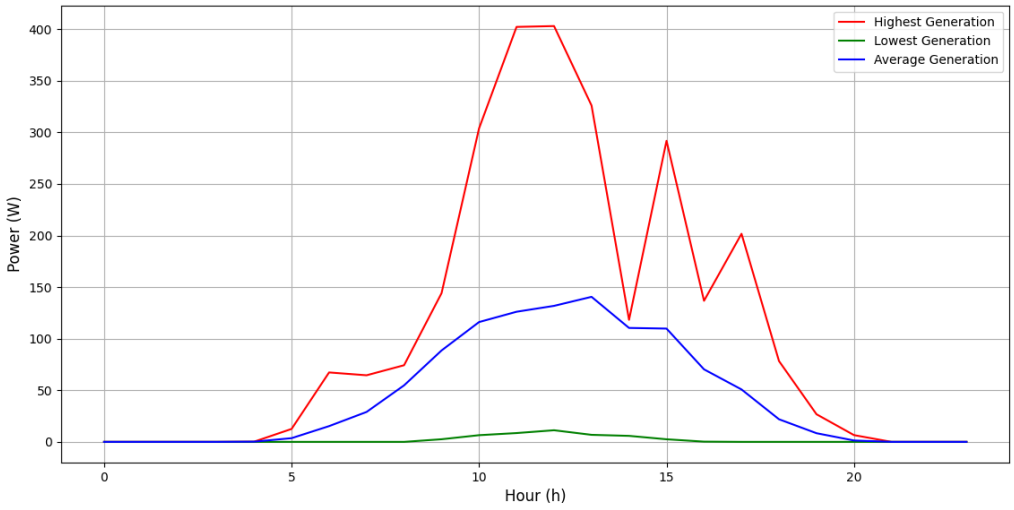


Figure 4.8: Comparison between the highest, average, and lowest generations day

### 4.3.4. Power Demand vs Generation

Normalization was employed as a preprocessing technique to standardize the scale of generation and power demand data. Given the substantial disparity in magnitude between the datasets, with power demand values seen in Figure 4.2 significantly exceeding those of generation as seen in Figures 4.4 and 4.7, normalization was necessary to facilitate meaningful comparison. Scaling the power demand datasets to a common range using the theory and equations as shown in Section 3.7 enables straightforward comparisons. In conjunction with Equation 3.26, the power imbalance was determined for a scenario involving one wind turbine and one PV panel and the results are presented in Figure 4.9. It is important to note that, due to the normalization applied for scaling, the average of the imbalance in the figure is zero. Figure 4.9 illustrates periods of positive and negative electricity imbalance. Positive imbalance occurs when renewable output exceeds power demand, resulting in a surplus of energy. Conversely, negative imbalance indicates instances when power demand surpasses the power generated.

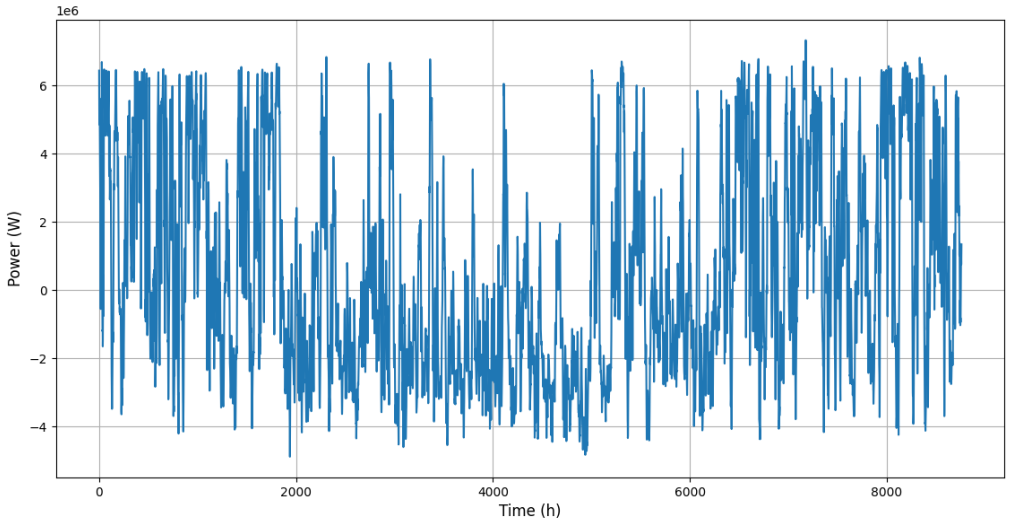


Figure 4.9: Power imbalance of a single wind turbine and pv panel and the normilised power demand

A histogram, as illustrated in Figure 4.10, has been constructed to emphasize the critical role of medium-term energy storage, as elaborated in Section 1.3. The x-axis delineates consecutive hours during which power demand surpasses generation, signifying periods of negative power imbalance. The y-axis represents the frequency of these occurrences, thereby highlighting how often mismatches of varying durations take place. The histogram reveals a notable prevalence of short-term storage needs, specifically for durations of less than four hours. Nevertheless, the data underscores a pronounced concentration of frequency within the medium-term storage range, particularly at the shorter end of this spectrum, underscoring its pivotal importance. It is imperative to recognize, however, that the analysis is inherently limited by its temporal scope, being confined to a single year. This limitation precludes the capture of seasonal variations and multi-year trends, which might otherwise indicate a greater necessity for both medium-term and long-term energy storage solutions.

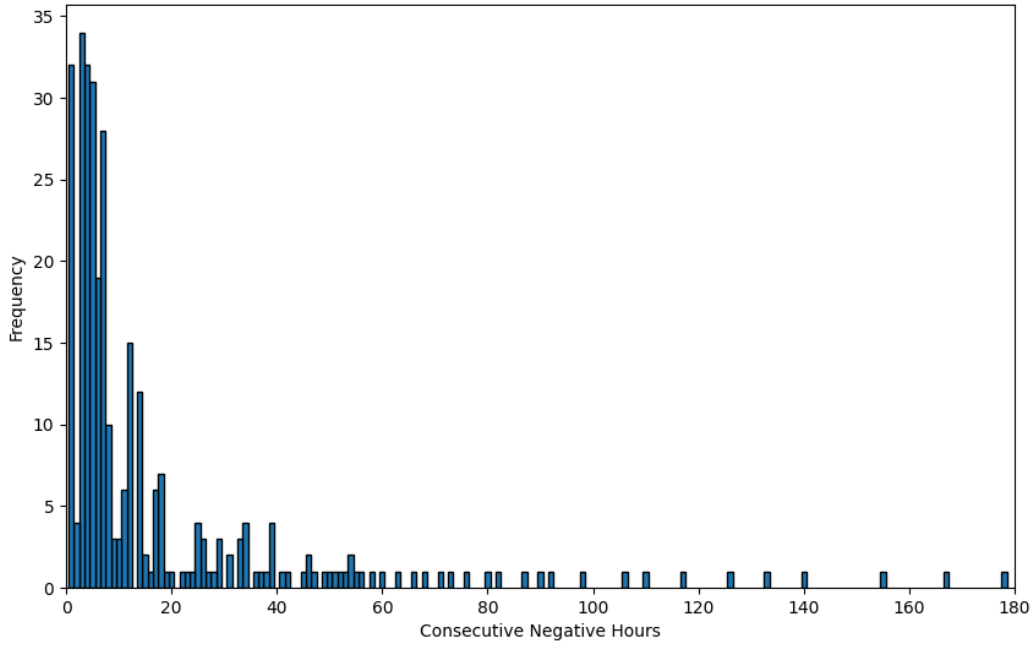


Figure 4.10: Histogram of Frequency Distribution of Energy Demand Mismatch Durations Highlighting the Importance of Medium-Term Storage

# 5

# Results

This chapter aims to explore the final two sub-objectives through detailed case studies. The first case study considers a scenario with a 100% generation from wind power. The optimization process identified the Pareto front for both capital cost and mismatch for the selected storage technology. From this, the solution with the lowest capital cost that meets all normalized demand (zero mismatch) was identified. In the second case study, the percentage of solar energy is incrementally increased to evaluate its impact and determine the optimal energy mix. This two-dimensional study aims to identify the most efficient hybrid generation system configuration with the cumulative negative mismatch over a year, without storage.

## 5.1. Base Case: Only Wind Power for Generation

In this section, the results produced by the model used to analyse the generation mix, comprising only of 100% wind power. To ensure realism and accuracy, the analysis is based on the Hollandse Kust (Noord) wind farm, which has a total capacity of 759 MW. For the base case scenario, the model uses a slightly adjusted and rounded total capacity of 760 MW. As discussed in Section 3.10, the total annual energy generated is kept constant to ensure direct comparisons across all scenarios. By doing so, the analysis remains realistic and applicable to real-world conditions. Thus, by applying the equations from Chapter 3 Figure 5.1 is created which illustrates the average monthly wind energy generation for the Base Case scenario.

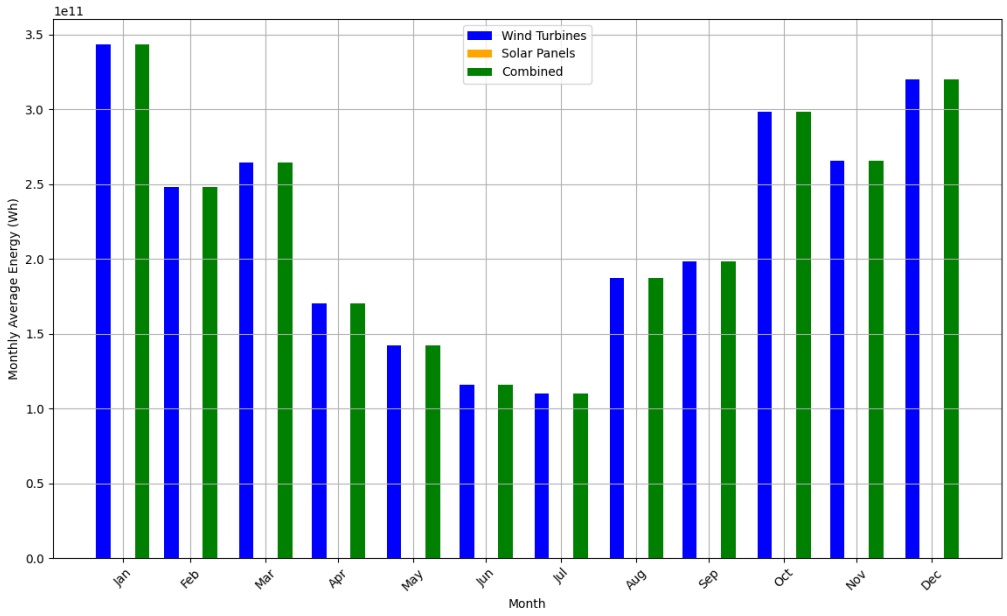


Figure 5.1: Monthly wind energy generation for the Base Case

According to the workflow in Figure 3.1 the third step involves normalizing the power demand. This step is crucial because it enables to adequately reflect the dynamic nature of power demand patterns in the Netherlands, as discussed in Section 3.4. Using the equations from Section 3.10, Figure 5.2 is obtained.

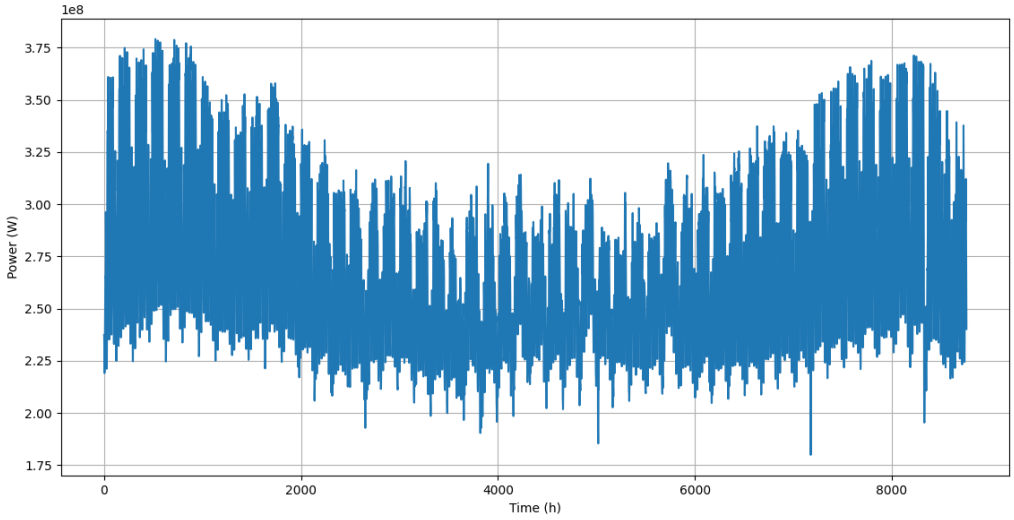


Figure 5.2: Normilised power demand for Base Case

The next step involves calculating the power imbalance using Equation 3.26, providing the requirements of the storage technology. Figure 5.3 depicts the variation between wind power generation and normalised power demand. As expected, and as discussed in Subsection 4.3.4, there are significant variations between generation and demand, especially during winter days. Conversely, during the summer period, there is a deficit as wind power generation is significantly lower compared to power demand. This graph clearly indicates the need for mid-term energy storage. However, due to the many short and swift variations observed in Figure 5.3 and the results shown in the histogram in Figure 4.10, the need for filtering is necessary.

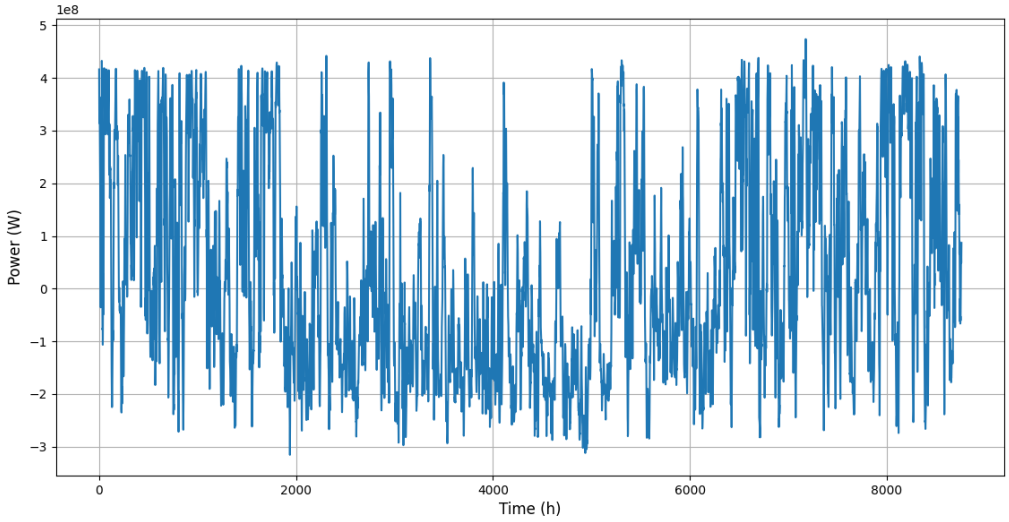


Figure 5.3: Power imbalance for Base Case

Thus, the power imbalance is filtered to meet the requirements of the timeframe for medium-duration storage, as shown in Figure 5.4 depicted by the orange line. This figure exhibits a marked reduction in short-term variations, achieving a smoother representation of the data compared to Figure 5.3 which is also visible in Figure 5.4a. The short-term fluctuations that dominate the unfiltered graph have been effectively minimized, demonstrating that the filter successfully excluded variations occurring over periods shorter than four hours. Additionally, Figure 5.4a shows a shift of the power imbalance values closer to zero. This shift closer to zero results from the filtering properties, which suppress extreme short-term fluctuations and minimize seasonal variations. By eliminating these spikes and dips, the data points are drawn closer to the mean value.

Furthermore, to ensure that the filtering is working properly, a sensitivity analysis was conducted. The two plots in Figure 5.4 illustrate the results of the sensitivity analysis. Each plot displays two time-series datasets: the unfiltered energy imbalance by the blue line also depicted in Figure 5.3 and the orange line depicts the filtered energy imbalance. The blue line remains constant across all plots, serving as a reference for comparing the effects caused by varying the low pass frequency of the band-pass filter.

Figure 5.4b, where the low cut frequency was increased to 1/40 samples per hour compared to the base case where the low cut frequency was 1/200 samples per hour, the filtered signal demonstrates a more aggressive smoothing effect. This is characterized by a substantial reduction in high-frequency oscillations and a more stable trend, suggesting a higher cutoff frequency. Consequently, the filter suppresses more noise, leading to a smoother signal but also beginning to smooth out some finer details present in the original data. This aligns with the expected behavior where increasing the low-cut frequency filters out more low-frequency noise, resulting in a smoother overall signal.

Figure 5.4c, where the low cut frequency was reduced to 1/400samples per hour compared to the base case where the low cut frequency was 1/200 samples per hour, the filtered energy imbalance shows a less aggressive smoothing effect compared Figure 5.4b and Figure 5.4a. This results in a signal that retains more low-frequency content and exhibits more fluctuations. This indicates that a lower cutoff frequency was used, filtering out less low-frequency noise and preserving more of the finer details in the data. This behavior is also expected, as reducing the low cut frequency should lead to less aggressive noise attenuation and a signal that closely follows the original energy imbalance. Thus, these observations confirm that the band-pass filter behaves as expected.

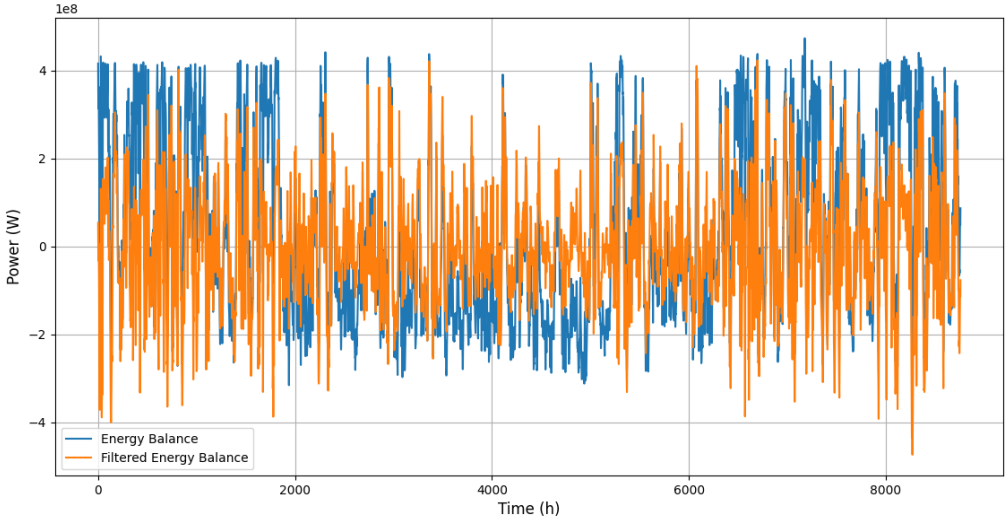


(a) Actual low pass frequency (1/200 samples per hour)

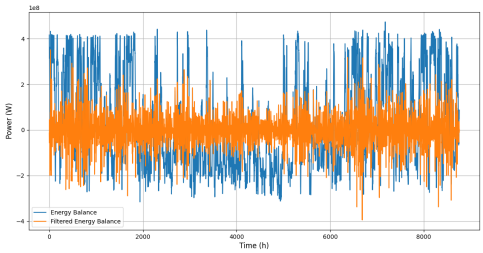

(b) Low pass frequency (1/40 samples per hour)

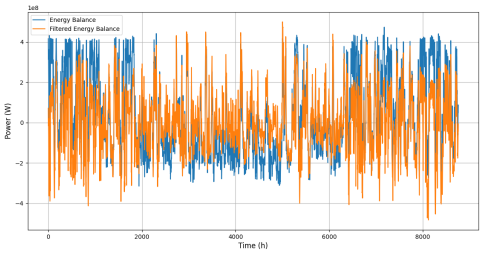

(c) Low pass frequency (1/400 samples per hour)

Figure 5.4: Comparison of the filtered power imbalance and unfiltered power imbalance including sensitivity analysis.

The final step of the process is the optimization step. An in-depth analysis has already been made in Section 3.11 enabling the determination of the most efficient and suitable optimisation technique to be adopted. The optimization problem is a multi-objective optimization, as it involves minimizing two conflicting objectives: Minimising the mismatch between energy generation and demand, Equation 5.1, and minimising the capital cost of the hybrid system, Equation 5.2.

Analyzing further the first objective function shown in Equation 5.1, the optimization seeks to determine the optimal storage capacity that minimizes the hourly loss of load. This objective function focuses on minimizing the discrepancy between power demand and generation shortfall by incorporating storage systems. This approach ensures that the system is not penalized for surplus generation and concentrates solely on unmet demand. The total mismatch is accumulated over an entire year, capturing the temporal dynamics of power generation, demand, and storage interactions.

The second objective function is defined in Equation 5.2 and aims to minimize the total capital costs associated with the hybrid renewable energy system. This optimization seeks to identify the optimal storage capacities that result in the lowest possible capital costs, including the capital cost for the generation systems.

Between the two objective functions, there are trade-offs because minimizing the net power capacity mismatch often necessitates a larger storage capacity, which increases capital costs. Conversely, minimizing capital costs involves limiting storage capacity, potentially leading to higher mismatches between generation and demand. Finally, the one constraint identified is depicted by Equation 5.3. which was introduced and

discussed in Section 3.10. This constraint ensures that the state of charge (SoC) of the storage system stays within specified minimum and maximum limits, which is essential for prolonging battery life.

Optimization Problem Formulation:

Objective Functions:

$$\text{Minimize (Mismatch)} = \sum_{t=1}^{8760} \left( \max_{\cdot} \{0, -( P_G(t) - P_{D_{\text{normalized}}}(t) + P_{\text{discharge}}(t)\} \right) \tag{5.1}$$

$$\text{Minimize (Cost)} = S_{\text{cap}} \times C_{\text{sto,cap}} + W_{\text{cap}} \times C_{\text{w,cap}} + P_{\text{cap}} \times C_{\text{PV,cap}} \tag{5.2}$$

Constraints:

$$SoC_{min} \leq SoC_i \leq SoC_{max} \tag{5.3}$$

Given the inherent trade-off between the two objectives, the use of Pareto optimality allows for the simultaneous consideration of both objectives. By exploring the trade-offs between minimizing mismatches and minimizing costs, Pareto optimal solutions offer a balanced approach where no objective can be improved without compromising the other. This ensures an efficient and effective configuration for the renewable energy system. As already discussed in Section 3.11, the Pareto front provides a range of optimal solutions rather than a single point solution, offering a broader perspective on the feasible solution range as seen in Figure 5.5. To determine the points for the Pareto front in this thesis, a stepwise approach was employed. This method involved incrementally increasing the storage size in predefined steps and determining the mismatch and costs for each step. This approach is more predictable and reproducible compared to evolutionary algorithms (EAs). The stepwise approach offers straightforward implementation, requires fewer computational resources, and converges more quickly to optimal or near-optimal solutions. Its deterministic nature enhances robustness and reliability.

For the optimization process, the storage capacity ranges were determined for three types of storage: Lithium-ion, Lead-acid, and Compressed Air Energy Storage (CAES). The ranges were as follows:

- Lithium-ion:
  - Capacity Range: 2.5 GWh to 35 GWh
  - Increment: 0.4 GWh
- Lead-acid:
  - Capacity Range: 2.7 Wh to 37 GWh
  - Increment: 0.4 GWh
- CAES:
  - Capacity Range: 2.6 GWh to 36 GWh
  - Increment: 0.4 GWh

These ranges were selected after determining the point at which each storage technology achieves zero negative mismatch. The incremental steps were chosen to balance accuracy and computational efficiency. While smaller increments offered only marginal improvements in accuracy, they significantly increased computation time. The selected storage capacities provide a comprehensive analysis of the relationship between costs and mismatch for each storage type. This stepwise approach, compared to EAs, offers a faster and more user-friendly optimization method. However, it lacks the flexibility and potential for discovering diverse solutions that EAs provide and requires detailed domain knowledge to set appropriate step sizes and evaluate their impacts accurately.

Figure 5.5 represents the Pareto optimal results, comparing the three distinct energy storage technologies: Li-ion, Lead-acid, and CAES, each represented by blue, orange, and green lines, respectively. The figure reveals an inverse relationship between cost and mismatch for each technology, as expected. As investment increases, the mismatch decreases, indicating an improved alignment between energy supply and demand. Interpreting the graph, a position more to the left indicates a higher dependence on grid energy, whereas moving towards the right signifies reduced grid dependency, approaching self-sufficiency. When the loss of

load is zero, the hybrid energy system fully meets the demand. Among the storage technologies analyzed, Compressed Air Energy Storage (CAES) exhibits the lowest capital cost to achieve this zero loss of load condition. However, its required capacity is neither the lowest nor the highest, which may seem contradictory given its low efficiency as shown in Table 3.1. Unlike electrochemical storage systems, CAES does not have a State of Charge (SoC) limitation, allowing it to store more energy. Lithium-ion batteries require the highest capital investment but need the lowest energy capacity, which is vital in regions with spatial limitations, particularly in Europe. As discussed in the paper [61], most developed countries, especially in Europe, face spatial and social limitations on the amount of onshore renewable systems that can be commissioned. Finally, lead acid has the largest required capacity and its capital cost is also quite high.

The graph succinctly illustrates the trade-offs between cost and mismatch for different storage technologies, aiding in the selection of the appropriate technology based on financial constraints and desired mismatch levels. This analysis is crucial for informed decision-making in energy storage and generation investments. Additionally, it highlights the importance of considering both capital cost and system efficiency when evaluating energy storage solutions.

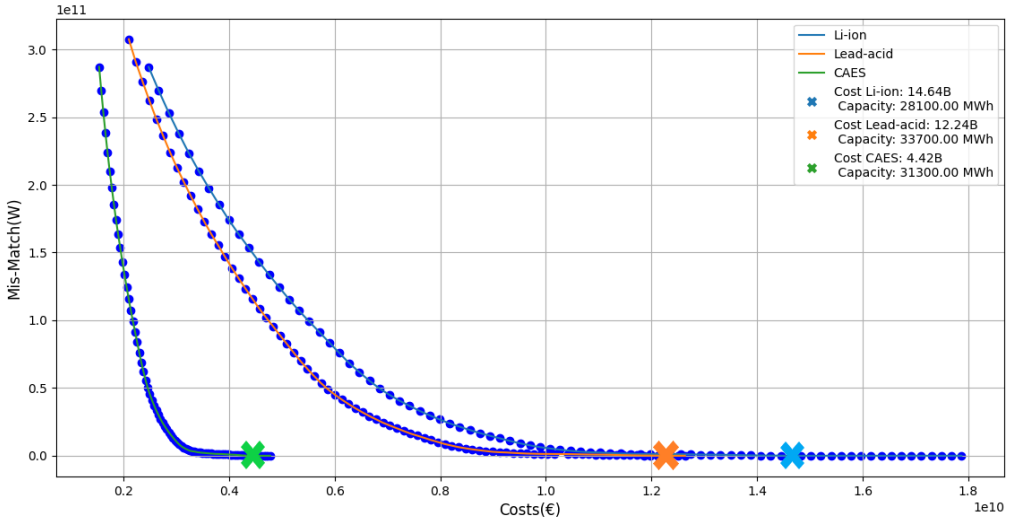


Figure 5.5: Cost-Mismatch Trade-offs for the three selected ESTs Base Case

A sensitivity analysis was conducted to investigate the relationship between storage technology parameters and the capital cost of the storage system. The parameter selected for this analysis was the efficiency of the storage technology, with values presented within the ranges specified in Table 3.1. Figures 5.6 and 5.7 illustrate the low-end and high-end efficiency points, respectively, within this range. Comparing these figures with the points (crosses) depicted in Figure 5.5, it is suggested that efficiency influences the total capital cost of the storage technologies. This influence can be observed through the changes in capital cost corresponding to different efficiency levels. While the relationship may not be strictly linear, a trend can be seen where variations in efficiency impact the overall cost. The comparison of Figure 5.6 with Figure 5.5 highlights this trend more clearly. At lower efficiency levels, the required storage capacity and consequently the total capital cost are significantly higher compared to scenarios with higher efficiency percentages. This is because lower efficiency necessitates more capacity to store the same amount of energy, leading to increased capital expenditure.

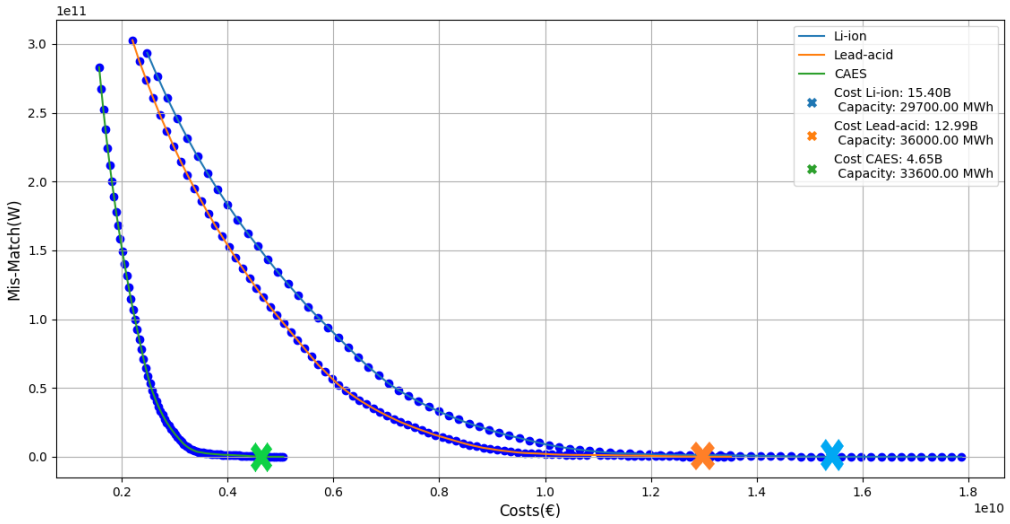


Figure 5.6: Impact of Low-End Efficiency on Cost-Mismatch Trade-offs for the three selected ESTs Base Case

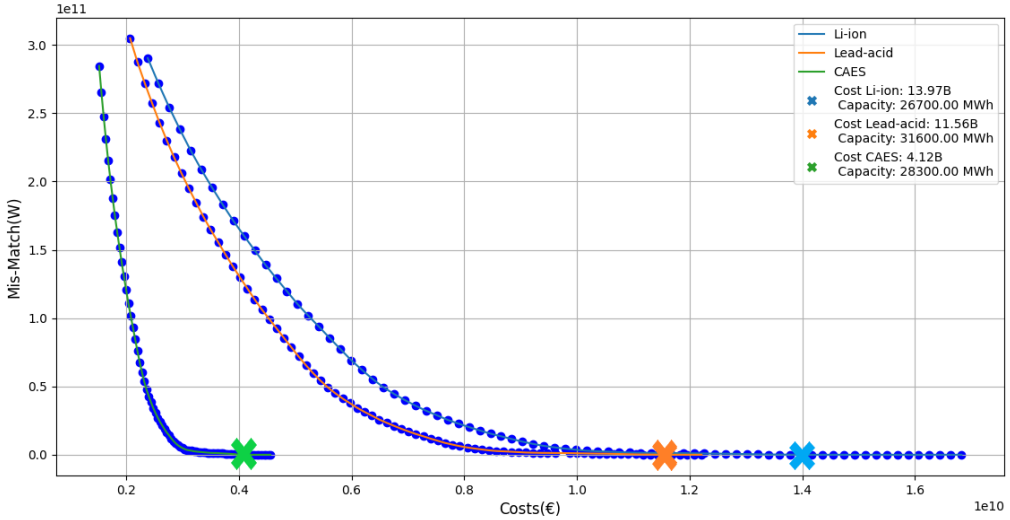


Figure 5.7: Impact of High-End Efficiency on Cost-Mismatch Trade-offs for the three selected ESTs Base Case

Finally referring to Figure 5.5, it is apparent that the representation of CAES is compressed due to the scale of the graph, making it challenging to discern its trend clearly. Referring to Figure 5.5, it is not immediately clear whether allowing for some excess energy generation or drawing energy from the grid would affect the total capital cost of the renewable energy system. Consequently, Figure 5.8 was developed to constrain scaling, offering a clear visual representation to facilitate analysis and decision-making. Allowing for excess energy generation involves producing more renewable energy than the immediate demand, which can be stored for later use or potentially curtailed if storage capacity is insufficient. This strategy can reduce the reliance on high-capacity storage systems, potentially lowering the capital costs associated with large-scale storage investments. However, it also requires an accurate assessment of the balance between generation, storage, and curtailment costs but this will not be analysed further in this thesis as it is not

part of the scope. Notably, examining the left side of Figure 5.8, allowing for a slight mismatch in energy generation and demand, presents the potential for significant reductions in capital costs. It becomes evident that with a mismatch ranging from 0.01 to $0.15 \times 10^{11}$, the capital cost could be reduced to approximately 0.5 billion euros.

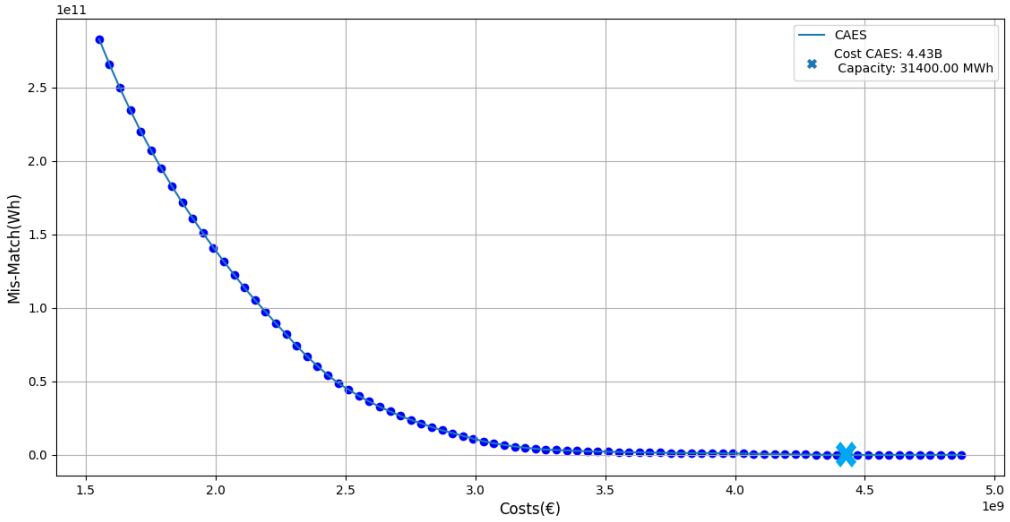


Figure 5.8: Cost-Mismatch Trade-offs for the CAES Base Case

## 5.2. Second Case: Optimum Wind and Solar mix

The main goal of this section is to determine the effects of varying the energy mix of the hybrid renewable energy system and to obtain the optimal energy mix. As detailed in Chapter 1 and Section 4.3, the profiles of wind power and solar power generation are promising when combined for a hybrid renewable energy system, due to their complementary nature. Further, by tuning the generation mix to closely match demand profile, it is possible to reduce the required storage capacity, as discussed in paper [86] and therefore also the capital cost of the system. Therefore, the percentage of solar power will be incrementally increased to evaluate its impact and identify the most efficient hybrid generation system configuration with the least annual negative mismatch. To achieve this, the analysis will proceed in two steps. In the first step, the optimal mix of wind and solar power will be determined without considering storage. This initial step will help identify the most effective combination of renewable sources based solely on their generation profiles and the required demand profile. Subsequently, the performance of this optimal mix will be evaluated with the inclusion of storage. By introducing storage, the analysis will determine how well the chosen mix can accommodate fluctuations in demand and generation, ultimately aiming to minimize the need for additional storage capacity and determine the effect it will have on the capital cost of the hybrid energy system.

By using Equations 3.17 to 3.26, an incremental analysis was performed to determine the lowest energy imbalance. Increments of 5% of solar mix were used from 0 to 100%. The focus is on periods where demand exceeds generation, computing the negative mismatch as shown in Equation 5.4. This parameter was identified as more accurate for the analysis required since the objective is to compensate for generation shortfalls to ensure reliability. By emphasizing the negative mismatch, the aim is to address and mitigate periods of energy deficit, thus enhancing the overall stability and performance of the hybrid renewable energy system.

$$M_{\text{neg}} = \sum_{t} \min(B(t), 0) \tag{5.4}$$

These incremental analysis results are illustrated in Figure (5.9).

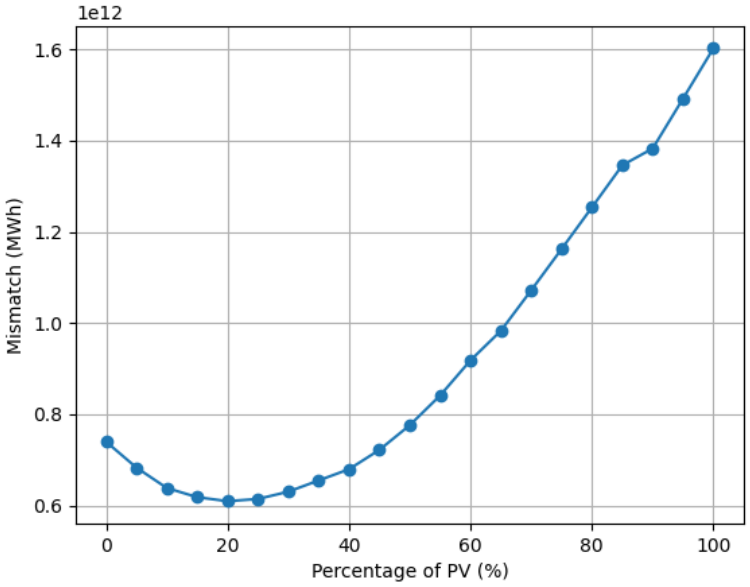


Figure 5.9: Negative Energy Imbalance Across Varying Solar Mix Percentages

From Figure 5.9, it can be deduced that the optimal energy mix is 80% wind and 20% solar. This outcome aligns with expectations due to the complementary nature of wind power generation patterns with power demand, and it is similar to the optimal energy mix concluded in literature [86], as the UK has similar weather conditions to the Netherlands. The results obtained from the incremental analysis together with the Base Case scenario results are depicted in Table 5.1 and Figure 5.10 below. These will be used as input for the model as outlined in Section 3.1.

Comparing the two cases, it is evident that the cumulative negative mismatch over a year, without storage, is significantly different. The optimal energy mix shows a reduction for the annual negative mismatch of 130.35 GWh, which is considered substantial. This demonstrates that determining the optimal energy mix effectively reduces the cumulative negative mismatch over a year.

Table 5.1: Simulation results comparing the Base Case and the Second Case

| Percentage (%) | Installed Wind Power(MW) | Installed Solar Power (MW) | Annual Negative Mismatch (GWh) |
|---|---|---|---|
| 0 | 760 | 0 | 739.90 |
| 20 | 610 | 538.37 | 609.55 |

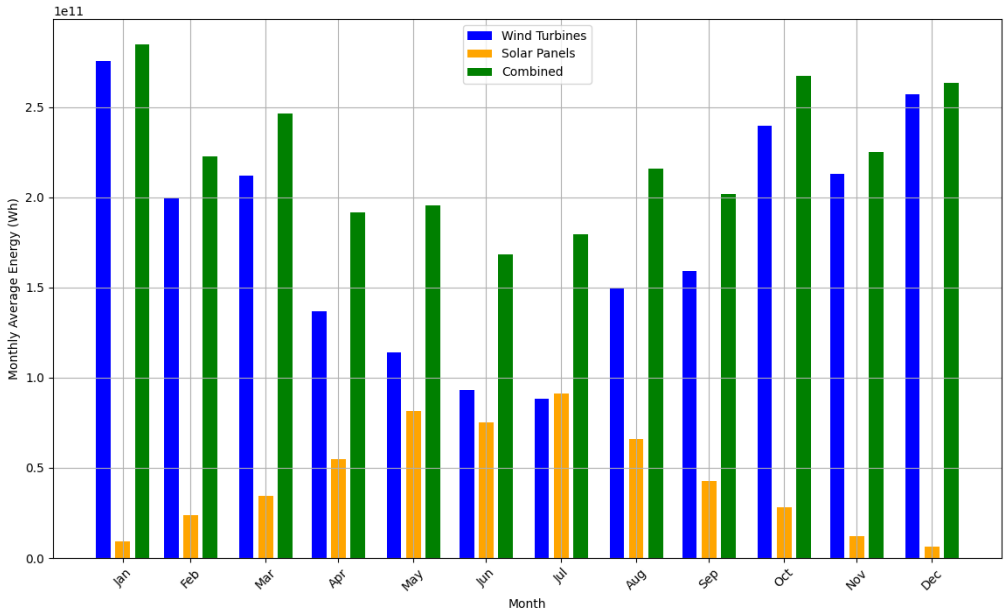


Figure 5.10: Monthly energy generation of solar and wind energy for the second case

Following the same methodology as described in the previous section and the workflow depicted in Figure (3.1) allows for determining the Pareto optimal solutions for the three selected storage technologies. The results of the Pareto optimal analysis are depicted in Figure 5.11. As expected, the hybrid energy system that includes CAES has the lowest capital cost requirement. Furthermore, comparing the capacities from the two cases reveals a noticeable decrease in the required storage capacity. For example, in CAES, the capacity was reduced from 31,300 MWh (Figure 5.5 to 24,800 MWh (Figure 5.11, thus the reduction is 6,500 MWh, which is considered substantial.

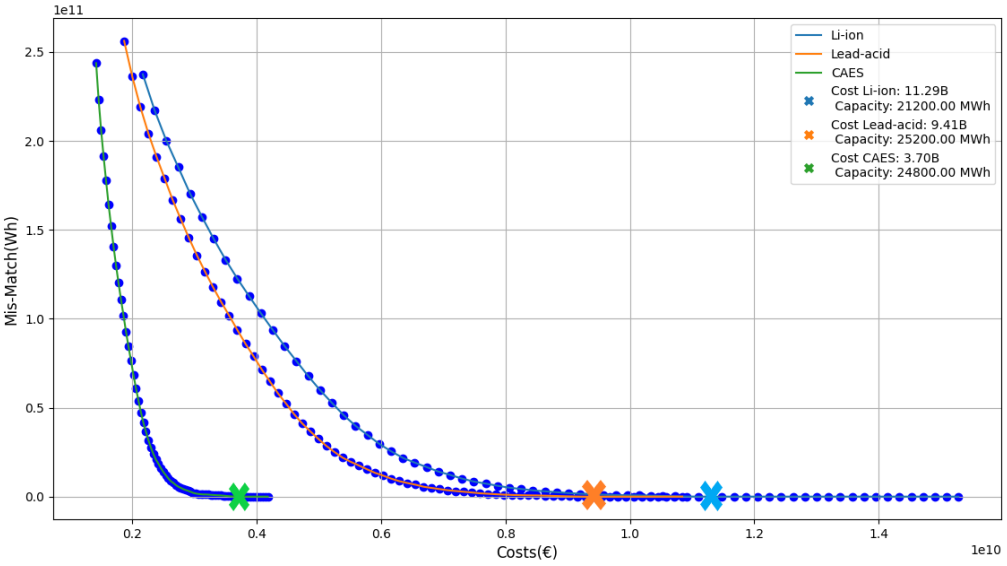


Figure 5.11: Cost-Mismatch Trade-offs for the three selected ESTs Second Case

Finally, as discussed in the Base Case, Figure 5.12 illustrates that a small amount of over-generation can lead to a significant reduction in capital costs. Comparing the misssmatch range from 0.01 to $0.15 \times 10^{11}$ Wh, the capital cost is reduced by approximately 1 billion euros.This point was further analysed in a paper [86], where the authors simulated various percentages of over-generation. They concluded that a small amount of over-generation (and subsequent curtailment) can reduce the need for energy storage and result in lower overall capital costs.

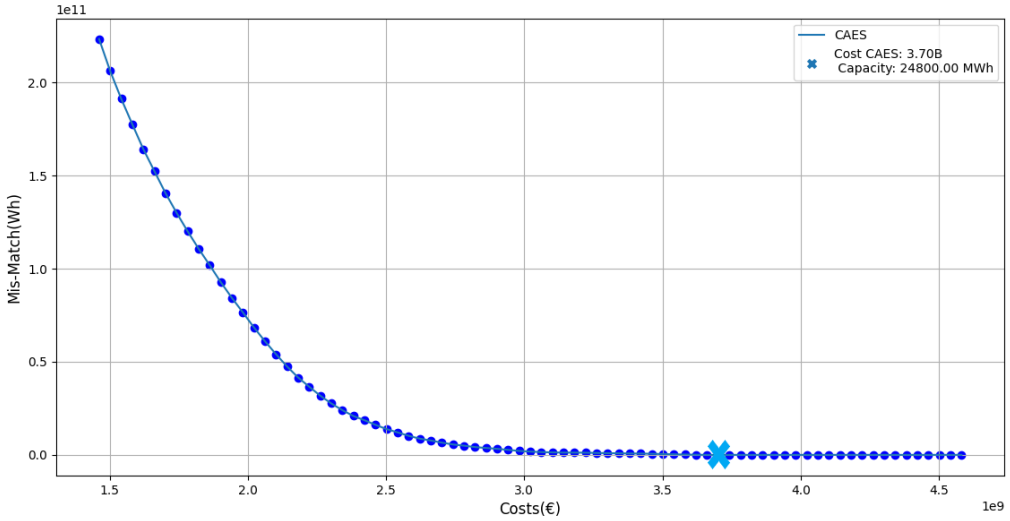


Figure 5.12: Cost-Mismatch Trade-offs for the CAES Second Case

# 6

# Conclusion and Recommendation

This is the final chapter of the paper and includes the conclusions derived from this thesis by answering the sub-objectives. Finally, recommendations for future work are also provided based on the outcome of the thesis.

## 6.1. Conclusion

This research evaluates the feasibility and effectiveness of integrating medium-term storage solutions into hybrid offshore renewable energy systems, specifically focusing on offshore wind and solar energy generation. The main objective is to develop the building blocks necessary to identify the optimal medium-term storage technology that aligns electricity generation from a hybrid offshore system with the desired demand. Through this study, three sub-objectives have been addressed and are now concluded:

First, the complementary nature of wind and solar energy sources was analyzed by examining the specified location, weather data, and electricity demand. Wind power exhibits higher short-term variability, while solar power offers predictable daily and seasonal patterns. When combined, these energy sources mitigate overall intermittency, enhancing the system's reliability. This finding underscores the importance of leveraging the complementary characteristics of wind and solar power in hybrid systems. By tuning the generation mix to closely match the generation profile with the demand profile, it is possible to reduce the required storage capacity.

Secondly, a Multi-Criteria Analysis (MCA) was employed to evaluate eight different energy storage technologies. These technologies were assessed using six criteria, which identified Compressed Air Energy Storage (CAES), Lithium-ion batteries, and Lead-acid batteries as the most suitable options for medium-term applications.

Thirdly, a multi-objective optimization approach was applied, focusing on minimizing net power capacity mismatch and total capital costs associated with the hybrid renewable energy system. Two energy mix scenarios were discussed: the base case and the optimized scenario. The base case, which examines a 100% wind power configuration, revealed CAES as the medium-term storage technology with the lowest total capital cost. Its lower total capital costs and high efficiency make it an attractive option for enhancing the reliability and economic viability of renewable energy systems.

In the optimized scenario, the study highlights the importance of the complementary nature of wind and solar power, resulting in an optimal energy mix of 80% offshore wind and 20% solar power. This configuration substantially decreases the net power capacity mismatch, thus reducing the total capital cost of the renewable hybrid system.

This thesis not only addresses the variability of renewable energy sources but also provides a robust framework for investigating, choosing and analysing future energy storage solutions. It contributes to the strategic planning and development of sustainable energy systems by offering a viable path for integrating renewable energy sources with efficient medium-term storage technologies.

## 6.2. Recommendations

From the methodology and logic used in this thesis, the research yielded some interesting findings. However, some recommendations can be made for future research. Due to time constraints and the limited resources

available for this thesis, certain simplifications were necessary.

### 6.2.1. Increase Weather Data Accuracy

The simulation study employed an hourly average for wind speed, solar radiation, and power demand, utilizing a one-hour time step to assess the general hourly performance of the generating system. This choice assumes constant conditions within each hour, though acknowledging the inherent intermittency of wind and solar resources. While this simplification doesn't significantly impact the overall hourly response, it may not accurately capture system behavior when detailed variability is of interest. Incorporating stochastic distribution curves, such as the Weibull distribution for wind, can address this by adjusting power generation within each hour. Previous research comparing hourly and 15-minute wind data showed minimal impact on general hourly wind power generation. For a more detailed system response, smaller simulation time steps (e.g., 15 minutes or one minute) can be used with corresponding data availability.

### 6.2.2. Seasonal Data Utilization

Utilizing seasonal data for the simulation study can enhance the accuracy of results, considering the seasonal variability of wind speed, solar radiation, and power demand. This approach not only improves system performance across different seasons but also enables informed engineering decisions regarding the sizing of system components based on season-specific outcomes [87]. Especially in the paper [86], it is evident that sizing an energy store based on monthly scenarios may not adequately address the variations in demand and generation throughout the year. For instance, using a single year's data for storage sizing might not be sufficient to meet demand in some years. This underscores the importance of considering inter-annual variability in renewables, indicating that the storage capacity required to manage such variability may be several times larger than what analyses based on a single year might suggest. This limitation was also discussed in Subsection ?? and is also visible from the results that were obtained from Figure 4.10.

### 6.2.3. Weather Forecasting

Renewable energy forecasting is critical for reducing the uncertainty associated with renewable energy generation, given the highly intermittent and variable nature of these sources. Accurate forecasting enables better decision-making and improves the accuracy and realism of data analysis. However, as discussed in this thesis and stated in Subsection 4.2, this aspect was beyond the scope of the current thesis and was not further investigated or incorporated into the data collection and analysis. Nevertheless, from paper [88], various forecasting models, including physical models, statistical models, artificial intelligence-based models, and machine learning and deep learning models, were identified. Through further research, these models could be implemented in the control strategy of this thesis to enhance the overall effectiveness and reliability of the energy management system.

### 6.2.4. Model Predictive Control (MPC)

Optimizing charging and discharging strategies is critical for the efficient management of medium-term energy storage systems in hybrid offshore power systems. Strategies relying on predictive algorithms, such as weather and energy demand forecasting, are essential for anticipating fluctuations in energy availability. Model Predictive Control (MPC) combined with stochastic optimization techniques offers a robust approach for optimizing the operation of storage systems. MPC employs predictive models of system dynamics to optimize control actions over a defined time horizon. By integrating stochastic optimization, which addresses uncertainties inherent in factors like energy demand and renewable energy generation, MPC can effectively enhance efficiency and cost-effectiveness in managing energy storage [89] and [90].

### 6.2.5. Integration of more Renewable Technologies and strategies for grid flexibility

A renewable energy system should not solely rely on variable renewable energy technologies such as PV and wind. Further optimization can be achieved by integrating other carbon-neutral and flexible options like biomass. Leveraging these technologies can reduce the required storage capacity[86]. To further enhance the system's efficiency, exploring various strategies for grid flexibility is essential. Demand-side management (DSM) is a key approach that involves adjusting consumer demand to match supply conditions, which helps alleviate grid stress during peak periods [91]. Other strategies include interconnecting different grids to balance generation and demand across regions and implementing supply response techniques. These approaches can significantly reduce the storage capacity required and should be considered in the

optimization process. By integrating these technologies and strategies, the hybrid energy system can achieve a lower mismatch and reduced capital costs, optimizing the overall performance.

# References


[1] energy agency. CO2 Emissions in 2022. Tech. rep. France: IEA, Mar. 2022. URL: https://www.iea.org/reports/co2-emissions-in-2022.

[2] IEA. Renewables 2022. Tech. rep. Paris, Dec. 2022.

[3] Guido Francesco Frate et al. "Energy storage for grid-scale applications: Technology review and economic feasibility analysis". In: Renewable Energy 163 (Jan. 2021), pp. 1754–1772. DOI: 10.1016/J.RENENE.2020.10.070.

[4] Marc Beaudin et al. "Energy storage for mitigating the variability of renewable electricity sources: An updated review". In: Energy for Sustainable Development 14.4 (Dec. 2010), pp. 302–314. DOI: 10.1016/J.ESD.2010.09.007.

[5] Bruno Cárdenas et al. "Short-, medium-, and long-duration energy storage in a 100% renewable electricity grid: A UK case study". In: Energies 14.24 (Dec. 2021). DOI: 10.3390/en14248524.

[6] Clemens van Gessel. Vattenfall's largest hybrid energy park is taking shape in the Netherlands. June 2020. URL: https://group.vattenfall.com/press-and-media/newsroom/2020/vattenfalls-largest-hybrid-energy-park-is-taking-shape-in-the-netherlands.

[7] Sonal Patel. A Fine Balance: Building One of Europe's Largest Hybrid Facilities. Aug. 2022. URL: https://www.powermag.com/a-fine-balance-building-one-of-europes-largest-hybrid-facilities/.

[8] David Vetter. China installed more offshore wind generation capacity than every other country installed over the last five years. Jan. 2022. URL: https://www.forbes.com/sites/davidrvetter/2022/01/26/china-built-more-offshore-wind-in-2021-than-every-other-country-built-in-5-years/?sh=1852cc9e4634.

[9] Darrell Proctor. China Unveils World's First Commercial Offshore Wind-Plus-Solar Project. Nov. 2022. URL: https://www.powermag.com/china-unveils-worlds-first-commercial-offshore-wind-plus-solar-project/.

[10] Igor Todorović. China completes world's first hybrid offshore wind-solar power plant. Nov. 2022. URL: https://balkangreenenergynews.com/china-completes-worlds-first-hybrid-offshore-wind-solar-power-plant/.

[11] J. P. Coelingh et al. "Analysis of wind speed observations over the North Sea". In: Journal of Wind Engineering and Industrial Aerodynamics 61.1 (June 1996), pp. 51–69. DOI: 10.1016/0167-6105(96)00043-8.

[12] J. P. Coelingh et al. "Analysis of wind speed observations on the North Sea coast". In: Journal of Wind Engineering and Industrial Aerodynamics 73.2 (Feb. 1998), pp. 125–144. DOI: 10.1016/S0167-6105(97)00285-7.

[13] Ronald B Stull. Practical meteorology: an algebra-based survey of atmospheric science. University of British Columbia, 2015.

[14] Simon P. Neill et al. "Offshore Wind". In: Fundamentals of Ocean Renewable Energy (Jan. 2018), pp. 83–106. DOI: 10.1016/B978-0-12-810448-4.00004-5.

[15] Seamus Garvey. Medium Duration Energy Storage. Presented at the Medium-Duration Energy Storage conference,IMechE. London, Mar. 2022.

[16] Marco Dean. A Practical Guide to Multi-Criteria Analysis. June 2022. DOI: 10.13140/RG.2.2.15007.02722. URL: https://www.researchgate.net/publication/358131153_A_Practical_Guide_to_Multi-Criteria_Analysis.

[17] Kambiz Shahroodi et al. “Application of Analytical Hierarchy Process (AHP) Technique to Evaluate and Selecting Suppliers in an Effective Supply Chain”. In: (June 2012). URL: https://www.researchgate.net/publication/256017441_Application_of_Analytical_Hierarchy_Process_AHP_Technique_to_Evaluate_and_Selecting_Suppliers_in_an_Effective_Supply_Chain.

[18] Omkarprasad S. Vaidya et al. “Analytic hierarchy process: An overview of applications”. In: European Journal of Operational Research 169.1 (Feb. 2006), pp. 1–29. DOI: 10.1016/J.EJOR.2004.04.028.

[19] A. B. Gallo et al. “Energy storage in the energy transition context: A technology review”. In: Renewable and Sustainable Energy Reviews 65 (Nov. 2016), pp. 800–822. DOI: 10.1016/J.RSER.2016.07.028.

[20] Mathew Aneke et al. “Energy storage technologies and real life applications – A state of the art review”. In: Applied Energy 179 (Oct. 2016), pp. 350–377. DOI: 10.1016/J.APENERGY.2016.06.097.

[21] Hasan Abumeteir et al. “The Determining Factors of Selecting Energy Storage Systems for the Renewable Energy Sources in the Energy- Efficient Building”. In: May 2016.

[22] Murat Çolak et al. “Multi-criteria evaluation of energy storage technologies based on hesitant fuzzy information: A case study for Turkey”. In: Journal of Energy Storage 28 (Apr. 2020), p. 101211. DOI: 10.1016/J.EST.2020.101211.

[23] Jingzheng Ren. “Sustainability prioritization of energy storage technologies for promoting the development of renewable energy: A novel intuitionistic fuzzy combinative distance-based assessment approach”. In: Renewable Energy 121 (June 2018), pp. 666–676. DOI: 10.1016/J.RENENE.2018.01.087.

[24] Dalia Štreimikiene et al. “Multi-criteria analysis of electricity generation technologies in Lithuania”. In: Renewable Energy 85 (Jan. 2016), pp. 148–156. DOI: 10.1016/J.RENENE.2015.06.032.

[25] Mads Troldborg et al. “Assessing the sustainability of renewable energy technologies using multi-criteria analysis: Suitability of approach for national-scale assessments and associated uncertainties”. In: Renewable and Sustainable Energy Reviews 39 (Nov. 2014), pp. 1173–1184. DOI: 10.1016/J.RSER.2014.07.160.

[26] Wolf Dieter Steinmann. “Overview of the Section on Mechanical Energy Storage”. In: Encyclopedia of Energy Storage: Volume 1-4 1-4 (Jan. 2022), pp. 1–4. DOI: 10.1016/B978-0-12-819723-3.00152-9.

[27] Andrew Blakers et al. “A review of pumped hydro energy storage”. In: Progress in Energy 3.2 (Mar. 2021), p. 22003. DOI: 10.1088/2516-1083/abeb5b. URL: https://dx.doi.org/10.1088/2516-1083/abeb5b.

[28] Seamus D. Garvey et al. “Compressed air energy storage (CAES)”. In: Storing Energy: with Special Reference to Renewable Energy Sources (Jan. 2022), pp. 117–140. DOI: 10.1016/B978-0-12-824510-1.00031-3.

[29] T. Kousksou et al. “Energy storage: Applications and challenges”. In: Solar Energy Materials and Solar Cells 120.PART A (Jan. 2014), pp. 59–80. DOI: 10.1016/J.SOLMAT.2013.08.015.

[30] Xing Luo et al. “Overview of Current Development in Compressed Air Energy Storage Technology”. In: Energy Procedia 62 (2014), pp. 603–611. DOI: https://doi.org/10.1016/j.egypro.2014.12.423. URL: https://www.sciencedirect.com/science/article/pii/S1876610214034547.

[31] Andrea Vecchi et al. “Liquid air energy storage (LAES): A review on technology state-of-the-art, integration pathways and future perspectives”. In: Advances in Applied Energy 3 (2021), p. 100047. DOI: https://doi.org/10.1016/j.adapen.2021.100047. URL: https://www.sciencedirect.com/science/article/pii/S2666792421000391.

[32] Yulong Ding et al. “10 - Liquid air energy storage”. In: Storing Energy (Second Edition). Ed. by Trevor M Letcher. Second Edition. Elsevier, 2022, pp. 191–205. DOI: https://doi.org/10.1016/B978-0-12-824510-1.00014-3. URL: https://www.sciencedirect.com/science/article/pii/B9780128245101000143.

[33] S. X. Wang et al. “The Application of Cryogens in Liquid Fluid Energy Storage Systems”. In: Physics Procedia 67 (Jan. 2015), pp. 728–732. DOI: 10.1016/J.PHPRO.2015.06.123.

[34] Qian Zhu. High-efficiency power generation – review of alternative systems. IEA Clean Coal Centre, Mar. 2015.

[35] Shuozhuo Hu et al. “Thermo-economic analysis of the pumped thermal energy storage with thermal integration in different application scenarios”. In: Energy Conversion and Management 236 (2021), p. 114072. DOI: https://doi.org/10.1016/j.enconman.2021.114072. URL: https://www.sciencedirect.com/science/article/pii/S019689042100248X.

[36] Zhenguo Yang et al. “Electrochemical Energy Storage for Green Grid”. In: Chemical Reviews 111.5 (2011), pp. 3577–3613. DOI: 10.1021/cr100290v. URL: https://doi.org/10.1021/cr100290v.

[37] Haisheng Chen et al. “Progress in electrical energy storage systems: a critical review. Prog Nat Sci”. In: Progress in Natural Science 19 (Sept. 2009), pp. 291–312. DOI: 10.1016/j.pnsc.2008.07.014.

[38] Helder Lopes Ferreira et al. “Characterisation of electrical energy storage technologies”. In: Energy 53 (2013), pp. 288–298. DOI: https://doi.org/10.1016/j.energy.2013.02.037. URL: https://www.sciencedirect.com/science/article/pii/S0360544213001515.

[39] Yangtao Liu et al. “Current and future lithium-ion battery manufacturing”. In: iScience 24.4 (2021), p. 102332. DOI: https://doi.org/10.1016/j.isci.2021.102332. URL: https://www.sciencedirect.com/science/article/pii/S258900422100300X.

[40] Peter Keil et al. “Lifetime Analyses of Lithium-Ion EV Batteries”. In: Sept. 2015.

[41] Álvaro Cunha et al. “Vanadium redox flow batteries: a technology review”. In: International Journal of Energy Research 39.7 (Oct. 2014), pp. 889–918. DOI: https://doi.org/10.1002/er.3260. URL: https://onlinelibrary.wiley.com/doi/abs/10.1002/er.3260.

[42] Aishwarya Parasuraman et al. “Review of material research and development for vanadium redox flow battery applications”. In: Electrochimica Acta 101 (2013), pp. 27–40. DOI: https://doi.org/10.1016/j.electacta.2012.09.067. URL: https://www.sciencedirect.com/science/article/pii/S0013468612015459.

[43] IRENA. Electricity Storage and Renewables: Costs and Markets to 2030, International Renewable Energy Agency. Tech. rep. Abu Dhabi: International Renewable Energy Agency, 2017.

[44] Paul Breeze. “Compressed Air Energy Storage”. In: Power System Energy Storage Technologies (Jan. 2018), pp. 23–31. DOI: 10.1016/B978-0-12-812902-9.00003-1. URL: https://linkinghub.elsevier.com/retrieve/pii/B9780128129029000031.

[45] Abdelhamid Kaabeche et al. “Techno-economic optimization of hybrid photovoltaic/wind/diesel/battery generation in a stand-alone power system”. In: Solar Energy 103 (2014), pp. 171–182. DOI: https://doi.org/10.1016/j.solener.2014.02.017. URL: https://www.sciencedirect.com/science/article/pii/S0038092X14000954.

[46] Stefan Emeis et al. “Comparison of Logarithmic Wind Profiles and Power Law Wind Profiles and their Applicability for Offshore Wind Profiles”. In: June 2007, pp. 61–64. DOI: 10.1007/978-3-540-33866-6{_}11.

[47] C. A. Lopez-Villalobos et al. “Analysis of the influence of the wind speed profile on wind power production”. In: Energy Reports 8 (Nov. 2022), pp. 8079–8092. DOI: 10.1016/J.EGYR.2022.06.046.

[48] Parikshit Jamdade et al. “Assessment of Power Coefficient of an Offline Wind Turbine Generator System”. In: Electronic Journal of Energy & Environment 1 (June 2013). DOI: 10.7770/ejee-V1N3-art683.

[49] Amir R. Nejad et al. “Drivetrains on floating offshore wind turbines: lessons learned over the last 10 years Antriebsstränge in schwimmenden Offshore-Windkraftanlagen: Erkenntnisse der letzten 10 Jahres”. In: Forschung im Ingenieurwesen 85 (June 2021). DOI: 10.1007/s10010-021-00469-8. URL: https://www.researchgate.net/publication/350468646_Drivetrains_on_floating_

offshore_wind_turbines_lessons_learned_over_the_last_10_yearsAntriebsstrange_in_schwimmenden_Offshore-Windkraftanlagen_Erkenntnisse_der_letzten_10_Jahres.

[50] Rabia Shakoor et al. “Wake effect modeling: A review of wind farm layout optimization using Jensen s model”. In: Renewable and Sustainable Energy Reviews 58 (May 2016), pp. 1048–1059. DOI: 10.1016/J.RSER.2015.12.229. URL: https://www.sciencedirect.com/science/article/pii/S1364032115016123.

[51] R Barthelmie et al. “Modelling and Measuring Flow and Wind Turbine Wakes in Large Wind Farms Offshore”. In: Wind Energy 12 (June 2009), pp. 431–444. DOI: 10.1002/we.348.

[52] Reza Hassanian et al. “A Practical Approach for Estimating the Optimum Tilt Angle of a Photovoltaic Panel for a Long Period—Experimental Recorded Data”. In: 1 (June 2021), pp. 41–51. DOI: 10.3390/solar1010005.

[53] Arno Smets et al. Solar Energy: The physics and engineering of photovoltaic conversion, technologies and systems. UIT Cambridge, 2015.

[54] Sugianto Sugianto. “Comparative Analysis of Solar Cell Efficiency between Monocrystalline and Polycrystalline”. In: INTEK: Jurnal Penelitian 7 (June 2020), p. 92. DOI: 10.31963/intek.v7i2.2625.

[55] Vladan Durkovic et al. “Analysis of the Potential for Use of Floating PV Power Plant on the Skadar Lake for Electricity Supply of Aluminium Plant in Montenegro”. In: Energies 10 (June 2017), p. 1505. DOI: 10.3390/en10101505.

[56] Adimas Pradityo Sukarso et al. “Cooling Effect on the Floating Solar PV: Performance and Economic Analysis on the Case of West Java Province in Indonesia”. In: Energies 13.9 (2020). DOI: 10.3390/en13092126. URL: https://www.mdpi.com/1996-1073/13/9/2126.

[57] Máté János Lőrincz et al. “Chapter 2 - Structural analysis of energy demand”. In: Handbook of Energy Economics and Policy. Ed. by Alessandro Rubino et al. Academic Press, 2021, pp. 67–107. DOI: https://doi.org/10.1016/B978-0-12-814712-2.00002-6. URL: https://www.sciencedirect.com/science/article/pii/B9780128147122000026.

[58] Bengt Sundén. “Thermal management of batteries”. In: Hydrogen, Batteries and Fuel Cells (Jan. 2019), pp. 93–110. DOI: 10.1016/B978-0-12-816950-6.00006-3.

[59] Tao Hong et al. “Calculating line losses in smart grid: A new rule of thumb”. In: IEEE PES T&D 2010. 2010, pp. 1–5. DOI: 10.1109/TDC.2010.5484368.

[60] Ward Bower et al. Performance Test Protocol for Evaluating Inverters Used in Grid-Connected Photovoltaic Systems Prepared by. Tech. rep. 2004.

[61] Paul Cosgrove et al. “Intermittency and periodicity in net-zero renewable energy systems with storage”. In: Renewable Energy 212 (Aug. 2023), pp. 299–307. DOI: 10.1016/J.RENENE.2023.04.135.

[62] Aixia Yuan et al. “A Novel Band-Stop Filter with Band-Pass, High-Pass, and Low-Pass Negative Group Delay Characteristics”. In: International Journal of Antennas and Propagation 2021 (Oct. 2021), pp. 1–15. DOI: 10.1155/2021/3207652.

[63] Jonathan M. Blackledget. “The Fourier Transform”. In: Digital Signal Processing (Jan. 2006), pp. 75–113. DOI: 10.1533/9780857099457.1.75. URL: https://linkinghub.elsevier.com/retrieve/pii/B9781904275268500051.

[64] Mokhtar Shouran et al. “Design and Implementation of Butterworth Filter”. In: International Journal of Innovative Research in Science Engineering and Technology 9 (Oct. 2020), p. 7975.

[65] MathWorks. Zero-phase digital filtering - MATLAB. 2023. URL: https://www.mathworks.com/help/signal/ref/filtfilt.html.

[66] Ibrahim Kyari et al. “Hybrid Renewable Energy Systems for Electrification: A Review”. In: Science Journal of Circuits, Systems and Signal Processing 8 (June 2019). DOI: 10.11648/j.cssp.20190802.11.

[67] Sunanda Sinha et al. “Review of software tools for hybrid renewable energy systems”. In: Renewable and Sustainable Energy Reviews 32 (Apr. 2014), pp. 192–205. DOI: 10.1016/J.RSER.2014.01.035.

[68] Hongxing Yang et al. “Optimal design and techno-economic analysis of a hybrid solar-wind power generation system”. In: Applied Energy 86.2 (2009), pp. 163–169. DOI: 10.1016/j.apenergy.2008.03.008.

[69] M. Thirunavukkarasu et al. “A comprehensive review on optimization of hybrid renewable energy systems using various optimization techniques”. In: Renewable and Sustainable Energy Reviews 176 (Apr. 2023), p. 113192. DOI: 10.1016/J.RSER.2023.113192.

[70] Kalyan Deb. “Multiobjective Optimization Using Evolutionary Algorithms. Wiley, New York”. In: Aug. 2001.

[71] Hasan Y. Alhammadi et al. “Process design and operation: Incorporating environmental, profitability, heat integration and controllability considerations”. In: Computer Aided Chemical Engineering 17.C (Jan. 2004), pp. 264–305. DOI: 10.1016/S1570-7946(04)80063-4.

[72] Er Mohapatra et al. “Multi-Objective Genetic Algorithm: A Comprhensive Survey”. In: (Aug. 2012).

[73] Wilfried Jakob et al. “Pareto Optimization or Cascaded Weighted Sum: A Comparison of Concepts”. In: Algorithms 7 (Aug. 2014), pp. 166–185. DOI: 10.3390/a7010166.

[74] Vignesh Ramasamy et al. Floating Photovoltaic System Cost Benchmark: Q1 2021 Installations on Artificial Water Bodies. Tech. rep. Denver: National Renewable Energy Laboratory, Oct. 2021. URL: www.nrel.gov/publications..

[75] The Crown Estate. Published on behalf of The Crown Estate and the Offshore Renewable Energy Catapult Guide to an offshore wind farm Subtitle Guide to an offshore wind farm The Crown Estate Offshore Renewable Energy Catapult. Tech. rep. 2019. URL: www.thecrownestate.co.uk.

[76] International Renewable Energy Agency. RENEWABLE ENERGY TECHNOLOGIES: COST ANALYSIS SERIES Volume 1: Power Sector Acknowledgement. Tech. rep. Bonn: IRENA, 2012. URL: www.irena.org/Publications.

[77] PBL Planbureau voor de Leefomgeving. COSTS OF OFFSHORE WIND ENERGY 2018 Note Sander Lensink and Iulia Pisca. Tech. rep. 2018. URL: www.pbl.nl/en..

[78] Kendall Mongird et al. “An Evaluation of Energy Storage Cost and Performance Characteristics”. In: Energies 13 (Apr. 2020), p. 3307. DOI: 10.3390/en13133307.

[79] Exchange Rates.org.uk. US Dollar to Euro Spot Exchange Rates for 2023. May 2024. URL: https://www.exchangerates.org.uk/USD-EUR-spot-exchange-rates-history-2023.html.

[80] The Netherlands Enterprise Agency. Dutch Offshore Wind Guide. Tech. rep. 2022. URL: https://windandwaterworks.nl/about.

[81] IEA. Renewable Electricity. Tech. rep. Paris: IEA, Sept. 2022. URL: https://www.iea.org/reports/renewable-electricity.

[82] Government of the Netherlands. Offshore wind energy. 2022. URL: https://www.government.nl/topics/renewable-energy/offshore-wind-energy.

[83] Richard Cullather et al. NASA’s MERRA2 reanalysis. URL: https://climatedataguide.ucar.edu/climate-data/nasas-merra2-reanalysis#:~:text=The%20Modern%2DEra%20Retrospective%20analysis,from%201980%20to%20the%20present.

[84] Christian Bak et al. The DTU 10-MW Reference Wind Turbine. English. 2013.

[85] H Hersbach et al. ERA5 hourly data on single levels from 1940 to present. May 2024. DOI: 10.24381/cds.adbb2d47. URL: https://cds.climate.copernicus.eu/cdsapp#!/dataset/reanalysis-era5-single-levels?tab=form.

[86] Bruno Cárdenas et al. “Energy storage capacity vs. renewable penetration: A study for the UK”. In: Renewable Energy 171 (June 2021), pp. 849–867. DOI: 10.1016/J.RENENE.2021.02.149.

[87] M Hashem Nehrir et al. “An approach to evaluate the general performance of stand-alone wind/photovoltaic generating systems”. In: Energy Conversion, IEEE Transactions on 15 (Mar. 2001), pp. 433–439. DOI: 10.1109/60.900505.

[88] Rajasekaran Meenal et al. “Weather Forecasting for Renewable Energy System: A Review”. In: Archives of Computational Methods in Engineering 29 (June 2022). DOI: 10.1007/s11831-021-09695-3.

[89] Bernhard Thaler et al. “Hybrid model predictive control of renewable microgrids and seasonal hydrogen storage”. In: International Journal of Hydrogen Energy 48.97 (2023), pp. 38125–38142. DOI: https://doi.org/10.1016/j.ijhydene.2023.06.067. URL: https://www.sciencedirect.com/science/article/pii/S0360319923029269.

[90] Masoud Sharafi et al. “Stochastic Optimization of Hybrid Renewable Energy Systems Using Sampling Average Method”. In: Renewable and Sustainable Energy Reviews 52 (June 2015). DOI: 10.1016/j.rser.2015.08.010.

[91] Joseph Elio et al. “Renewable Energy Systems for Demand-Side Management in Industrial Facilities”. In: June 2021. DOI: 10.1115/POWER2021-64381.

[92] Monocrystalline Solar Modules. Solar Power Supply. URL: https://cdn.solarpowersupply.eu/files/_166%20Mono%20400W-66%20Technical%20Data%20Sheet1906X1043X35-compressed-20221227.pdf.

[93] CanadianSolar. HiKu6 Mono PERC. Aug. 2022. URL: https://static.csisolar.com/wp-content/uploads/sites/3/2022/02/18013254/CS-Datasheet-HiKu6_CS6R-MS-HL_v1.1C25_F23_J1_NA.pdf.

[94] Eagle module. EAGLE CONTINENTAL. URL: https://jinkosolar.us/wp-content/uploads/2022/09/EAGLE-Continental-JKM380-400M-72HBL-V-F1-US.pdf.

# A

# Appendix

**Solar Power Supply**

### Electrical Characteristics

| | |
|---|---|
| Model No. | SPS-M400 |
| Maximum Power (Pmax) | 400W |
| Max-power Voltage (Vmp) | 37.62V |
| Max-power Current (Imp) | 10.64A |
| Open-circuit Voltage (Voc) | 45.52V |
| Short-circuit Current (Isc) | 11.27A |
| Module Efficiency | 20.12% |
| Operating Temperature | -40℃~+85℃ |
| Maximum System Voltage | 1000Vdc |
| Maximum Series Fuse Rating | 15A |
| Power Tolerance | ±5% |

*STC condition：1000 W/m²,1.5AM and 25℃ cell temperature.

### Temperature Characteristics

| | |
|---|---|
| NMOT | 46℃±2℃ |
| Temperature Co-efficient of Pmax | -0.398%/℃ |
| Temperature Co-efficient of Voc | -0.340%/℃ |
| Temperature Co-efficient of Isc | 0.0576%/℃ |

### Mechanical Characteristics

| | |
|---|---|
| Mono Power | 400W |
| Cell Type | Mono 166mm |
| Cell Arrangement | 66(6*11) |
| Dimensions | 1906*1043*35mm |
| Weight | 20.5kg |
| Front Cover | 3.2mm tempered glass |
| Frame Material | Anodized aluminium alloy |
| Junction Box | IP67 rated |
| Output Cables | 4mm²,Length 900mm+MC4 |

*All specifications and data described in this data sheet are tested under Standard Test Conditions (STC - Irradiance: 1000W/m₂ , Temperature: 25 C,
Air Mass: 1.5) and may deviate marginally from actual values. Solar Power Supply and any of its affiliates has reserved the right to make any modifications to the information on this data sheet without notice. It is our goal to supply our customers with the most recent information regarding our products. These data sheets can be found in the downloads section of our website, www.solarpowersupply.eu

### I-V Curve

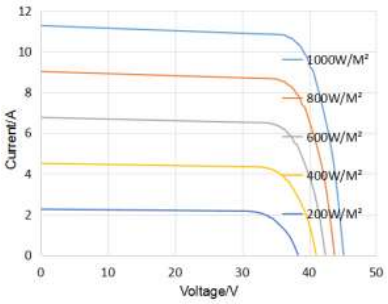


### Module Diagram

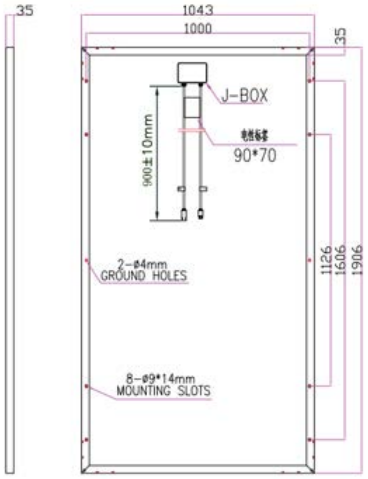


MONOCRYSTALLINE SOLAR MODULES

Figure A.1: Technical data sheet for the 400W Mono 166 PV panel [92].

## ENGINEERING DRAWING (mm)

Rear View

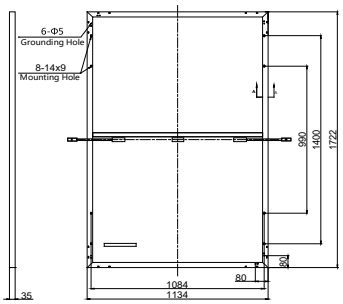


Frame Cross Section A-A

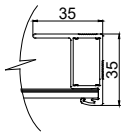


Mounting Hole

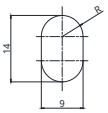


## CS6R-405MS-HL / I-V CURVES

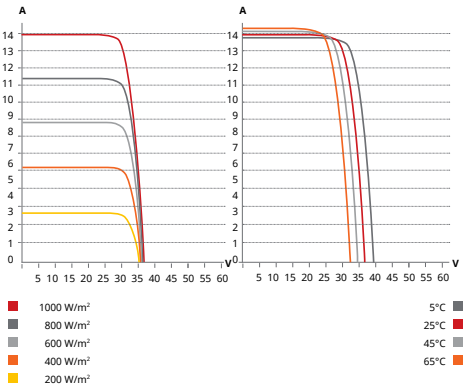


## ELECTRICAL DATA | STC*

CS6R-395/400/405/410/415/420MS-HL

| | | | | | | |
|---|---|---|---|---|---|---|
| Nominal Max. Power (Pmax) | 395 W | 400 W | 405 W | 410 W | 415 W | 420 W |
| Opt. Operating Voltage (Vmp) | 30.6 V | 30.8 V | 31.0 V | 31.2 V | 31.4 V | 31.6 V |
| Opt. Operating Current (Imp) | 12.91 A | 12.99 A | 13.07 A | 13.15 A | 13.23 A | 13.31 A |
| Open Circuit Voltage (Voc) | 36.6 V | 36.8 V | 37.0 V | 37.2 V | 37.4 V | 37.6 V |
| Short Circuit Current (Isc) | 13.77 A | 13.85 A | 13.93 A | 14.01 A | 14.09 A | 14.17 A |
| Module Efficiency | 20.2% | 20.5% | 20.7% | 21.0% | 21.3% | 21.5% |
| Operating Temperature | -40°C ~ +85°C | | | | | |
| Max. System Voltage | 1000V (IEC/UL) | | | | | |
| Module Fire Performance | TYPE 2 (UL 61730 1000V) or CLASS C (IEC 61730) | | | | | |
| Max. Series Fuse Rating | 25 A | | | | | |
| Application Classification | Class A | | | | | |
| Power Tolerance | 0 ~ + 10 W | | | | | |

* Under Standard Test Conditions (STC) of irradiance of 1000 W/m², spectrum AM 1.5 and cell temperature of 25°C.

## MECHANICAL DATA

| Specification | Data |
|---|---|
| Cell Type | Mono-crystalline |
| Cell Arrangement | 108 [2 X (9 X 6) ] |
| Dimensions | 1722 × 1134 × 35 mm (67.8 × 44.6 × 1.38 in) |
| Weight | 22.4 kg (49.4 lbs) |
| Front Cover | 3.2 mm tempered glass with anti-reflective coating |
| Frame | Anodized aluminium alloy, |
| J-Box | IP68, 3 bypass diodes |
| Cable | 4 mm² (IEC), 12 AWG (UL) |
| Connector | T6, MC4, MC4-EVO2 or MC4-EVO2A |
| Cable Length (Including Connector) | 1550 mm (61.0 in) (+) / 1100 mm (43.3 in) (-)* |
| Per Pallet | 30 pieces |
| Per Container (40' HQ) | 780 pieces |

* For detailed information, please contact your local Canadian Solar sales and technical representatives.

## ELECTRICAL DATA | NMOT*

CS6R-395/400/405/410/415/420MS-HL

| | | | | | | |
|---|---|---|---|---|---|---|
| Nominal Max. Power (Pmax) | 296 W | 300 W | 304 W | 307 W | 311 W | 315 W |
| Opt. Operating Voltage (Vmp) | 28.7 V | 28.9 V | 29.1 V | 29.2 V | 29.4 V | 29.6 V |
| Opt. Operating Current (Imp) | 10.33 A | 10.39 A | 10.45 A | 10.52 A | 10.58 A | 10.65 A |
| Open Circuit Voltage (Voc) | 34.6 V | 34.8 V | 35.0 V | 35.1 V | 35.3 V | 35.5 V |
| Short Circuit Current (Isc) | 11.09 A | 11.15 A | 11.21 A | 11.28 A | 11.34 A | 11.41 A |

* Under Nominal Module Operating Temperature (NMOT), irradiance of 800 W/m² spectrum AM 1.5, ambient temperature 20°C, wind speed 1 m/s.

## TEMPERATURE CHARACTERISTICS

| Specification | Data |
|---|---|
| Temperature Coefficient (Pmax) | -0.34 % / °C |
| Temperature Coefficient (Voc) | -0.26 % / °C |
| Temperature Coefficient (Isc) | 0.05 % / °C |
| Nominal Module Operating Temperature | 41 ± 3°C |

## PARTNER SECTION

* The specifications and key features contained in this datasheet may deviate slightly from our actual products due to the on-going innovation and product enhancement. CSI Solar Co., Ltd. reserves the right to make necessary adjustment to the information described herein at any time without further notice.
Please be kindly advised that PV modules should be handled and installed by qualified people who have professional skills and please carefully read the safety and installation instructions before using our PV modules.




Figure A.2: Technical data sheet for the HiKu6 CS6R-MS PV panel produced by Canadian Solar [93].

## ENGINEERING DRAWINGS

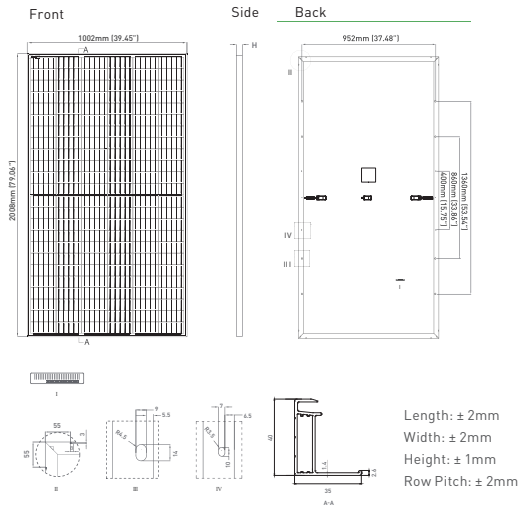


Length: ± 2mm
Width: ± 2mm
Height: ± 1mm
Row Pitch: ± 2mm

## ELECTRICAL PERFORMANCE & TEMPERATURE DEPENDENCE

Current-Voltage & Power-Voltage Curves (400W)

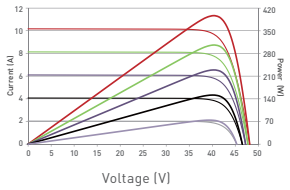


Temperature Dependence of Isc, Voc, Pmax

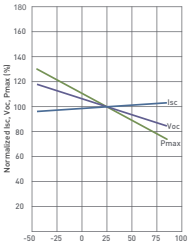


## MECHANICAL CHARACTERISTICS

| | |
|---|---|
| Cells | Mono PERC Diamond Cell (158.75 x 158.75mm) |
| No. of Half Cells | 144 (6 x 24) |
| Dimensions | 2008 x1002 x 40mm (79.06 x 39.45 x 1.57in) |
| Weight | 22.5kg (49.6lbs) |
| Front Glass | 3.2mm, Anti-Reflection Coating<br>High Transmission, Low Iron, Tempered Glass |
| Frame | Anodized Aluminum Alloy |
| Junction Box | IP68 Rated |
| Output Cables | 12 AWG, 1400mm (55.12in) |
| Connector | Staubli MC4 Series |
| Fire Type | Type 1 |
| Pressure Rating | 5400Pa (Snow) & 2400Pa (Wind) |
| Hailstone Test | 50mm Hailstones at 35m/s |

## TEMPERATURE CHARACTERISTICS

| | |
|---|---|
| Temperature Coefficients of Pmax | -0.35%/°C |
| Temperature Coefficients of Voc | -0.29%/°C |
| Temperature Coefficients of Isc | 0.048%/°C |
| Nominal Operating Cell Temperature (NOCT) | 45±2°C |

## MAXIMUM RATINGS

| | |
|---|---|
| Operating Temperature (°C) | -40°C~+85°C |
| Maximum System Voltage | 1500VDC (UL and IEC) |
| Maximum Series Fuse Rating | 20A |

## PACKAGING CONFIGURATION

(Two pallets = One stack)

27pcs/pallet, 54pcs/stack, 594pcs/40'HQ Container

## WARRANTY

**25-year product and 25-year linear power warranty**

1st year degradation not to exceed 2.5%, each subsequent year not to exceed 0.6%, minimum power at year 25 is 83.1% or greater.

## ELECTRICAL CHARACTERISTICS

| Module Type | JKM380M-72HBL-V | | JKM385M-72HBL-V | | JKM390M-72HBL-V | | JKM395M-72HBL-V | | JKM400M-72HBL-V | |
|---|---|---|---|---|---|---|---|---|---|---|
| | STC | NOCT | STC | NOCT | SCT | NOCT | STC | NOCT | STC | NOCT |
| Maximum Power (Pmax) | 380Wp | 280Wp | 385Wp | 283Wp | 390Wp | 287Wp | 395Wp | 291Wp | 400Wp | 294Wp |
| Maximum Power Voltage (Vmp) | 39.10V | 36.5V | 39.37V | 36.8V | 39.64V | 37.0V | 39.90V | 37.4V | 40.16V | 37.6V |
| Maximum Power Current (Imp) | 9.72A | 7.67A | 9.78A | 7.71A | 9.84A | 7.75A | 9.90A | 7.77A | 9.96A | 7.82A |
| Open-circuit Voltage (Voc) | 48.2V | 45.4V | 48.4V | 45.6V | 48.6V | 45.8V | 48.8V | 46.0V | 49.1V | 46.2V |
| Short-circuit Current (Isc) | 10.30A | 8.32A | 10.38A | 8.38A | 10.46A | 8.45A | 10.54A | 8.51A | 10.61A | 8.57A |
| Module Efficiency STC (%) | 18.89% | | 19.13% | | 19.38% | | 19.63% | | 19.88% | |

***STC:** Irradiance 1000W/m² Cell Temperature 25°C AM = 1.5
**NOCT:** Irradiance 800W/m² Ambient Temperature 20°C AM = 1.5 Wind Speed 1m/s

*Power measurement tolerance: ±3%

*The company reserves the final right for explanation on any of the information presented hereby. JKM380-400M-72HBL-V-F1-US*

**BUILDING YOUR TRUST IN SOLAR. WWW.JINKOSOLAR.US**

Figure A.3: Technical data sheet for the JKM380-400M-72HBL-V Eagle Continental PV panel produced by JinkoSolar [94].